CO_2 utilization using bio/photo-hybrid catalysts with visible light energy

(可視光をエネルギー源とする 生体―光触媒による二酸化炭素利用)

Takayuki Katagiri

(片桐　毅之)

CO_2 utilization using bio/photo-hybrid catalysts with visible light energy

(可視光をエネルギー源とする 生体―光触媒による二酸化炭素利用)

理学研究科

物質分子系専攻

令和 3 年度

Takayuki Katagiri

(片桐　毅之)

Abstract

The goal of this doctoral work was to establish a system of CO_2 utilization with visible light energy using biocatalysts. Although many groups have reported visible-light-driven CO_2 utilization systems, most of these involve CO_2 reduction to CO, formate, and methanol by using a metal, complex, and biocatalyst. Several studies on carbon–carbon (C–C) bond formation from CO_2 and organic compounds were reported. However, there are few studies on C–H bond activation and C–C bond formation from CO_2. Furthermore, for biocatalytic CO_2 utilization, most researchers used ferredoxin-$NAD(P)^+$ reductase and rhodium (Rh) complexes for NADH regeneration and focused on the development of photosensitizers to improve NAD^+ reduction activity. To address this issue, two approaches for CO_2 utilization with visible light energy are proposed in this thesis. First, a novel system not based on the NAD^+/NADH redox system is suggested. In addition, a novel type of catalyst for NADH regeneration, a Rh colloidal catalyst, is reported.

This dissertation consists of five chapter. Chapter 1 introduces CO_2 utilization, the conventional CO_2 utilization system using visible light energy, and the scope and outline of this study. In chapter 2, a photoredox system for enzymatic CO_2 fixation using a viologen derivative (PV) as an artificial coenzyme was developed. A novel and simple coenzyme for malic enzyme (ME) was designed and developed. By using this coenzyme, a visible-light-driven C–C bond formation system with ME was developed. In addition, the function of multi-electron-reduced viologen (PV^0) in C–C bond formation was clarified. PV^0 derivatives act as a base and were involved in oxaloacetate production via C–H bond activation and carboxylation of pyruvate by CO_2. In addition, the kinetic parameters of oxaloacetate production based on forming a C–C bond of a coupling pyruvate and CO_2 with PV^0 and ME were determined upon analysis of the enzymatic kinetics.

In Chapter 3, the regioselective NAD^+ reduction to enzymatically active NADH was accomplished using a system comprising photosensitizer and homogeneously polymer-dispersed Rh nanoparticles. The catalytic activity of homogeneous Rh nanoparticles for NADH regeneration was demonstrated for the

first time. The reduction product of NAD^+ was solely 1,4-NADH, which was validated using HPLC and an enzymatic assay. NADH regeneration mechanisms were also proposed.

In Chapter 4, by using the proposed visible-light-driven NADH regeneration system, photochemical conversion using visible light was successfully achieved. As models of enantioselective synthesis, L-lactate-dehydrogenase-catalyzed pyruvate reduction to L-lactate and 3-hydroxybutyrate-dehydrogenase-catalyzed acetoacetate reduction to D-3-hydroxybutyrate were attempted. As a model of C–C bond formation with CO_2 based on C–H bond activation, NAD^+-dependent ME catalyzed pyruvate carboxylation with CO_2, and subsequent reduction to L-malate was performed using visible light energy. This work provides a platform for using Rh nanoparticles as highly efficient homogeneous catalysts for regioselective NADH regeneration, which is central to biological solar energy conversion, energy storage, and artificial photosynthesis.

In Chapter 5, the research carried out during my doctoral studies is summarized. In addition, the prospects of the proposed visible-light-driven molecular conversion system are discussed.

Table of contents

List of Abbreviations

Materials

MV : methylviologen, 1,1'-dimethyl-4,4'bipyridinium salt

MV_{red} : single-electron reduced MV

PV : diphenylviologen, 1,1'-diphenyl-4,4'-bipyridinium salt

$PV^{\bullet+}$: single-electron reduced PV

PV^0 : double-electron reduced PV

PSV : 1,1'-bis(p-sulfonatophenyl)-4,4'-bipyridinium salt

$PSV^{\bullet+}$: single-electron reduced PSV

PSV^0 : double-electron reduced PSV

PCV : 1,1'-bis(p-carboxyphenyl)-4,4'-bipyridinium salt

$PCV^{\bullet+}$: single-electron reduced PCV

PSV^0 : double-electron reduced PCV

DNP : 1,1'-bis(2,4-dinitrophenyl)-4,4'-bipyridinium salt

TEOA : Triethanolamine

H_2TPPS : Tetraphenylporphine tetrasulfonate

ZnTPPS : Zinc tetraphenylporphine tetrasulfonate

Bis-tris : bis(2-hydroxyethyl)iminotris(hydroxymethyl)methane

HEPES : 2-[4-(2-hydroxyethyl)-1-piperazinyl] ethanesulfonic acid

NAD^+ : nicotinamide adenine dinucleotide (Oxidized form)

NADH : nicotinamide adenine dinucleotide (Reduced form)

$NADP^+$: nicotinamide adenine dinucleotide phosphate (Oxidized form)

NADPH : nicotinamide adenine dinucleotide phosphate (Reduced form)

PVP : polyvinylpyrrolidone

$[Cp^*RhCl_2]_2$: (pentamethylcyclopentadienyl)rhodium(III) dichloride dimer

$[Cp^*Rh(bpy)(H_2O)]^{2+}$: pentamethylcyclopentadienyl rhodium bipyridine

Enzymes

CODH : carbon monoxide dehydrogenase

FDH : formate dehydrogenase

AldDH : aldehyde dehydrogenase

ADH : alcohol dehydrogenase

ME : malate dehydrogenase (oxaloacetate-decarboxylating) ($NADP^+$)

MDH : malate dehydrogenase (oxaloacetate-decarboxylating) (NAD^+)

HBDH : 3-hydroxybutyrate dehydrogenase

LDH : L-lactate dehydrogenase

6-PGDH : 6-Phosphogluconate dehydrogenase

Measuring Equipment

TEM : transmission electron microscope

HPLC : high-performance liquid chromatography

UV–Vis : ultraviolet–visible

CV : cyclic voltammetry

NMR : nuclear magnetic resonance

Others

EC number : Enzyme Commission number

List of Figures, Tables and Schemes

after enzymatic assay. A sample solution contained TEOA (0.1 M), ZnTPPS (9.5 μM), Rh-PVP (125 μM), LDH (2 U), and pyruvate (2 mM).

Fig. 3-5. UV-Vis absorption spectral changes during the reduction process with UV-Vis spectroscopy and enzymatic assay. (a) Different UV-Vis absorption spectral changes of sample solution including TEOA, ZnTPPS, and NAD^+ with visible-light irradiation time. Baseline is HEPES-NaOH buffer. (b) Baseline was recorded before irradiation. (c) Different UV-Vis absorption spectral changes of after enzymatic assay. A sample solution contained TEOA (0.1 M), ZnTPPS (9.5 μM), LDH (2 U), and pyruvate (2 mM).

Fig. 3-6. The gas chromatogram of H_2 gas and Air (a), and analysis of the gas phase in the system of TEOA, ZnTPPS, and Rh-PVP after 3 h irradiation (b).

Fig. 3-7. Analytical HPLC chromatograms. (a) After the reduction of NAD^+ with sodium borohydride. (b) Visible-light-driven NAD^+ reduction with the system including TEOA, ZnTPPS, Rh-PVP, and NAD^+. (c) Enzymatic assay for visible-light-driven NAD^+ reduction after 300 min irradiation. A sample solution contained TEOA (0.1 M), ZnTPPS (9.5 μM), Rh-PVP (125 μM), pyruvate (2 mM) and LDH (2 U, — or 0 U, —).

Fig. 3-8. Difference UV-Vis absorption spectral changes of before and after enzymatic assay. A sample solution contained TEOA (0.1 M), ZnTPPS (9.5 μM), Rh-PVP (125 μM), LDH (2 U), and pyruvate (2 mM). (a) 30 min irradiation, (b) 60 min irradiation, (c) 180 min irradiation, (d) 300 min irradiation.

Fig. 3-9. Time course of 1,4-NADH production with the system of TEOA, ZnTPPS, Rh-PVP, and NAD^+ in HEPES-NaOH buffer under continuous irradiation.

Fig. 3-10. Fluorescence spectral changes of ZnTPPS with Rh-PVP.

Fig. 3-11. Modified Stern-Volmer plot for the fluorescence quenching of ZnTPPS by Rh-PVP. The excitation and fluorescence wavelength were 422 and 606 nm, respectively.

Fig. 3-12. UV-Vis absorption spectral changes of ZnTPPS with addition of Rh-PVP. The sample solution contained ZnTPPS (1.0 μM) and Rh-PVP in HEPES-NaOH buffer (pH 7.4).

Chapter 1

General introduction

1.1 CO_2 utilization

1.1.1 Social background

Greenhouse gases are chemical compounds that absorb and emit radiant energy within the thermal infrared range, thereby inducing the greenhouse effect on Earth. The rapid increase in atmospheric concentrations of the three main man-made greenhouse gases—CO_2, methane, and nitrous oxide—is clear from the datasets for these gases over the last 400,000 years. Among these anthropogenic gases, CO_2 is the most important and is primarily generated through the consumption of fossil fuels. Its concentration in the atmosphere has risen by more than 30% since the Industrial Revolution. Therefore, the development of technologies for drastic CO_2 gas reduction is important for the future.[1] With ambitious CO_2 reduction targets set at the 21st Conference of the Parties to the Climate Change Convention (COP21) in 2015 (Paris Agreement),[2] the CO_2 utilization technologies including capture and conversion to resources and fuel are eagerly awaited for protection of the global environment. In 2021, an emissions reduction plan to not exceed a temperature increase of 1.5 °C compared to pre-industrial levels was agreed upon at the United Nations Climate Change Conference (COP26) (Glasgow Climate Pact).[3] CO_2 is the most stable final oxide product from organic compounds. In order to reduce organic molecules or use CO_2 as a feedstock for the synthesis of new organic molecules, it is necessary to input external energy such as electricity and sunlight in addition to the catalyst. Therefore, the production of hydrogen, low-carbon fuels, CO_2-based alcohols, and so on using renewable energy such as solar energy is important to mitigate global warming.

1.1.2 Concept for CO_2 utilization with visible light energy

As in natural photosynthesis, solar energy is used as external energy, and CO_2 can be converted into fuel and resources.[4-10] In natural photosynthesis, CO_2 is reduced with solar energy, the number of carbon atoms is expanded, and finally, glucose with six carbon atoms is produced, as shown in Eq. 1-1.

$$6H_2O + 6CO_2 \rightarrow C_6H_{12}O_6 + 6O_2 \quad \text{(Eq. 1-1)}$$

However, many previous studies that mimicked natural photosynthesis used visible light energy to reduce CO_2 to carbon monoxide, formate, formaldehyde, and methanol.[11-16] Many researchers are currently developing systems using organic dye molecules–catalysts, semiconductor photocatalysts, systems that directly use biomaterials, and hybrid catalyst systems that combine these systems. With its single carbon atom, CO_2 can be multi-electron-reduced with multiple protons; only molecules with a single carbon atom are produced in these systems. On the other hand, natural photosynthesis can fix CO_2, expand its carbon number, and produce glucose with six carbon atoms. In developing CO_2 conversion into various valuable materials using solar energy as a practical technology, various organic-molecule syntheses that mimic natural photosynthesis are promising, especially those using CO_2 as a resource.

To establish this technology, an effective catalyst for the binding of CO_2 to organic molecules is essential. In other words, a catalyst needs to be developed for activating the C–H bonds in organic molecules and promoting carbon–carbon (C–C) bond formation with CO_2. The concept of light-driven C–H bond activation and building C–C bonds with CO_2 using various catalysts is shown in Fig. 1-1.

As shown in Fig. 1-1, an efficient electron-transfer process among photofunctional dyes (photocatalytic materials or molecular dyes), electron mediators (electron carrier or molecules coenzymes), and catalysts is an important factor in constructing the system for light-driven C–H bond activation and C–C bond formation with CO_2. In the concept shown in Fig. 1-1, reduction of the electron mediator and radical formation by photosensitization of an organic dye, semiconductor photocatalyst, or coordination complex has been widely studied. Furthermore, research on light-driven hydrogen production and CO_2 reduction by linking these photoredox systems with biocatalysts, molecular catalysts, or metal nanoparticles has been extensively reported. In order to construct the system shown in Fig. 1-1, it is important to choose a useful catalyst that can activate the C–H bond in organic molecules and promote C–C bond formation with CO_2, which can be linked with the reduction of the electron mediator and radical formation utilizing the photosensitization of an organic dye, semiconductor photocatalyst, or coordination complex. In other words, by searching for and developing a catalyst for activating the

C–H bond in organic molecules and promoting C–C bond formation with CO_2 that can be applied to the photoredox system, various light-driven CO_2 utilization technologies using the system shown in Fig. 1-1 can be constructed.

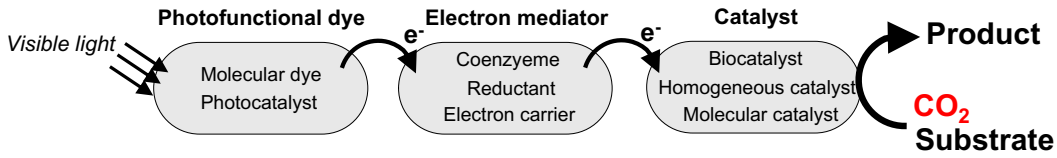

Fig. 1-1. The concept of the light-driven carboxylation of organic molecule with CO_2 using the system of a photofunctional dye, an electron mediator, and a catalyst.

1.1.3 Biocatalysts for CO_2 utilization

Biocatalysts are biological systems or their parts used to catalyze chemical reactions. Natural catalysts, such as enzymes, perform chemical transformations of organic compounds in biocatalytic processes. Enzymes have high catalytic activity and selectivity in ambient conditions. Therefore, they have been used in biodegradation reactions, pharmaceuticals, chemical syntheses, and so on.[17] Enzymes are classified into six groups based on reaction specificity: oxidoreductases, transferases, hydrolases, lyases, isomerases, and ligases. Enzymes are known to catalyze more than 5000 types of biochemical reactions and have strict selectivity for substrates; they decrease the activation energy of a particular biochemical reaction, which is impossible to accomplish using molecular or solid catalysts.

Biocatalysts for CO_2 reduction and utilization are classified into two categories:

(i) CO_2 reduction to CO or formate

(ii) C–C bond formation from CO_2 and an organic molecule to produce a carboxylic acid

Biocatalysts with the function of CO_2 reduction for light-driven redox systems include a set of enzymes that catalyze the oxidation of C1 materials such as formate and CO into CO_2, donating the electrons to a second substrate, $NAD(P)^+$. In addition, these biocatalysts, $NAD(P)^+$-dependent dehydrogenases, catalyze the reverse

reaction, donating the electrons to a second substrate, NAD(P)H. Carbon monoxide dehydrogenase (CODH)[18-22] and formate dehydrogenase (FDH)[23-25] catalyze CO_2 reduction to CO and formate, respectively. CO_2 reduction to ethanol has been achieved by combining FDH, aldehyde dehydrogenase (AldDH),[26–28] and alcohol dehydrogenase (ADH). [29–31]

Biocatalysts with the capability to utilize CO_2 based on C–H bond activation and C–C bond formation for light-driven redox systems are classified into two categories: (i) an oxidoreductase used in the pentose–phosphate cycle,[32–35] tricarboxylic acid (TCA) cycle,[36] and reductive TCA cycle[37–39]; and (ii) a carboxylase producing new C–C bonds by introducing HCO_3^- or CO_2 into target organic molecules. The enzyme belonging to category (i) uses $NAD(P)^+$ or NAD(P)H as a coenzyme and catalyzes the decarboxylation or carboxylation. A malic enzyme (ME)[40–44] and isocitrate dehydrogenase (IDH)[45–47] are typical biocatalysts for CO_2 utilization.

The ME existing in mitochondria is also a useful enzyme that catalyzes the introduction of CO_2 into an organic molecule. ME are classified into three types.

(1) Malate dehydrogenase (oxaloacetate-decarboxylating) (MDH) (EC 1.1.1.38)[48,49] catalyzes the following reaction:

$$\text{(s)-malate} + NAD^+ \leftrightarrows \text{pyruvate} + CO_2 + NADH \quad \text{(Eq. 1-2)}$$

This enzyme belongs to the family of oxidoreductases and participates in pyruvate metabolism.

(2) Malate dehydrogenase (decarboxylating) (EC 1.1.1.39)[50–53] or NAD^+-malic enzyme (NAD^+-ME) catalyzes the following reaction:

$$\text{(s)-malate} + NAD^+ \leftrightarrows \text{pyruvate} + CO_2 + NADH \quad \text{(Eq. 1-3)}$$

This enzyme participates in pyruvate metabolism and carbon fixation.

(3) $NADP^+$-malic enzyme (oxaloacetate-decarboxylating) ($NADP^+$-ME) (EC 1.1.1.40)[40–42,54,55] catalyzes the following reaction in the presence of a divalent metal ion:

$$\text{(s)-malate} + NADP^+ \leftrightarrows \text{pyruvate} + CO_2 + NADPH \quad \text{(Eq. 1-4)}$$

$NADP^+$-ME, as with all other C4 decarboxylases, did not evolve de novo for CO_2 pooling to aid RuBisCO catalysis. Instead, $NADP^+$-ME was directly transformed

from a C3 species during photosynthesis and can be traced to even earlier origins from an ancient cytosol. The typical reaction mechanism of ME involves catalysis of the carboxylation of pyruvate with CO_2 to produce a malate in the presence of NAD(P)H, as shown in Fig. 1-2.

IDH (NAD^+, EC 1.1.1.41) and ($NADP^+$, 1.1.1.42)[56–63] catalyzes the oxidation of isocitrate to produce oxalosuccinate as an intermediate with reduction of $NADP^+$ and decarboxylation of oxalosuccinate to produce 2-oxoglutarate (Eq. 1-5).

Isocitrate + $NAD(P)^+$ ⇆ 2-oxoglutarate + CO_2 + NAD(P)H + H^+ (Eq. 1-5)

In the reverse reaction, an amino acid residue serving as a base in the IDH or an external base abstracts the hydrogen atom of 2-oxoglutarate, and then CO_2 is bonded as a carboxyl group to form an intermediate oxalosuccinate, followed by reduction of the carbonyl group of oxalosuccinate by NADPH to produce an isocitrate.

6-Phosphogluconate dehydrogenase (decarboxylating) (6-PGDH) (NAD^+, EC 1.1.1.343) and $NADP^+$ (EC 1.1.1.44) catalyzes the interconversion of 6-phospho-D-gluconate and D-ribulose 5-phosphate with the $NAD(P)^+$/NAD(P)H redox couple in the pentose phosphate pathway.[64–68] 6-PGDH catalyzes the carboxylation of D-ribulose 5-phosphate with CO_2 to produce a 6-phospho-D-gluconate-assisted $NAD(P)^+$/NAD(P)H redox couple (Eq. 1-6).

6-phospho-D-gluconate + $NAD(P)^+$

⇆ 6-phospho-2-dehydro-D-gluconate + NAD(P)H + H^+ (eq. 1-6)

Acetone carboxylase (EC 6.4.1.6) is an enzyme that catalyzes the reaction of CO_2 with acetone to produce acetoacetate using ATP as a coenzyme.[69]

Oxidoreductases have the potential to achieve the carboxylation of organic molecules with CO_2 by using basic amino-acid residues in the enzyme or external bases and the redox couple $NAD(P)^+$/NAD(P)H. Therefore, visible-light-driven CO_2 utilization based on C–C bond formation can be achieved by using the light-driven $NAD(P)^+$ reduction system with these oxidoreductases.

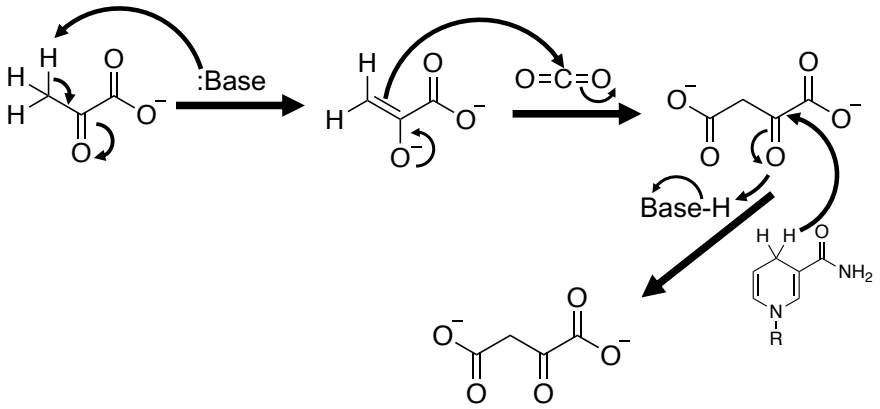

Fig. 1-2. Reaction mechanism for the carboxylation of pyruvate with CO_2 to produce malate with ME.

1.2 Visible-light-driven CO_2 utilization system based on C-H bond activation and C–C bond formation

1.2.1 Photocatalytic dye and molecular catalyst hybrid system

Visible-light-driven C–C bond formation with CO_2 and organic compounds using molecular catalysts have been described. Light-driven CO_2 fixation was reported as early as 1975.[70] The first example in a non-biological system was the conversion of phenanthrene to 9,10-dihydrophenanthrene-9-carboxylic acid using UV irradiation in the presence of various amines and CO_2 in dimethylformamide (DMF) or dimethyl sulfoxide (DMSO) solution.[70] Afterward, many efforts have been devoted to building C–C bonds with CO_2 by using visible-light irradiation as a driving force.[71,72] Although much progress has been made in the field of C(sp^2)–H bond functionalization with CO_2, the direct carboxylation of inactive C(sp^3)–H remains a challenge. Therefore, C(sp^3)–H bond activation and C–C bond formation with CO_2 using visible light energy is a popular research target.

Recently, the first carboxylation based on C(sp^3)–H bond activation and C–C bond formation using *o*-alkylphenyl ketones and CO_2 with UV light or sunlight to generate the corresponding *o*-acylphenylacetic acids was reported (Fig. 1-3).[73]

Site-selective and remote C(sp^3)-H carboxylation enabled by the merging of photoredox and nickel (Ni) catalysis has been reported.[74] The visible-light-driven carboxylation of alkyl halides with CO_2 at remote C(sp^3)-H sites using photoredox and Ni catalysts is shown in Fig. 1-4. A protocol based on a Ni–phenanthroline complex, organic photocatalyst (1,2,3,5-tetrakis(carbazol-9-yl)-4,6-dicyanobenzene; 4-CzIPN), K_2CO_3, and dimethyl 1,4-dihydro-2,6-dimethyl-3,5-pyridine-dicarboxylate (or Hantzsch ester; HEH) as the terminal reductant provided good results.[75]

Very recently, a breakthrough for visible-light-driven C–H bond activation and C–C bond formation with CO_2 has been achieved.[76] The visible-light-driven direct carboxylation of benzylic C(sp^3)-H bonds with CO_2 to prepare 2-arylpropionic acids by using a catalytic amount of photosensitizer and hydrogen-atom-transfer

catalyst was reported for the first time (Fig.1-5). 4-CzIPN is a catalyst for the direct carboxylation of the benzylic C(sp^3)-H bond.[77–80]

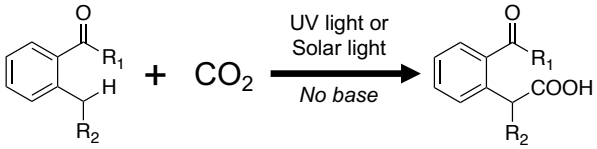

Fig. 1-3. Light-driven the carboxylation of benzylic C(sp^3)-H with CO_2 using the system without base.

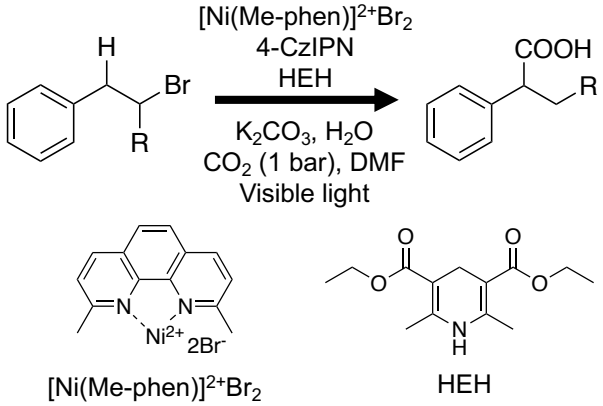

Fig. 1-4. Visible-light-driven carboxylation at remote C(sp^3)-H sites by merging $[Ni(Me- phen)]^{2+}$ and photoredox catalysis.

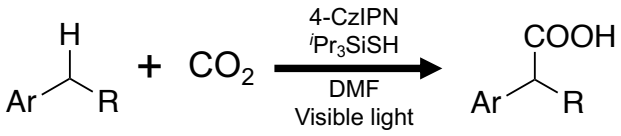

Fig. 1-5. Visible-light-driven carboxylation of benzylic C(sp^3)-H bonds with CO_2 using benzonitrile derivative 4-CzIPN as a catalyst.

1.2.2 Photocatalytic dye and biocatalyst hybrid system

As mentioned in Chapter 1.1.3, ME and IDH are attractive biocatalysts for C–H bond activation and C–C bond formation with CO_2 and an organic molecule. For the C–C bond formation to proceed for ME or IDH, NAD(P)H is needed. Therefore, to construct the photoredox system with these biocatalysts, a redox cycle

of $NAD(P)^+$ to NAD(P)H is necessary. In simple terms, $NAD(P)^+$ is reduced directly with a photocatalytic dye such as a tris(bypyridine)ruthenium(II) ($[Ru(bpy)_3]^{2+}$) or water-soluble porphyrin. Then, a single-electron-reduced $NAD(P)^+$ forms and can undergo dimerization to a biologically inactive reduction product (4,4'- or 4,6-NAD dimer). Therefore, to produce NAD(P)H from $NAD(P)^+$, a photoredox system with ferredoxin-$NAD(P)^+$ reductase (FNR; EC 1.18.1.2) is developed. FNR catalyzes a reduction of $NAD(P)^+$ to NADPH by coupling with ferredoxin, as shown in Eq. 1-5.

2 reduced ferredoxin + $NAD(P)^+$ + H^+

$$\rightleftharpoons \text{ 2 oxidized ferredoxin + NAD(P)H (Eq. 1-5)}$$

FNR also catalyzes the reduction of $NADP^+$ to NADPH by coupling with a 1,1'-dimethyl-4,4'bipyridinium salt (methylviologen, MV) and single-electron-reduced MV (MV_{red}), as shown in Eq. 1-6.[81]

$$MV_{red} + NADP^+ + H+ \rightleftharpoons MV + NADPH \text{ (Eq. 1-6)}$$

A visible-light-driven redox system with ME using the FNR-catalyzed $NAD(P)^+$ reduction to NAD(P)H as the electron was reported.[82,83] In this case, the use of $[Ru(bpy)_3]^{2+}$, MV, FNR, and 2-mercaptoethanol results in malate production from HCO_3^- and pyruvic acid, as shown in Scheme 1-1. In this system, MV_{red} does not act as a coenzyme for ME in malate production from CO_2 and pyruvate. Thus, an $NAD(P)^+$/NAD(P)H redox system with FNR is necessary for the system. Several groups reported ME-catalyzed malate production systems comprising a TiO_2 semiconductor,[84] CdS photocatalyst,[84] Zn chlorin-e_6 (ZnChl-e_6),[85,86] and polyethylene-glycol-modified chlorophyll-a (PEG-Chl-a) [87] as a photosensitizer with an FNR-catalyzed $NADP^+$/NADPH redox cycle.

A successful CO_2 fixation system for preparing isocitrate using IDH and the $NADP^+$/NADPH redox cycle is shown in Scheme 1-2.[82,83] This visible-light-driven redox system consists of DL-dithiothreitol (DTT) as an electron donor, $[Ru(bpy)_3]^{2+}$, MV, FNR, $NADP^+$, IDH, HCO_3^-, and α-oxoglutarate.

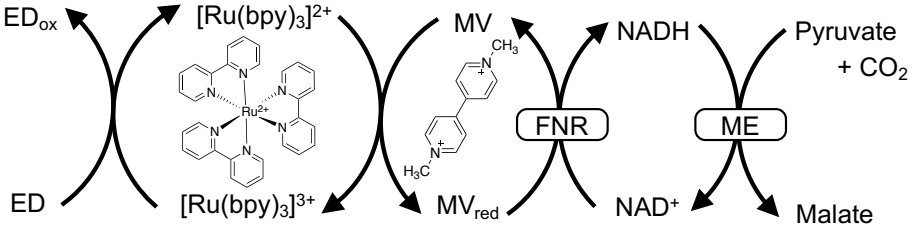

Scheme 1-1. Visible-light-driven malate production system consisted of 2-mercaptoethanol, $[Ru(bpy)_3]^{2+}$, MV, FNR, $NADP^+$, ME, HCO_3^-, and pyruvic acid.

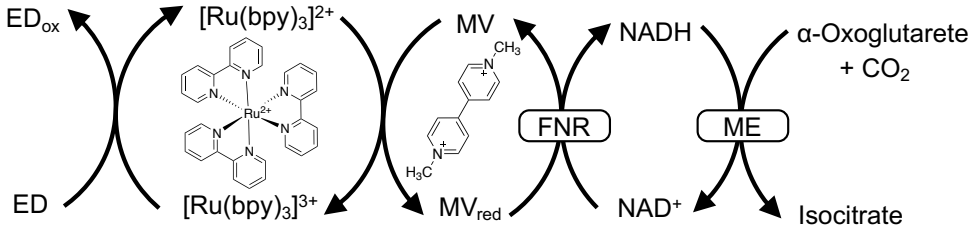

Scheme 1-2. Visible-light-driven isocitrate production system consisted of DL-dithiothreitol, $[Ru(bpy)_3]^{2+}$, MV, FNR, $NADP^+$, IDH, HCO_3^-, and α-oxoglutarate.

Light-driven C–H bond activation and C–C bond formation with CO_2 using molecular catalysts is limited to unsaturated hydrocarbons, alkenes, alkynes, and aromatics as substrates. To date, several studies on the carboxylation of saturated hydrocarbons using a photoredox system with molecular catalysts have been reported, although these systems are limited to organic solvents. On the other hand, for photoredox systems with molecular catalysts, a high yield and selective carboxylation can be achieved using reaction-inert CO_2 as a raw material.

In contrast, light-driven C–H bond activation and C–C bond formation with CO_2 using biocatalysts has limited variety in terms of reaction substrates. However, the reaction can be accomplished in aqueous solvents. It is expected that the strict selectivity of biocatalytic reactions will be diversified depending on the structures and functions of various electron mediators as the coenzyme in light-driven C–H bond activation and C–C bond formation with CO_2.

1.3 Scope and outline of the dissertation

The goal of this doctoral work is to establish a system of CO_2 utilization with visible light energy using biocatalysts.

As mentioned earlier in this chapter, many groups have reported visible-light-driven CO_2 utilization systems. Most of these systems involve CO_2 reduction to CO, formate, and methanol by using a metal, complex, and biocatalyst. Although some researchers have investigated C–C bond formation from CO_2 and organic compounds, the number of studies exploring C–H bond activation and C–C bond formation is still low. For biocatalytic CO_2 utilization, most researchers employed FNR and a Rh complex for NADH regeneration; however, their main focus was to develop a photosensitizer to improve NAD^+ reduction activity. Here, a novel system that omits the NAD^+/NADH redox system is suggested. In addition, a novel type of catalyst for NADH regeneration—an Rh colloidal catalyst—is reported.

The dissertation is composed of five chapters. Chapter 1 introduces the concept of CO_2 utilization, the conventional CO_2 utilization system using visible light energy, and the scope and outline of this study.

Chapter 2 describes the photoredox system for enzymatic CO_2 fixation using a viologen derivative as an artificial coenzyme. A novel and simple coenzyme for ME was designed, developed and used in the visible-light-driven C–C bond formation system with ME. In addition, the function of viologen derivatives in the C–C formation mechanism was clarified.

Chapter 3 describes the regioselective NAD^+ reduction to NADH using a system composed of photosensitizer and homogeneously polymer-dispersed metal nanoparticles. The catalytic activity of homogeneous Rh nanoparticles for NADH regeneration was studied.

Chapter 4 describes the photochemical conversion using a visible-light-driven NADH regeneration system described in Section 3. By using this system, the enantioselective synthesis of L-lactate from pyruvate with lactate dehydrogenase and C–C bond formation from CO_2 and pyruvate to produce L-malate with MDH, were successfully achieved.

In Chapter 5, my doctoral research is summarized, and the potential applications of the visible-light-driven molecular conversion system are discussed.

1.4 References

1. E. S. Sanz-Pérez, C. R. Murdock, S. A. Didas and C. W. Jones, "Direct Capture of CO_2 from Ambient Air", *Chem. Rev.*, 2016, **116**, 11840–11876.
2. https://unfccc.int/sites/default/files/english_paris_agreement.pdf (PARIS AGREEMENT).
3. https://unfccc.int/sites/default/files/resource/cop26_auv_2f_cover_decision.pdf (Glasgow Climate Pact).
4. M. P. Johnson, "Photosynthesis", *Essays Biochem.*, 2016, **60**, 255–273
5. R. E. Blankenship, "Early Evolution of Photosynthesis", *Plant Physiol.*, 2010, **154**, 434-438.
6. R. E. Blankenship, *Molecular Mechanisms of Photosynthesis*, Wiley–Blackwell Publishing, Chichester, 2014.
7. N. Nelson and A. Ben Shem, "The complex architecture of oxygenic photosynthesis", *Nat. Rev. Mol. Cell Biol.*, 2004, **5**, 971–982.
8. C. A. Raines, "The Calvin cycle revisited", *Photosynth. Res.*, 2003, **75**, 1–10.
9. A. V. Ruban, "Evolution under the sun: optimizing light harvesting in photosynthesis", *J. Exp. Bot.*, 2015, **66**, 7–23.
10. R. F. Sage, "The evolution of C4 photosynthesis", *New Phytol.*, 2004, **161**, 341-–370.
11. T. Zhanga, and W. Lin, "Metal–organic frameworks for artificial photosynthesis and photocatalysis", *Chem. Soc. Rev.*, 2014,**43**, 5982–5993.
12. Y. Amao, "Formate dehydrogenase for CO_2 utilization and its application", *J. CO_2. Util.*, 2018, **26**, 623–641.
13. N. Zhang, R. Long, C. Gao and Y. Xiong, "Recent progress on advanced design for photoelectrochemical reduction of CO_2 to fuels", *Sci. China Mater.*, **2018**, 61, 771–-805.
14. C. Wang, Z. Sun, Y. Zheng and Y. H. Hu, "Recent progress in visible light photocatalytic conversion of carbon dioxide", *J. Mater. Chem. A*, 2019, **7**, 865–887.

15. D. Li, M. Kassymova, X. Cai, S.-Q. Zang and H.-L. Jiang, "Photocatalytic CO_2 reduction over metal-organic framework-based materials", *Coord. Chem. Rev.*, 2020, **412**, 21362.
16. P. R. Yaashikaa, P. S. Kumar, S. J. Varjani and A. Saravanan, "A review on photochemical, biochemical and electrochemical transformation of CO_2 into value-added products", *J. CO_2. Util.*, 2019, **33**, 131–147.
17. U. T. Bornscheuer, G. W. Huisman, R. J. Kazlauskas, S. Lutz, J. C. Moore and K. Robins, "Engineering the third wave of biocatalysis", *Nature*, 2012, **485**, 185–194.
18. O. Meyer and H. G. Schlegel, "Carbon monoxide: methylene blue oxidoreductase from *Pseudomonas carboxydovorans*", *J. Bacteriol.*, 1980, **141**, 74–80.
19. S. W. Ragsdale, J. E. Clark, L. G. Ljungdahl, L. L. Lundie and H. L. Drake, "Properties of purified carbon monoxide dehydrogenase from *Clostridium thermoaceticum*, a nickel, iron-sulfur protein", *J. Biol. Chem.*, 1983, **258**, 2364–2369.
20. T. I. Doukov, T. M. Iverson, J. Seravalli, S. W. Ragsdale and C. L. Drennan, "A Ni-Fe-Cu Center in a Bifunctional Carbon Monoxide Dehydrogenase/ Acetyl-CoA Synthase", *Science*, 2002, **298**, 567–572.
21. C. L. Drennan, J. Heo, M. D. Sintchak, E. Schreiter and P. W. Ludden, "Life on carbon monoxide: X-ray structure of Rhodospirillum rubrum Ni-Fe-S carbon monoxide dehydrogenase", *Proc. Natl. Acad. Sci.*, 2001, **98**, 11973–11978.
22. H. Dobbek, V. Svetlitchnyi, L. Gremer, R. Huber and O. Meyer, "Crystal Structure of a Carbon Monoxide Dehydrogenase Reveals a [Ni-4Fe-5S] Cluster", *Science*, 2001, **293**, 1281–1285.
23. D. C. Davison, "Studies on plant formic dehydrogenase", *Biochem. J.*, 1950, **49**, 520–526.
24. J. R. Quayle, "Formate dehydrogenase", *Methods Enzymol.*, 1966, **9**, 360–364
25. D. R. Jollie and J. D. Lipscomb, "Formate dehydrogenase from *Methylosinus trichosporium* OB3b. Purification and spectroscopic characterization of the cofactors", *J. Biol. Chem.*, 1991, **266**, 21853–21863.

26. B. A. Manjasetty, J. Powlowski and A. Vrielink, “Crystal structure of a bifunctional aldolase-dehydrogenase: Sequestering a reactive and volatile intermediate”, *Proc. Natl. Acad. Sci.*, 2003, **100**, 6992–6997.
27. S. Harada, “Genetic Polymorphism of Alcohol Metabolyzing Enzymes and Its Implication to Human Ecology”, *J. Anthrop. Soc. Nippon*, 1991, **99**, 123–139.
28. Y. Lei, P. D. Pawelek and J. Powlowski, “A Shared Binding Site for NAD^+ and Coenzyme A in an Acetaldehyde Dehydrogenase Involved in Bacterial Degradation of Aromatic Compounds”, *Biochemistry*, 2008, **47**, 6870–6882.
29. E. Racker, “Crystalline alcohol dehydrogenase from baker's yeast”, *J. Biol. Chem.*, 1950, **184**, 313–319.
30. E. G. Brandt, M. Hellgren, T. Brinck, T. Bergman and O. Edholm, “Molecular dynamics study of zinc binding to cysteines in a peptide mimic of the alcohol dehydrogenase structural zinc site”, *Phys. Chem. Chem. Phys.*, 2009, **11**, 975–983.
31. P. Zucca, M. Littarru, A. Rescigno and E. Sanjust, “Cofactor Recycling for Selective Enzymatic Biotransformation of Cinnamaldehyde to Cinnamyl Alcohol”, *Biosci., Biotechnol., Biochem.*, 2009, **73**, 1224–1226.
32. M. A. Keller, A. V. Turchyn and M. Ralser, “Non-enzymatic glycolysis and pentose phosphate pathway-like reactions in a plausible Archean ocean”, *Mol. Syst. Biol.*, 2014, **10**, 725.
33. Y. P. Wang, L. S. Zhou, Y. Z. Zhao, S. W. Wang, L. L. Chen, L. X. Liu, Z. Q. Ling, F. J. Hu, Y. P. Sun, J. Y. Zhang, C. Yang, Y. Yang, Y. Xiong, K. L. Guan and D. Ye, “Regulation of G6PD acetylation by KAT9/SIRT2 modulates NADPH homeostasis and cell survival during oxidative stress.”, *EMBO J.*, 2014, **33**, 1304–1320.
34. S. N. Xu, T. S. Wang, X. Li and Y. P. Wang, “SIRT2 activates G6PD to enhance NADPH production and promote leukaemia cell proliferation”, *Sci. Rep.*, 2016, **6**, 32734.
35. E. S. Cho, Y. H. Cha, H. S. Kim, N. H. Kim and J. I. Yook, “The Pentose Phosphate Pathway as a Potential Target for Cancer Therapy”, *Biomol. Ther.*, 2018, **26**, 29–38.

36. J. M. Lowenstein, Methods in Enzymology, *Citric Acid Cycle*, Academic Press, Boston, 1969, vol. 13.
37. M. C. Evans, B. B. Buchanan and D. I. Arnon, "A new ferredoxin-dependent carbon reduction cycle in a photosynthetic bacterium", *Proc. Natl. Acad. Sci. U. S. A.*, 1966, **55**, 928–934B.
38. X. V. Zhang and S. T. Martin, "Driving Parts of Krebs Cycle in Reverse through Mineral Photochemistry", *J. Am. Chem. Soc.*, 2006, **128**, 16032–16033.
39. K. B. Muchowska, S. J. Varma, E. Chevallot-Beroux, L. Lethuillier-Karl, G. Li and J. Moran, "Metals promote sequences of the reverse Krebs cycle", *Nat. Ecol. Evol.*, 2017, **1**, 1716–1721.
40. I. Harary, S. R. Korey and S. Ochoa, "Biosynthesis of dicarboxylic acids by carbon dioxide fixation. VII. Equilibrium of malic enzyme reaction", *J. Biol. Chem.*, 1953, **203**, 595–604.
41. S. Ochoa, A. H. Mehler and A. Kornberg, "Biosynthesis of dicarboxylic acids by carbon dioxide fixation. I. Isolation and properties of an enzyme from pigeon liver catalyzing the reversible oxidative decarboxylation of l-malic acid.", *J. Biol. Chem.*, 1948, **74**, 979–1000.
42. W. J. Rutter and H. A. Lardy, "Purification and properties of pigeon liver malic enzyme", *J. Biol. Chem.*, 1958, **233**, 374–378.
43. Y. Ohno, T. Nakamori, H. Zheng and S. Suye, "Reverse Reaction of Malic Enzyme for HCO_3^- Fixation into Pyruvic Acid to Synthesize L-Malic Acid with Enzymatic Coenzyme Regeneration", *Biosci., Biotechnol., Biochem.*, 2008, **72**, 1278–1282.
44. H. Zheng, T. Nakamori and S. Suye, "Production of l-malic acid with fixation of HCO_3^- by malic enzyme-catalyzed reaction based on regeneration of coenzyme on electrode modified by layer-by-layer self-assembly method", *J. Biosci. Bioeng.*, 2009, **107**, 16–20.
45. D. B. Cherbavaz, M. E. Lee, R. M. Stroud and D. E. Koshland, "Active site water molecules revealed in the 2.1 Å resolution structure of a site-directed mutant of isocitrate dehydrogenase", *J. Mol. Biol.*, 2000, **295**, 377–385.

46. H. Tarhonskaya, A. M. Rydzik, I. K. H. Leung, N. D. Loik, M. C. Chan, A. Kawamura, J. S. McCullagh, T. D. W. Claridge, E. Flashman and C. J. Schofield, “Non-enzymatic chemistry enables 2-hydroxyglutarate-mediated activation of 2-oxoglutarate oxygenases”, *Nat. Commun.*, 2014, **5**, 3423.
47. F. J. Corpas, J. B. Barroso, L. M. Sandalio, J. M. Palma, J. A. Lupiáñez and L. A. del Río, “Peroxisomal NADP-Dependent Isocitrate Dehydrogenase. Characterization and Activity Regulation during Natural Senescence”, *Plant Physiol.*, 1999, **121**, 921–928.
48. S. Kaufman, S. Korkes and A. Del Campillo, “Biosynthesis of dicarboxylic acids by carbon dioxide fixation. V. Further study of the "malic" enzyme of Lactobacillus arabinosus”, *J. Biol. Chem.*, 1951, **192**, 301–312.
49. M. Yamaguchi, “Studies on Regulatory Functions of Malic Enzymes: IV. Effects of Sulfhydryl Group Modification on the Catalytic Function of NAD-linked Malic Enzyme from Escherichia coli”, *J. Biochem.*, 1979, **86**, 325–333.
50. R. T. Wedding, “Malic Enzymes of Higher Plants: Characteristics, Regulation, and Physiological Function”, *Plant Physiol.*, 1989, **90**, 367–371.
51. R. T. Voegele, J. M. Mitsch and T. M. Finan, “Characterization of two members of a novel malic enzyme class”, *Biochim. Biophys. Acta*, 1999, **1432**, 275–285.
52. I. Sato, J. Yoshikawa, A. Furusawa, K. Chiku, S. Amachi and T. Fujii, “Isolation and Properties of Malic Enzyme and Its Gene in Rhodopseudomonas palustris No. 7”, *Biosci. Biotechnol. Biochem.*, 2010, **74**, 75–81.
53. M. A. Tronconi, M. C. G. Wheeler, G. Maurino, M. F. Drincovich and C. S. Andreo, “NAD-malic enzymes of Arabidopsis thaliana display distinct kinetic mechanisms that support differences in physiological control”, *Biochem. J.*, 2010, **430**, 295–303.
54. R. G. Strickland, “Some properties of the malic enzyme of pigeon liver. 1. Conversion of malate into pyruvate”, *Biochem. J.*, 1959, **73**, 646–654.
55. R. G. Strickland, “Some properties of the malic enzyme of pigeon liver. 2. Synthesis of malate from pyruvate”, *Biochem. J.*, 1959, **73**, 654–659.

56. C. E. Quartararo, S. Hazra, T. Hadi and J. S. Blanchard, “Structural, Kinetic and Chemical Mechanism of Isocitrate Dehydrogenase-1 from Mycobacterium tuberculosis”, *Biochemistry*, 2013, **52**, 1765–1775.
57. I. Maeting, G. Schmidt, H. Sahm and K. P. Stahmann, “Role of a peroxisomal NADP-specific isocitrate dehydrogenase in the metabolism of the riboflavin overproducer Ashbya gossypii”, *J. Mol. Catal. B: Enzym.*, 2000, **10**, 335–343.
58. J. McMurry and P. B. Tadhg, *The Organic Chemistry of Biological Pathways*, Roberts and Co. Publishers, 2005, 189190.
59. M. Cox, E. R. Nelson and A. L. Lehninger, *Principles of Biochemistry*, W.H. Freeman, San Francisco, 2005, 609611.
60. Y. Yasutake, S. Watanabe, M. Yao, Y. Takada, N. Fukunaga and I. Tanaka, “Crystal Structure of the Monomeric Isocitrate Dehydrogenase in the Presence of $NADP^+$: INSIGHT INTO THE COFACTOR RECOGNITION, CATALYSIS, AND EVOLUTION”, *J. Biol. Chem.*, 2003, **278**, 36897–36904.
61. R. Garrett and C. M. Grisham, *Biochemistry*, Cengage Learning, 2012, 621.
62. M. Aoshima and Y. Igarashi, “Nondecarboxylating and Decarboxylating Isocitrate Dehydrogenases: Oxalosuccinate Reductase as an Ancestral Form of Isocitrate Dehydrogenase”, *J. Bacteriol.*, 2008, **190**, 2050–2055.
63. A. E. Fedøy, N. Yang, A. L. Martinez and I. H. Steen, “Structural and Functional Properties of Isocitrate Dehydrogenase from the Psychrophilic Bacterium Desulfotalea psychrophila Reveal a Cold-active Enzyme with an Unusual High Thermal Stability”, *J. Mol. Biol.*, 2007, **372**, 130–149.
64. C. Phillips, S. Gover and M. J. Adams, “Structure of 6-phosphogluconate dehydrogenase refined at 2 Å resolution”, *Acta Crystallogr., Sect. D: Biol. Crystallogr.*, 1995, **51**, 290–301.
65. W. He, Y. Wang, W. Liu and C. Z. Zhou, “Crystal structure of Saccharomyces cerevisiae 6-phosphogluconate dehydrogenase Gnd1”, *BMC Struct. Biol.*, 2007, **7**, 38.
66. Y. Y. Chen, T. P. Ko, W. H. Chen, L. P. Lo, C. H. Lin and A. H. Wang, “Conformational changes associated with cofactor/substrate binding of 6-phosphogluconate dehydrogenase from Escherichia coli and Klebsiella

pneumoniae: Implications for enzyme mechanism", *J. Struct. Biol.*, 2010, **169**, 25–35.

67. M. Rippa, P. P. Giovannini, M. P. Barrett, F. Dallocchio and S. Hanau, "6-Phosphogluconate dehydrogenase: the mechanism of action investigated by a comparison of the enzyme from different species", *Biochim. Biophys. Acta*, 1998, **1429**, 83–92.
68. W. He, Y. Wang, W. Liu and C. Z. Zhou, "Crystal structure of *Saccharomyces cerevisiae* 6-phosphogluconate dehydrogenase Gnd1", *BMC Struct. Biol.*, 2007, **7**, 38.
69. M. K. Sluis and S. A. Ensign, "Purification and characterization of acetone carboxylase from *Xanthobacter* strain Py2", *Proc. Natl. Acad. Sci. U. S. A.*, 1997, **94**, 8456.
70. S. Tazuke and H. Ozawa, "Photofixation of carbon dioxide: formation of 9,10-dihydrophenanthrene-9-carboxylic acid from phenanthrene-amine-carbon dioxide systems", *J. Chem. Soc., Chem. Commun.*, 1975, 237–238.
71. J. Hou, J.-S. Li and J. Wu, "Recent Development of Light-Mediated Carboxylation Using CO_2 as the Feedstock", *Asian J. Org. Chem.*, 2018, **7**, 1439–1447.
72. S. Wanga and C. Xi, "Recent advances in nucleophile-triggered CO_2-incorporated cyclization leading to heterocycles", *Chem. Soc. Rev.*, 2019, **48**, 382–404.
73. Y. Masuda, N. Ishida and M. Murakami, "Light-Driven Carboxylation of o-Alkylphenyl Ketones with CO_2", *J. Am. Chem. Soc.*, 2015, **137**, 14063–14066.
74. B. Sahoo, P. Bellotti, F. Juliá-Hernández, Q. Y. Meng, S. Crespi, B. König and R. Martin, "Site-Selective, Remote sp^3 CH Carboxylation Enabled by the Merger of Photoredox and Nickel Catalysis", *Chem. - Eur. J.*, 2019, **25**, 9001–9005.
75. P. Z. Wang, J. R. Chen and W. J. Xiao, "Hantzsch esters: an emerging versatile class of reagents in photoredox catalyzed organic synthesis", *Org. Biomol. Chem.*, 2019, **17**, 6936–6951.

76. Q. Y. Meng, T. E. Schirmer, A. L. Berger, K. Donabauer and B. König, “Photocarboxylation of Benzylic C-H Bonds”, *J. Am. Chem. Soc.*, 2019, **141**, 11393–11397.
77. T. Y. Shang, L. H. Lu, Z. Cao, Y. Liu, W. M. He and B. Yu, “Recent advances of 1,2,3,5-tetrakis(carbazol-9-yl)-4,6-dicyanobenzene (4CzIPN) in photocatalytic transformations”, *Chem. Commun.*, 2019, **55**, 5408–5419.
78. H. Uoyama, K. Goushi, K. Shizu, H. Nomura and C. Adachi, “Highly efficient organic light-emitting diodes from delayed fluorescence”, *Nature*, 2012, **492**, 234–238.
79. J. Lu, B. Pattengale, Q. Liu, S. Yang, W. Shi, S. Li, J. Huang and J. Zhang, “Donor–Acceptor Fluorophores for Energy-Transfer-Mediated Photocatalysis”, *J. Am. Chem. Soc.*, 2018, **140**, 13719–13725.
80. E. Speckmeier, T. G. Fischer and K. Zeitler, “A Toolbox Approach To Construct Broadly Applicable Metal-Free Catalysts for Photoredox Chemistry: Deliberate Tuning of Redox Potentials and Importance of Halogens in Donor-Acceptor Cyanoarenes”, *J. Am. Chem. Soc.*, 2018, **140**, 15353–15365.
81. M. Ito and T. Kuwana, “Spectroelectrochemical study of indirect reduction of triphosphopyridine nucleotide: I. Methyl viologen, ferredoxin-TPN-reductase and TPN”, *J. Electroanal. Chem.*, 1971, **32**, 415–425.
82. L. Willner, D. Mandler and A. Riklin,” Photoinduced carbon dioxide fixation forming malic and isocitric acid”, *J. Chem. Soc., Chem. Commun.*, 1986, 1022–1024.
83. D. Mandler and I. Willner, “Photochemical fixation of carbon dioxide: enzymic photosynthesis of malic, aspartic, isocitric, and formic acids in artificial media”, *J. Chem. Soc., Perkin Trans.2*, 1988, 997–1003.
84. H. Inoue, M. Yamachika and H. Yoneyama, “Photocatalytic conversion of lactic acid to malic acid through pyruvic acid in the presence of malic enzyme and semiconductor photocatalysts”, *J. Chem. Soc., Faraday Trans.*, 1992, **88**, 2215–2219.

85. Y. Amao and M. Ishikawa, “Photochemical and Enzymatic Synthesis of Malic Acid from Pyruvic Acid and HCO_3^- with Combination System of Zinc Chlorin-e_6 and Malic Enzyme in Aqueous Medium”, *J. Jpn. Pet. Inst.*, 2007, **50**, 272–277.
86. Y. Amao and M. Ishikawa, “Visible light and enzymatic induced synthesis of malic acid from pyruvic acid and HCO_3^- with the combination system of zinc chlorophyll derivative and malic enzyme in water media”, *Catal. Commun.*, 2007, **8**, 523–526.
87. T. Itoh, H. Asada, K. Tobioka, Y. Kodera, A. Matsushima, M. Hiroto, H. Nishimura, T. Kamachi, I. Okura and Y. Inada, “Hydrogen Gas Evolution and Carbon Dioxide Fixation with Visible Light by Chlorophyllin Coupled with Polyethylene Glycol”, *Bioconjugate Chem.*, 2000, **11**, 8–13.

Chapter 2

Photoredox system for enzymatic CO_2 fixation using a viologen derivative as an artificial coenzyme

2.1 Introduction

Recently, several global environmental and resource issues such as global warming and depletion of fossil-fuel resources have come to the forefront.[1] To solve these problems, technologies for solar-energy-based CO_2 utilization, including artificial photosynthesis, have attracted considerable attention. As one of these technologies, a system of light-driven CO_2 photoreduction to CO, formate, or methanol using a photosensitizer, electron mediator, and biocatalyst was developed.[2–26] In this system, the products were mainly C1 compounds. On the other hand, light-driven CO_2 conversion to organic molecules has been actively investigated in green, sustainable chemistry. For example, upon C–H bond activation and C–C bond formation, CO_2 bound to an organic molecule as a carboxy group produces carboxylic acid.[27–35] In order to utilize CO_2 as a carbon feedstock for the synthesis of organic molecules, effective catalysts for building C–C bonds are required. Of the various catalysts, biocatalysts are useful owing to their favorable catalytic activity in aqueous media at room temperature and pressure. Among the biocatalysts, malate dehydrogenase (oxaloacetate-decarboxylating, EC 1.1.1.40), commonly called malic enzyme (ME), is a talented catalyst for forming C–C bonds using CO_2. ME catalyzes the incorporation of CO_2 into pyruvate (C3 compound) as a carboxy group to produce malate (C4 compound) via the intermediate oxaloacetate (C4 compound) with the coenzyme NADPH, as shown in Fig. 2-1.[36–38]

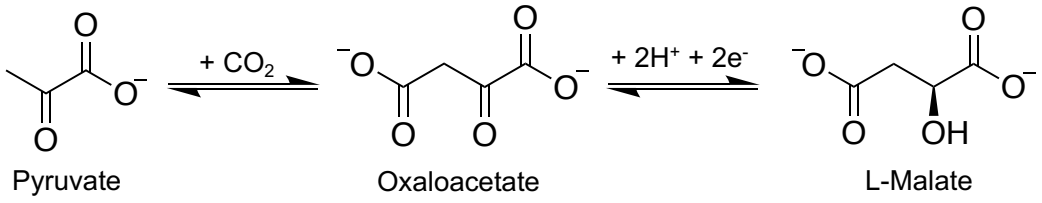

Fig. 2-1. Malate production from CO_2 and pyruvate via oxaloacetate as an intermediate.

Several studies of visible-light-driven malate production from pyruvate and CO_2 using a system composed of an electron donor (ED), photosensitizer (PS), methylviologen (MV, Fig. 2-2) as an electron mediator, ferredoxin-$NADP^+$ reductase

(FNR), $NADP^+$, and ME, as shown in Scheme 2-1, have been reported.[39–41] Although MV has been widely used as an electron mediator for formate (FDH), aldehyde (AldDH), and alcohol dehydrogenase (ADH), a single-electron-reduced MV ($MV^{\bullet}$) does not directly act as a coenzyme for ME. Therefore, to produce malate from pyruvate and CO_2 with ME, NADPH (the reduced form of $NADP^+$) is needed. This system is highly complex, necessitating simplification by using a simple electron mediator in place of $NADP^+$ reduction with FNR. Even if reduction of $NADP^+$ to NADPH with the photoredox system could be achieved, expensive biological reagents $NADP^+$ and FNR are needed. Thus, it is necessary to ameliorate their usage and of $NADP^+$/NADPH redox coupling. As long as redox coupling of $NADP^+$/NADPH takes place, no change in the affinity between $NADP^+$ or NADPH and ME is accomplished; thus, the catalytic activity of ME cannot be controlled in the photoredox system. Moreover, as NADPH acts as an electron donor and is consumed, the redox coupling of $NADP^+$/NADPH is unsuitable for use in the photoredox system. More recently, we reported the potential of 1,1'-diphenyl-4,4'-bipyridinium (diphenylviologen, PV), as shown Fig. 2-2 (b), to act as an electron mediator for ME, instead of NADPH.[42]

In this chapter, the construction of a photoredox system for enzymatic CO_2 fixation using a viologen derivative as an artificial coenzyme is described. First, water-soluble PV derivatives, 1,1'-bis(*p*-sulfonatophenyl)-4,4'-bipyridinium salt (PSV; Fig. 2-2 (c)) and 1,1'-bis(*p*-carboxyphenyl)-4,4'-bipyridinium salt (PCV; Fig. 2-2 (d)), were synthesized. Next, their chemical and photoredox properties were investigated. In addition, PV and PSV were applied to visible-light-induced malate production from CO_2 and pyruvate by using the system with ME (Scheme 2-1). Elucidation of the carboxylation process is essential for developing novel processes of the light-driven formation of C–C bonds from CO_2 as a chemical feedstock. Kinetic analyses can assist in achieving this goal by revealing the kinetic parameters of enzymatic pyruvate carboxylation by CO_2 with ME and PV. The kinetic parameters of the reaction of CO_2 with pyruvate using the double-electron-reduced water-soluble PV derivative PCV (PCV^0) along with ME were determined by enzymatic kinetic analysis.

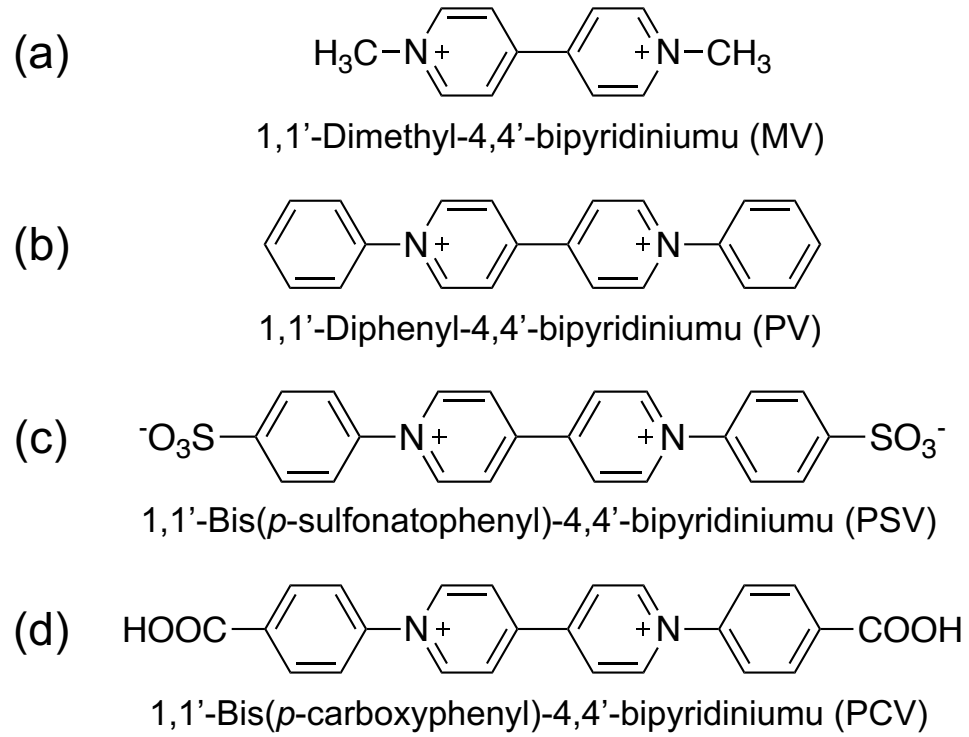

Fig. 2-2. Chemical structures of 4,4'-bipyridinium derivatives.

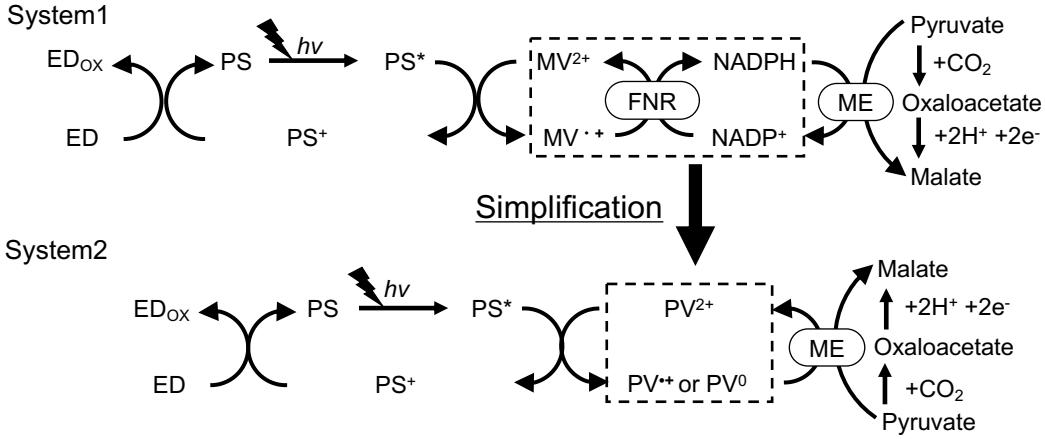

Scheme 2-1. Visible-light-induced malate production from pyruvate and CO_2 *via* oxaloacetate with the system consisted of an electron donor (ED), a photosensitizer (PS), MV, ferredoxin-$NADP^+$ reductase (FNR), $NADP^+$ and ME (System 1), and the simplified system using an electron mediator PV (System 2).

2.2 Experimental

2.2.1 Materials

Tetraphenylporphyrin tetrasulfonate (H_2TPPS) was purchased from Dojindo Laboratories (Kumamoto, Japan). Triethanolamine (TEOA), zinc acetate dihydrate, and methanol, acetonitrile, sodium sulfanilate dihydrate, and sodium hydrosulfite were purchased from FUJIFILM Wako Pure Chemical Corporation (Osaka, Japan). 4,4'-Bipyridyl, 1-chloro-2,4-dinitrobenzene, 1,1'-bis(2,4-dinitrophenyl)-4,4'-bipyridinium dichloride, PV, and MV were obtained from Tokyo Chemical Industry Co., Ltd. (Tokyo, Japan). 4-(2-Hydroxyethyl)-1-piperazineethanesulfonic acid (HEPES) was purchased from NACALAI TESQUE, INC. (Kyoto, Japan). ME derived from chicken liver (EC 1.1.1.40) was obtained from Sigma-Aldrich Co. LLC. The oxidized form of β-nicotinamide adenine dinucleotide (NAD^+) was purchased from Oriental Yeast Co., Ltd. (Tokyo, Japan). All other materials were of analytical grade or the highest grade available and used as received without further purification. Ar gas of ultrahigh purity (≧99.9999 %, Grade 1) was supplied by TAIYO NIPPON SANSO CORPORATION (Toyko, Japan). Water was purified using a Milli-Q purification system (18.2 M Ω cm @ 25 °C).

Zinc tetraphenylporphyrin tetrasulfonate (ZnTPPS) was synthesized by refluxing H_2TPPS with about three times the molar equivalent of zinc acetate dihydrate in 150 mL of methanol at 50 ℃ for 3 h according to the previously reported method, as shown in Scheme 2-2.[43,44]

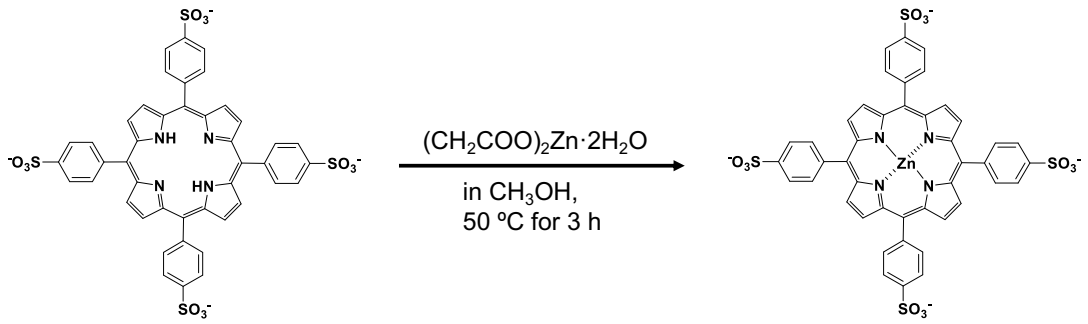

Scheme 2-2. Synthesis root of zinc tetraphenylporphyrin tetrasulfonate (ZnTPPS).

2.2.2 Preparation of water-soluble diphenylviologen derivaives

1,1,'-Bis(*p*-sulfonatophenyl)-4,4'-bipyridinium dichloride (PSV)

The synthesis route of PSV is summarized in Scheme 2-3. First, 1,1'-bis(2,4-dinitrophenyl)-4,4'-bipyridinium dichloride was synthesized according to a published procedure.[45] 4,4'-Bipyridyl (1.6 g, 10 mmol) and 1-chloro-2,4-dinitrobenzene (7.1 g, 35 mmol) were dissolved in anhydrous acetonitrile (30 mL), and the solution was stirred at 90 °C for 72 h under reflux. After cooling to room temperature, the mixture was diluted with acetonitrile and filtered to obtain a yellow-white solid, which was dried under vacuum overnight. Next, PSV was synthesized according to the previously reported method[46,47] with modifications, as follows. 1,1'-Bis(2,4-dinitrophenyl)-4,4'-bipyridinium dichloride (1.1 g, 2.0 mmol) was dissolved in distilled water (40 mL), and a solution of sodium sulfanilate dihydrate (2.1 g, 9.0 mmol) in distilled water (50 mL) was added dropwise. The mixture was stirred at 20 °C for 24 hours and refluxed at 80 °C for 48 h. The red solution was evaporated to obtain a dark red solid (PSV).

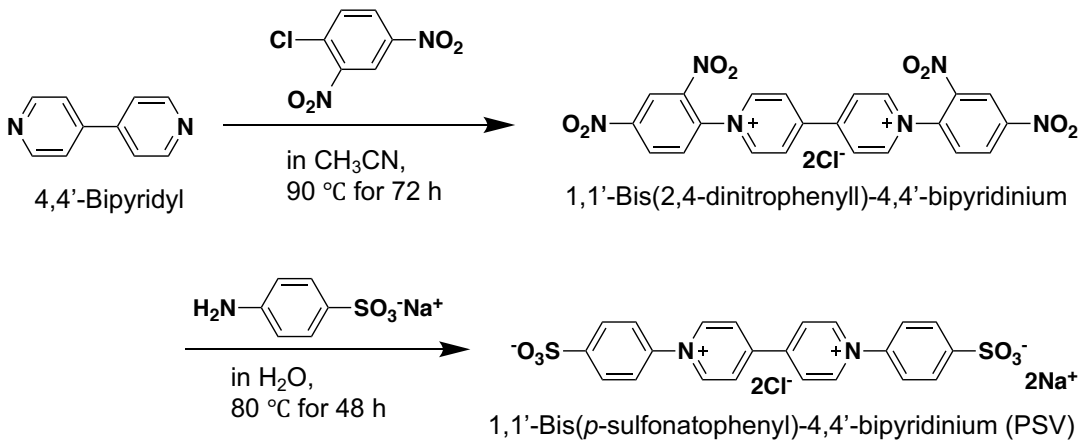

Scheme 2-3. Synthesis scheme of 1,1'-bis(*p*-sulfonatophenyl)-4,4'-bipyridinium dichloride (PSV).

1,1'-Bis(*p*-carboxyphenyl)-4,4'-bipyridinium dichloride (PCV)

The synthesis route of PCV is summarized in Scheme 2-4. The following procedure was carried out.[46-48] 1,1'-Bis(2,4-dinitrophenyl)-4,4'-bipyridinium dichloride (1.1 g, 2.0 mmol) was dissolved in ethanol (40 mL), and a solution of 4-

aminobenzoic acid (2.3 g, 9.0 mmol) in ethanol (50 mL) was added dropwise. The mixture was refluxed at 80 °C and then cooled at room temperature. The red solution was evaporated to obtain PCV as a dark red solid.

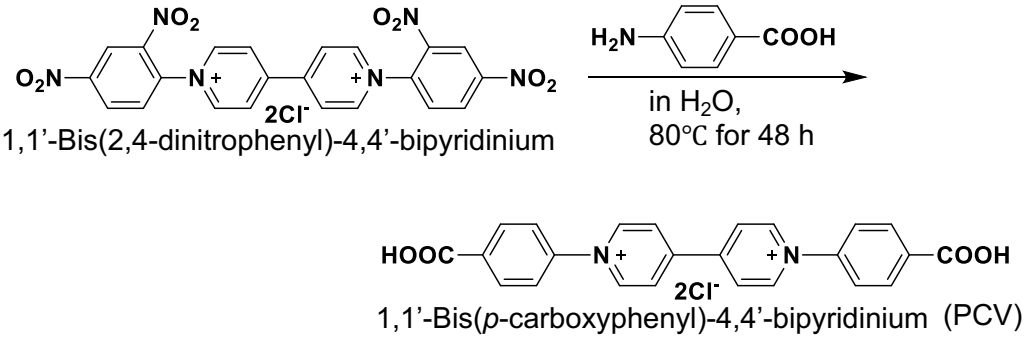

Scheme 2-4. Synthesis scheme of 1,1'-bis(*p*-carboxyphenyl)-4,4'-bipyridinium dichloride (PCV).

2.2.3 Fluorescence quenching behavior of ZnTPPS by PV derivatives

Quenching of the photoexcited state of ZnTPPS by PV derivatives (PV and PSV) was investigated using steady-state fluorescence spectroscopy. The sample solution contained ZnTPPS (0.5 μM) and PV derivatives in 10 mM Bis-tris buffer (pH 7.4). The excitation wavelength was 422 nm owing to the Soret band of ZnTPPS. The fluorescence intensity of ZnTPPS in the presence of the PV derivative was measured using a fluorescence spectrophotometer (SHIMADZU, RF-5300PC). In addition, quenching of the photoexcited state of ZnTPPS by MV was analyzed as a reference.

2.2.4 Reduction potential measurement of PV derivatives

To determine the electrochemical properties of the PV derivatives, their reduction potentials were measured using cyclic voltammetry (HOKUTO DENKO HZ-3000) with a glassy carbon electrode as the working electrode, platinum as the

counter electrode, and Ag/AgCl as the reference electrode. The electrolyte solution was nitrogen-saturated 0.2 M KCl solution. The scan rate was adjusted to 100 mV min^{-1}. In addition, the reduction potentials of MV were also measured as a reference.

2.2.5 Spectroscopic properties of the reduced form of water-soluble PV derivatives

The optical properties of single- and double-electron-reduced PSV ($PSV^{\bullet+}$ and PSV^{0}) and PCV ($PCV^{\bullet+}$ and PCV^{0}) were investigated by measuring the UV–Vis absorption spectra. The single- and double-electron-reduced form of the water-soluble PV derivatives were prepared as follows. PSV or PCV solution was prepared using Bis-tris buffer (pH 7.4) in the cell, and 2 mM of sodium hydrosulfite was added to the sample solution. Then, double-electron-reduced PSV was produced and oxidized to single-electron-reduced PSV by oxygen. The single- and double-electron-reduced forms of PSV and PCV were detected using UV–Vis absorption spectroscopy (SHIMADZU, MultiSpec-1500).

2.2.6 Photoreduction of PV derivatives by photosensitization of ZnTPPS

The sample solution contained TEOA (0.3 M), ZnTPPS (10 μM), and PV derivative (0.1 mM) in 5.0 mL of 10 mM Bis-tris buffer (pH 7.4). The sample solution was deaerated by repeating freeze–pump–thaw cycles six times and then irradiated with a 250 W halogen lamp (TOSHIBA) having a light intensity of 200 J m^{-2} s^{-1}; wavelengths under 390 nm were blocked with a cut-off filter at 30 ℃. Production of the reduced form of the PV derivative was monitored using UV–Vis absorption spectroscopy. An outline of the steady-state irradiation system is shown in Fig. 2-3.

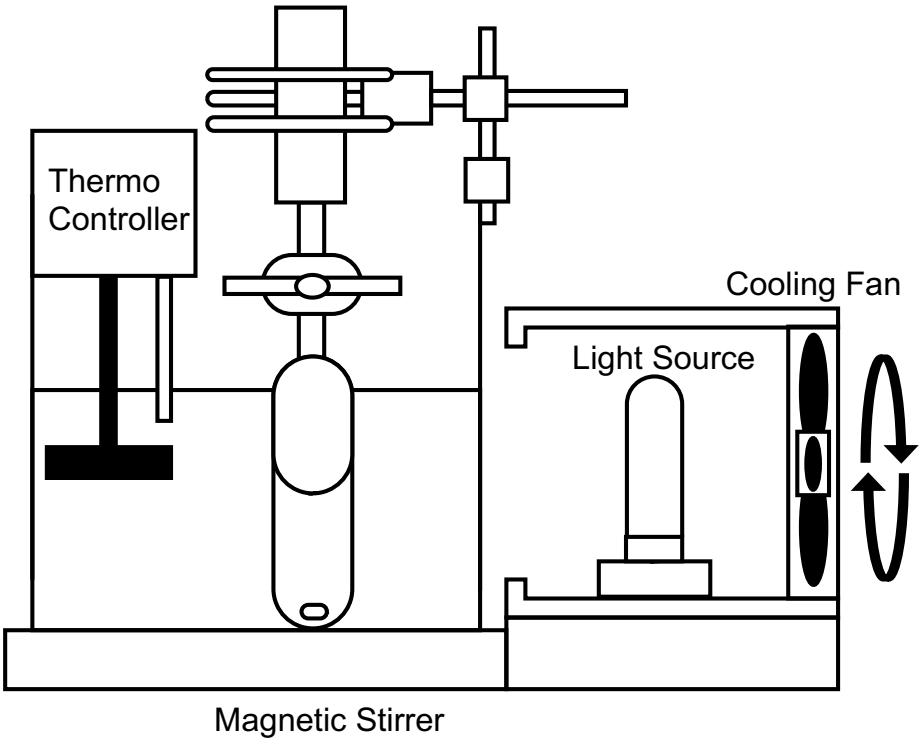

Fig. 2-3. Outline of steady state irradiation system.

2.2.7 Photoinduced malate production from CO_2 and pyruvate with ME and PV derivatives

Visible-light-induced malate production from CO_2 and pyruvate with H_2TPPS, PV, and ME in the presence of co-factor Mg^{2+} was carried out as follows. A sample solution containing TEOA (0.2 M), H_2TPPS (40 μM), PV derivative (0.4 mM), sodium pyruvate (12 mM), $MgCl_2$ (10 mM), and ME (0.95 μM; 4.0 U) in 5 mL of 10 mM Bis-tris buffer (pH 7.4) was deaerated by repeating freeze–pump–thaw cycles six times and then flushing with CO_2 gas for 10 min. The sample solution in the cell equipped with a magnetic stirrer was irradiated with visible light from a 250 W halogen lamp with a light intensity of 200 J m^{-2} s^{-1} at 30 ºC. UV rays with wavelengths shorter than 390 nm were blocked with a cut-off filter. The concentrations of oxaloacetate and malate were detected using an ionic chromatography system (Thermo Fisher Scientific, Dionex IC-1100). Since zinc

acetate was added in excess for the ZnTPPS synthesis, traces of zinc ion remained in the visible-light-induced malate synthesis. Zinc ion is divalent, which affects the activity of the ME,[49] so metal-free porphyrin (H_2TPPS) with a similar photosensitization activity to that of ZnTPPS was used as a photosensitizer. UV–Vis absorption spectroscopy confirmed that Mg^{2+} in this condition is not coordinated to H_2TPPS.

2.2.8 Function of PV derivative for the malate oxidation with ME

The function of the oxidized form of the PV derivative PCV for ME in the malate oxidation was investigated. The sample solution contained PCV (0.2 mM), $MgCl_2$ (1.0 mM), and sodium malate (1.2 mM) in 10 mL of HEPES-NaOH buffer (pH 7.4). The solution was deaerated over six freeze–pump–thaw cycles and sealed with argon gas. Then, the reaction was initiated by injecting ME (0.95 μM; 4U). The concentration of $PCV^{\bullet+}$ or PCV^0 produced was determined by the absorbance change.

The malate oxidation using NADPH as a coenzyme of ME was also investigated. The amount of NADPH produced was estimated from the absorbance of NADPH at 340 nm and the absorption coefficient, $\varepsilon_{340} = 6.2 \times 10^3\ M^{-1}\ cm^{-1}$.[50,51]

2.2.9 Function of multi-electron reduced PV derivative for the oxaloacetate production with ME in the presence of pyruvate and bicarbonate

The sample solution contained sodium pyruvate (1.2 mM), sodium bicarbonate (1.2 mM) as a CO_2 source, $MgCl_2$ (1.0 mM), ME (0.95 μM) from chicken liver, and PCV dissolved in a pH 7.4 solution of 10 mM HEPES-NaOH buffer. In this reaction, sodium dithionite (1.1 mM) was used as a reducing reagent for PCV, which was fully reduced to PCV^0, as confirmed by the UV–Vis absorption spectrum. The solution was deaerated by performing six freeze–pump–thaw cycles and then sealed with argon gas. The reaction was initiated by injecting ME into the vessel. The oxaloacetate concentration was determined using an ionic chromatography system

(Thermo Fisher Scientific, Dionex IC-1100). Lowering of the pH by adding sodium dithionite was suppressed using a pH 7.4 HEPES-NaOH buffer solution, indicating that ME was stably maintained in the sodium-dithionite-saturated solution. As the concentration of oxaloacetate increased linearly over the 5 min incubation period, the initial rate was determined by the linear gradient in the relationship between incubation time and the concentration of the produced oxaloacetate.

2.2.10 Oxaloacetate production using 1-methyl-4,4-bipyridiniumu salt with ME in the presence of pyruvate and bicarbonate

Oxaloacetate production using the 1-methyl-4,4'-bipyridinium salt (Fig. 2-4) has a 4,4,'-bipyridine skeleton and retains the lone electron pair on the nitrogen atom was investigated. A sample solution containing sodium pyruvate (1.2 mM), sodium bicarbonate (1.2 mM), $MgCl_2$ (1.0 mM), and 1-methyl-4,4'-bipyridinium iodide (0.2 mM) was prepared in 10 mM HEPES-NaOH buffer (pH 7.4). ME (0.95 μM; 4 U) was added to the sample solution to initiate the conversion of CO_2–pyruvate to oxaloacetate. The concentration of oxaloacetate produced was determined using an ionic chromatography system (Thermo Fisher Scientific, Dionex IC-1100).

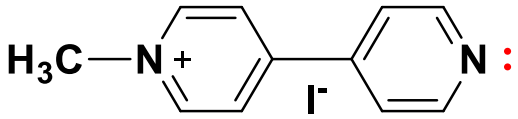

Fig. 2-4. The chemical structure of 1-methyl-4,4’-bipyridinium iodide.

2.3 Results and Discussion

2.3.1 Synthesis of 1,1'-bis(*p*-carboxyphenyl)-4,4'-bipyridinium dichloride (PCV) and ZnTPPS

The purity of the prepared PCV was determined using proton nuclear magnetic resonance spectroscopy (^{1}H-NMR; JEOL JNM-ECZ400S). ^{1}H-NMR in D_2O: δ (ppm) 7.83 (d, 4H), 8.20 (d, 4H), 8.71 (d, 4H), and 9.35 (d, 4H). The chemical shifts were referenced to the solvent peak calibrated against tetramethylsilane (TMS).

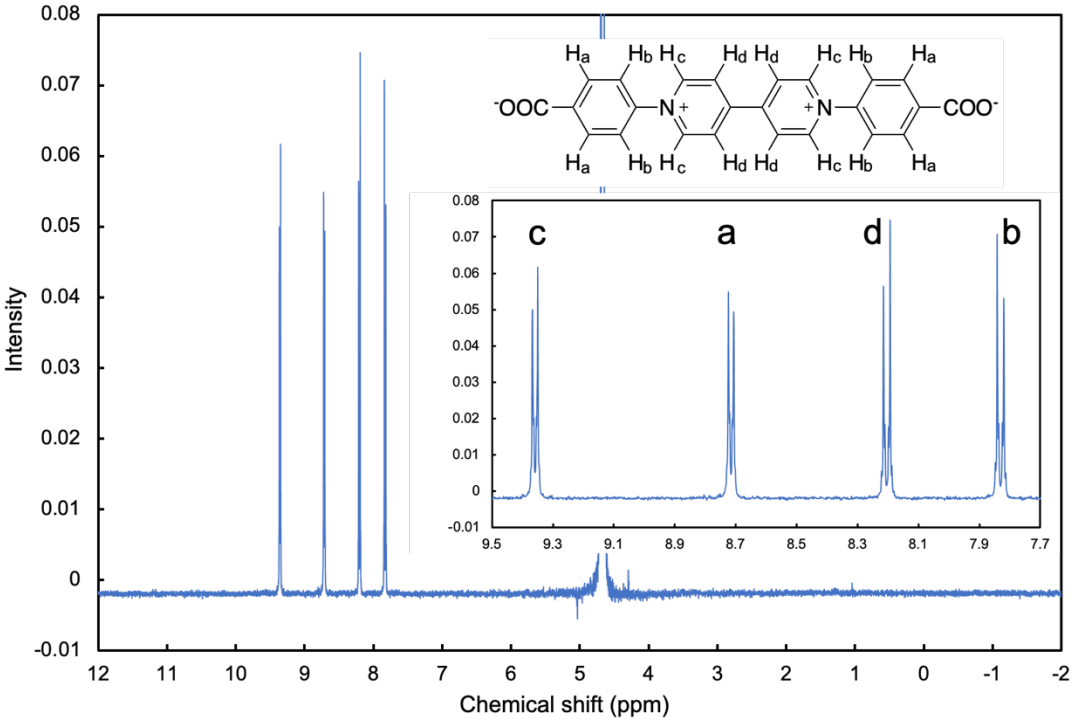

Fig. 2-5. ^{1}H-NMR spectrum of PCV in D_2O.

The absorption spectra of H_2TPPS and ZnTPPS are shown in Fig. 2-6. By coordination of zinc ion to H_2TPPS, the absorption peak at 414 nm based on the Soret band of the porphyrin was shifted to 422 nm. In addition, the four absorption peaks based on the Q band of the porphyrin transformed into two absorption peaks because the porphyrin became more symmetrical by the coordination of zinc ions.

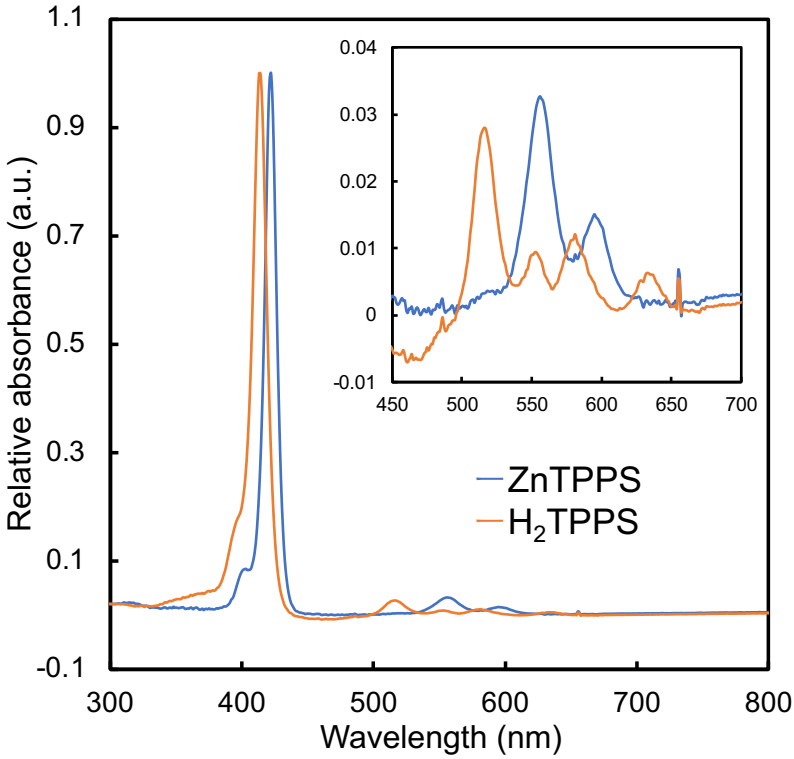

Fig. 2-6. Absorption spectra of H_2TPPS and ZnTPPS in 10 mM Bis-tris buffer (pH 7.4). H_2TPPS (—, orange), ZnTPPS (—, blue).

2.3.2 Fluorescence quenching behavior of ZnTPPS by PV derivatives

The interactions between ZnTPPS and PV derivatives were studied by measuring the fluorescence of ZnTPPS in the presence of PV, PSV, or PCV. The fluorescence quenching behavior of the excited singlet state of ZnTPPS by PV derivatives was studied, and the spectral changes of ZnTPPS according to MV, PV, and PSV concentration are shown in Fig. 2-7, Fig. 2-8, and Fig. 2-9, respectively. The fluorescence maximum of the ZnTPPS at 606 and 656 nm decreased with increasing viologen concentration. The fluorescence from the excited singlet state of ZnTPPS was quenched by viologen.

Fig. 2-10 shows the relative fluorescence intensity change according to MV and PV derivative concentration (Stern-Volmer plot[52,53]), where

$$\frac{I_0}{I} = 1 + K_{SV}[Q]$$

In this equation, I_0 and I are the fluorescence intensities in the absence and presence of Q, respectively; K_{SV} is the Stern–Volmer quenching constant (M^{-1}); and [Q] is the quencher concentration (M^{-1}). The K_{SV} value is obtained from the slope of the line for the plot of I_0/I vs. [Q]. The K_{SV} values of MV, PV, and PSV toward ZnTPPS were determined to be 12×10^4, 8.3×10^4, and 4.9×10^3 L mol^{-1}, respectively. Since the K_{SV} values of PV and MV are close, it can be inferred that the interaction between ZnTPPS and PV is similar to that between ZnTPPS and MV. In general, when a linear correlation with a positive K_{SV} value is observed in the Stern–Volmer plot, intermolecular quenching is occurring, indicating energy transfer from the excited state of ZnTPPS to PV.[54] Kaneko et al.[55] reported that the electron transfer from the photoexcited state of ZnTPPS to MV proceeded by a static mechanism owing to the electrostatic effect between ZnTPPS and MV. The fluorescence intensity of ZnTPPS

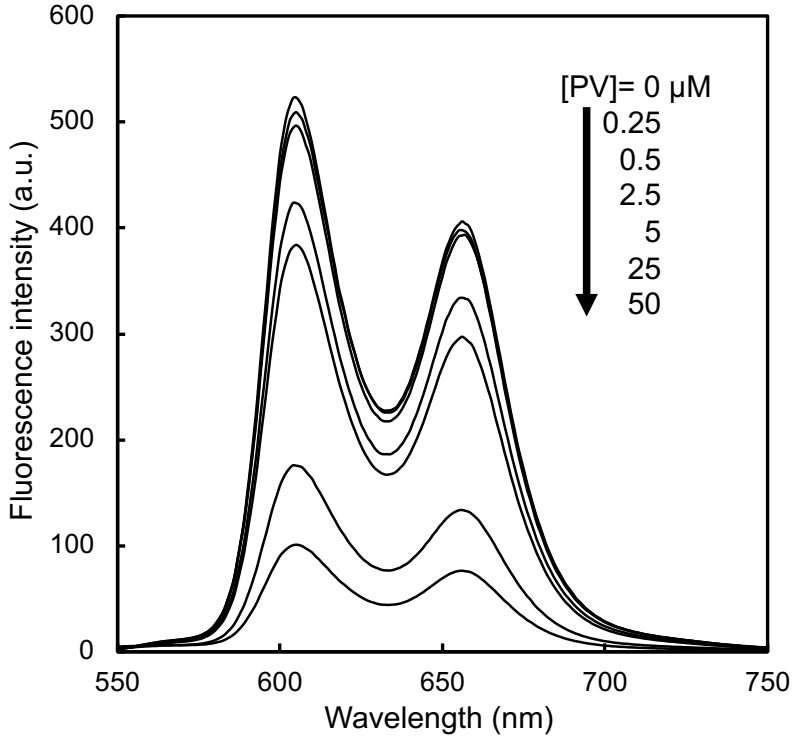

Fig. 2-7. Fluorescence spectral changes of ZnTPPS with addition of PV. The sample solution contained ZnTPPS (0.5 μM) and PV in Bis-tris buffer (pH 7.4). The excitation wavelength was 422 nm.

was decreased by the MV, but the lifetime of the photoexcited singlet state of ZnTPPS (^{1}ZnTPPS*) was not changed by MV. This indicates that the electron transfer from the photoexcited single state of ZnTPPS (^{1}ZnTPPS*) to MV did not occur. In addition, Amao et al.[56] found that electron transfer occurred from the photoexcited triplet state of ZnTPPS (^{3}ZnTPPS*) to MV by measuring the lifetime of the photoexcited triplet state of ZnTPPS (^{3}ZnTPPS*). Therefore, it can be considered that electron transfer from the excited triplet state of ZnTPPS (^{3}ZnTPPS*) to PV also occurred.

The K_{SV} value of PSV was smaller than that of PV. As an anion containing sulfonato groups, PSV is electrostatically repelled by the sulfonato groups of ZnTPPS. This interaction between ZnTPPS and PSV was smaller than that between ZnTPPS and PV.

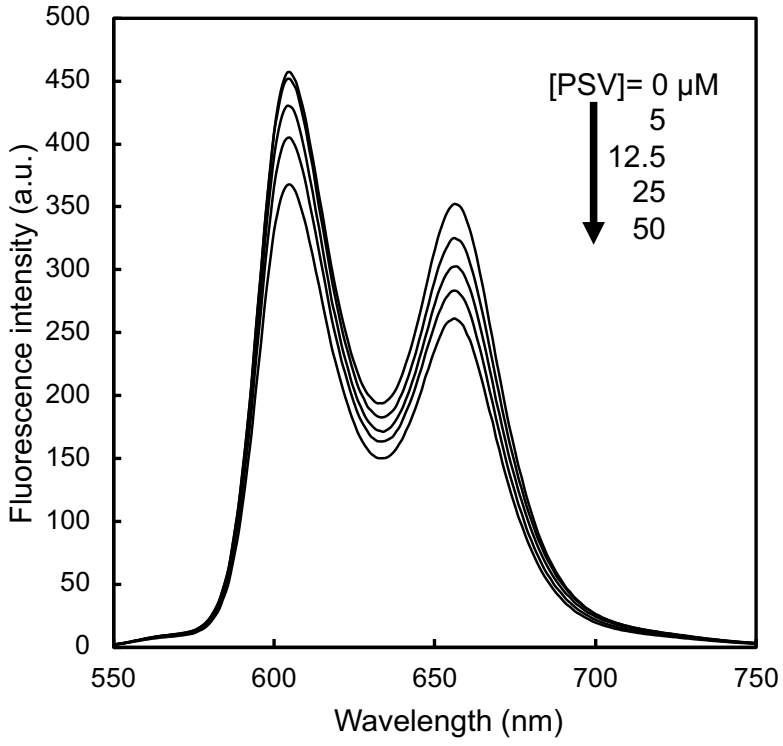

Fig. 2-8. Fluorescence spectral changes of ZnTPPS with addition of PSV. The sample solution contained ZnTPPS (0.5 μM) and PSV in Bis-tris buffer (pH 7.4). The excitation wavelength was 422 nm.

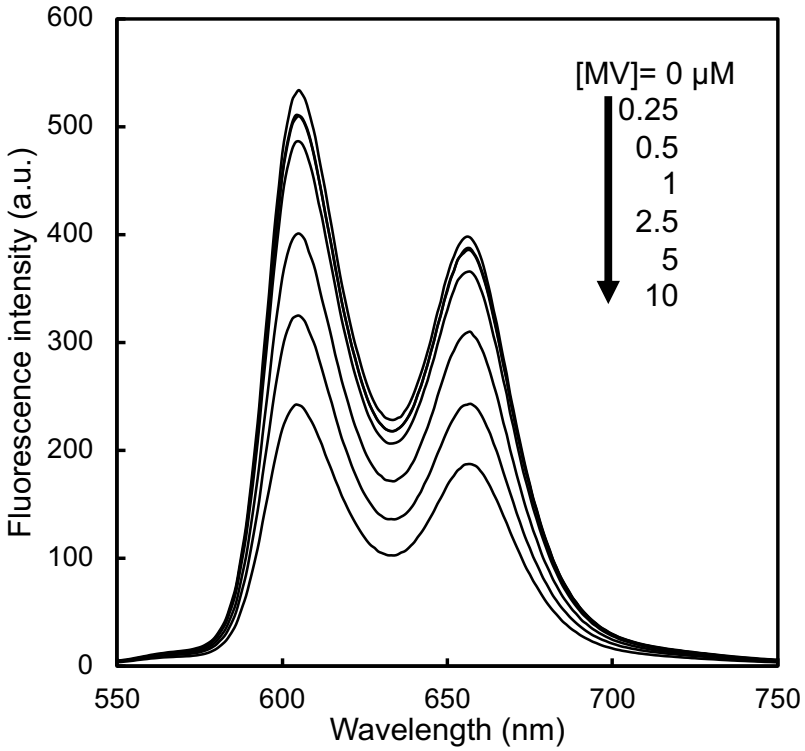

Fig. 2-9. Fluorescence spectral changes of ZnTPPS with addition of MV. The sample solution cintained of ZnTPPS (0.5 μM) and MV in Bis-tris buffer (pH 7.4). The excitation wavelength was 422 nm.

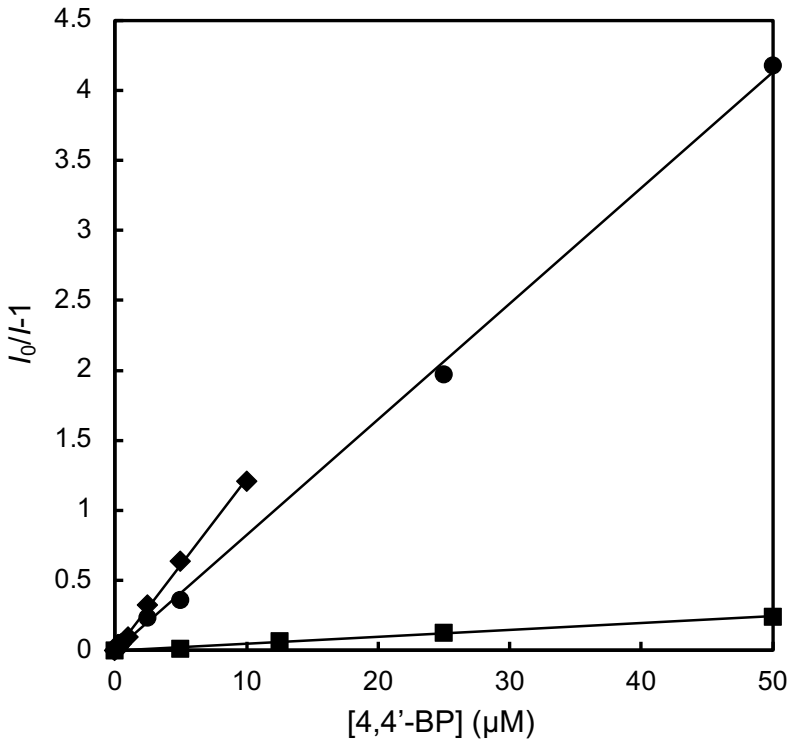

Fig. 2-10. Stern-Volmer plot for the fluorescence quenching of ZnTPPS by PV^{2+} (●), PSV^{2+} (■), and MV^{2+} (◆). The excitation and fluorescence wavelengths were 422 and 606 nm, respectively.

2.3.3 Reduction potentials for PV derivatives

The reduction potentials of MV and PV derivatives are listed in Table 2-1. The first and second reduction potentials were determined using cyclic voltammetry with Ag/AgCl as a reference electrode. The first and second reduction potentials of MV, widely used as an electron mediator, were estimated to be –0.65 and –1.08 V, respectively. On the other hand, the first and second reduction potentials of PV were estimated to be –0.39 and –0.74 V, respectively. The reduction potentials of PV were shifted in the positive direction compared with those of MV. This is because phenyl, an electron-withdrawing group, affected the redox potentials of 4,4'-bipyridinium salts (4,4'-BPs) owing to a decrease in the electron density of the bipyridine portion. On the other hand, the first and second reduction potentials of PSV were estimated to be –0.38 and –0.72 V, respectively. Compared to the reduction potential differences

between PV and MV, there is little difference between those of PV and PSV. The results indicate that the sulfonato group has little effect on the reduction potential in PV. Similarly, the first and second reduction potentials of PCV were estimated to be –0.38 and –0.70 V, respectively. Therefore, it is considered that the carboxy group bonded to the phenyl group also has a minor effect on the reduction potential in 4,4-BP. The effect of the phenyl group on the reduction potential is dominant.

In addition, the reduction efficiency of 4,4'-BPs with photosensitization of ZnTPPS depends on the reduction potential of 4,4'-BPs.[57] The redox potential of ^{3}ZnTPPS*, E(ZnTPPS$^+$/^{3}ZnTPPS*), was reported to be –0.75 (vs. Ag/AgCl).[58] Therefore, PV derivatives are reduced more readily by ZnTPPS than MV and are converted to their double-electron-reduced form (i.e., PV^{0}s).

PV$^{\bullet+}$, PSV$^{\bullet+}$, and PCV$^{\bullet+}$ were also expected to be able to reduce the carbonyl group in oxaloacetate to malate.

Table 2-1. Reduction potentials of 4,4'-BPs. (*vs* Ag/AgCl, 0.2 M KCl)

	E_{red1} (V)	E_{red2} (V)
MV	-0.65	-1.08
PV	-0.39	-0.72
PSV	-0.38	-0.72
PCV	-0.42	-0.70

The reduction potentials of 4,4'-BPs were measured by cyclic voltammetry with glassy carbon (GC) as a working electrode, Pt as a counter electrode, and Ag/AgCl as a reference electrode in 0.2 M KCl aqueous solution. The scan rate was adjusted to 100 mV min^{-1}.

2.3.4 Spectroscopic properties of the reduced form of water-soluble PV derivatives

The UV–Vis absorption spectra of single- and double-electron-reduced PSV (PSV$^{\bullet+}$ and PSV^0, respectively) are shown in Fig. 2-11. The absorbance baseline was the oxidized form of PSV, which produced a yellow solution. The chemical

structures of $PSV^{\bullet+}$ and PSV^{0} are also shown in Fig. 2-11. When the $PSV^{\bullet+}$ was formed, the color of the solution changed to dark orange and gave rise to an absorption band with a maximum of 490 nm. When PSV^{0} was produced, the solution color changed to green, which led to absorption bands with maxima of 590, 640, and 710 nm.

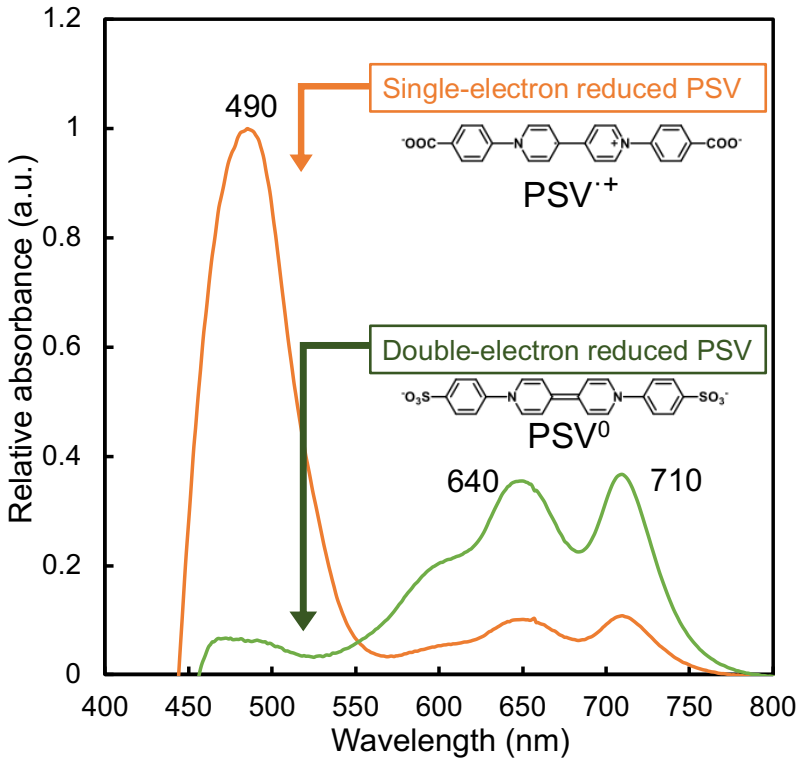

Fig. 2-11. UV-Vis absorption spectra of single-electron reduced PSV ($PSV^{\bullet+}$, orange) and double-electron reduced PSV (PSV^{0}, green).

In addition, the UV–Vis absorption spectra of single- and double-electron-reduced PCV ($PCV^{\bullet+}$ and PCV^{0}, respectively) are shown in Fig. 2-12. The absorbance baseline was a solution of the oxidized form of PCV. The chemical structures of $PCV^{\bullet+}$ and PCV^{0} are also shown in Fig. 2-12. The spectra show an absorption maximum for $PCV^{\bullet+}$ at 490 nm, and the maxima of of PCV^{0} are located at 600, 650, and 710 nm. The colors of $PCV^{\bullet+}$ and PCV^{0} in solution were orange and green, respectively; thus, $PCV^{\bullet+}$ and PCV^{0} differed significantly in their optical properties.

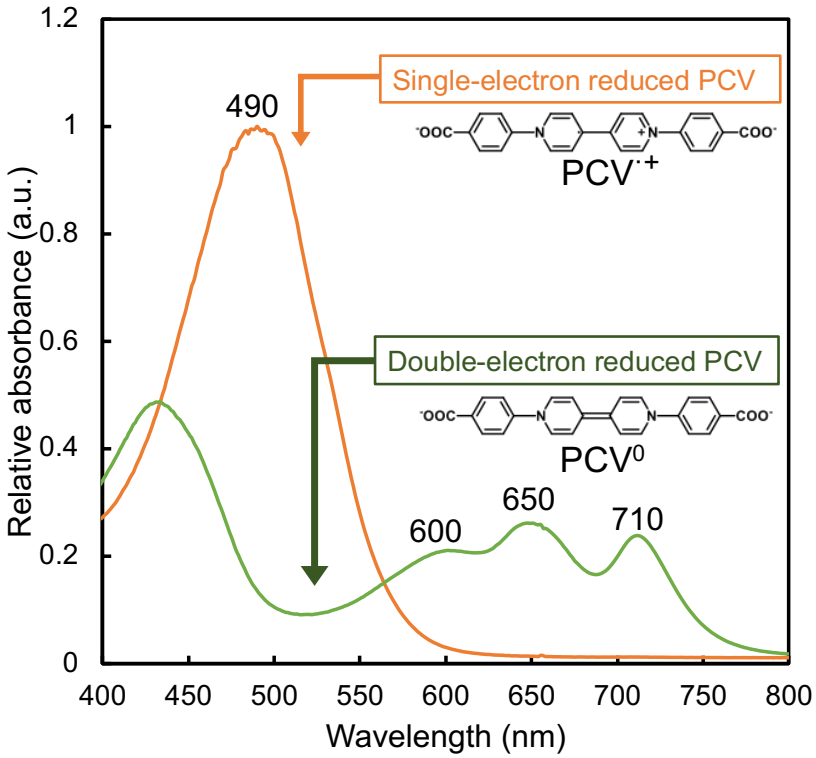

Fig. 2-12. UV-visible absorption spectra of single-electron reduced PCV ($PCV^{\bullet +}$, orange) and double-electron reduced PCV (PCV^{0}, green).

2.3.5 Photoreduction of PV derivatives with visible-light sensitization of ZnTPPS

The difference UV–Vis absorption spectra upon visible-light irradiation in a reaction system consisting of TEOA, ZnTPPS and, PV are shown in Fig. 2-13. The absorption bands at 610 and 710 nm based on the double-electron-reduced form of PV increased with irradiation time. The spectrum increased overall because part of the single- or double-electron-reduced form of PV was insoluble in aqueous media. The color of the sample solution changed to pale green in response to the formation of the double-electron-reduced form of PV. In this system, the photoinduced electron transfer from ^{3}ZnTPPS* to PV proceeded. The redox potentials of ^{3}ZnTPPS*, $E(ZnTPPS^{+}/^{3}ZnTPPS^{*})$, and $E(^{3}ZnTPPS^{*}/ZnTPPS^{-})$ were reported to be –0.75 and 0.45 V (vs. Ag/AgCl), respectively.[58] The first and second reduction potentials of PV

were estimated to be –0.39 and –0.74 V, respectively. The redox potential diagram of ZnTPPS and PV derivatives is shown in Fig. 2-16. The Gibbs free energy for the photoinduced electron transfer from ^{3}ZnTPPS* to PV to produce the double-electron-reduced form of PV was estimated to be –2.0 kJ mol^{-1}; thus, this is a thermodynamically feasible reaction. The oxidation potential of TEOA was reported to be 0.87 V (vs. Ag/AgCl).[59] Therefore, the single- and double-electron-reduced forms of PV were produced by photosensitization with ZnTPPS via the reductive-quenching process.

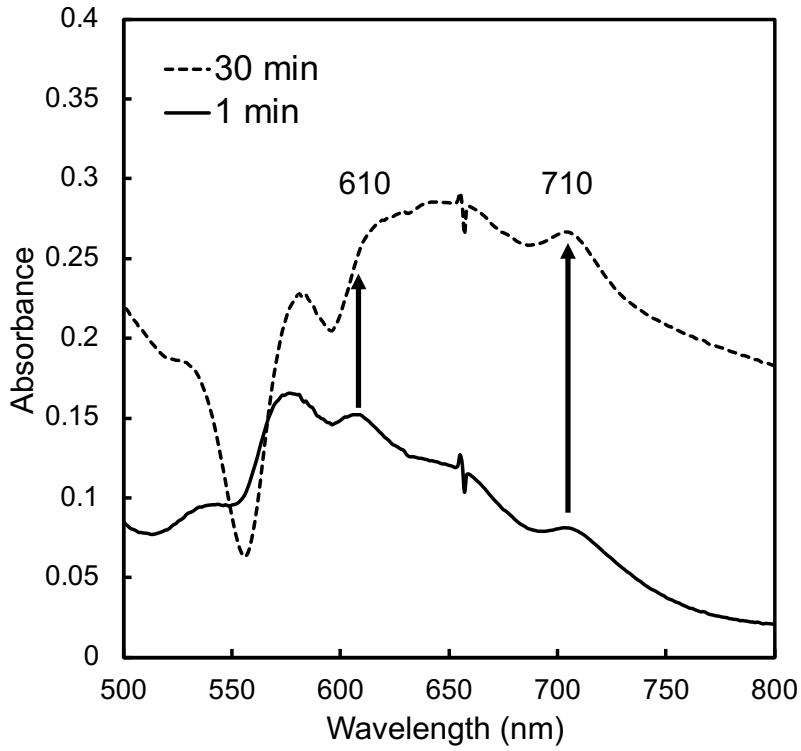

Fig. 2-13. Difference UV-Vis absorption spectral changes of the sample solution containing TEOA, ZnTPPS, and PV in Bis-tris buffer (pH 7.4) with visible-light irradiation time at 30 ℃.

Fig. 2-14 shows the difference UV–Vis spectral upon visible-light irradiation in a reaction system consisting of TEOA, ZnTPPS, and PSV. The absorption bands at 650 and 710 nm based on PSV^0 increased with irradiation time. The color of the sample solution changed to pale green owing to PSV^0 production. In

addition, no precipitation was observed, which is in contrast with the photoreduction of PV. This was due to the incorporation of the water-soluble sulfonato group from PV, which improved the solubility of PSV. The first and second reduction potentials of PSV were estimated to be –0.38 and –0.72 V, respectively. Thus, double-electron reduction of PSV to PSV^0 proceeded with visible-light sensitization of ZnTPPS in this system. The Gibbs free energy for the photoinduced electron transfer from ^{3}ZnTPPS* to PSV to produce the PSV^0 was estimated to be –5.8 kJ mol^{-1}; thus, this reaction is thermodynamically feasible. Therefore, $PSV^{\cdot+}$ and PSV^0 were produced by photosensitization with ZnTPPS via the reductive-quenching process. PSV is expected to function as an efficient electron mediator in aqueous solution.

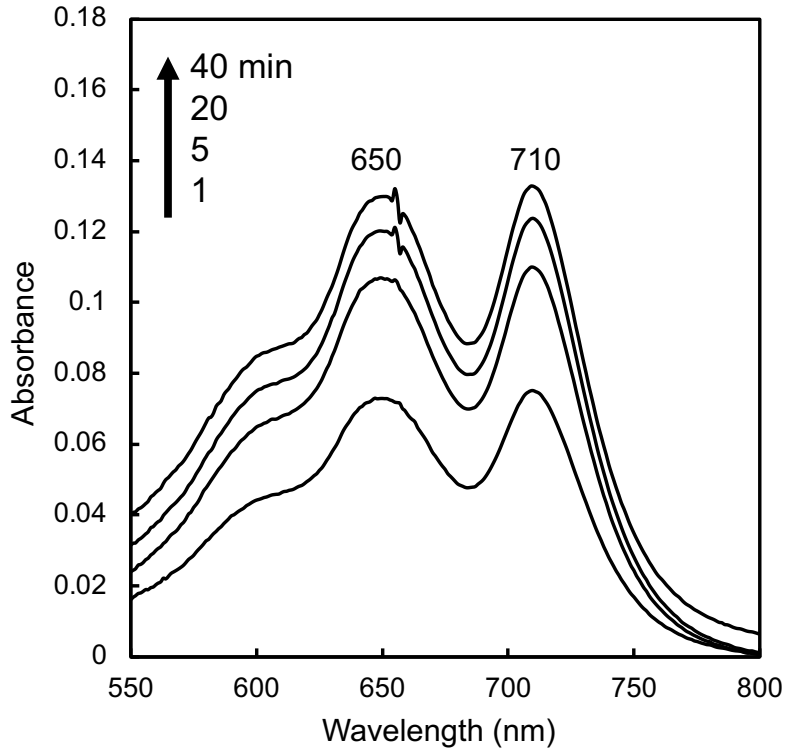

Fig. 2-14. Difference UV-Vis absorption spectral changes of the sample solution containing TEOA, ZnTPPS, and PSV in Bis-tris buffer (pH 7.4) with visible-light irradiation time at 30 ºC.

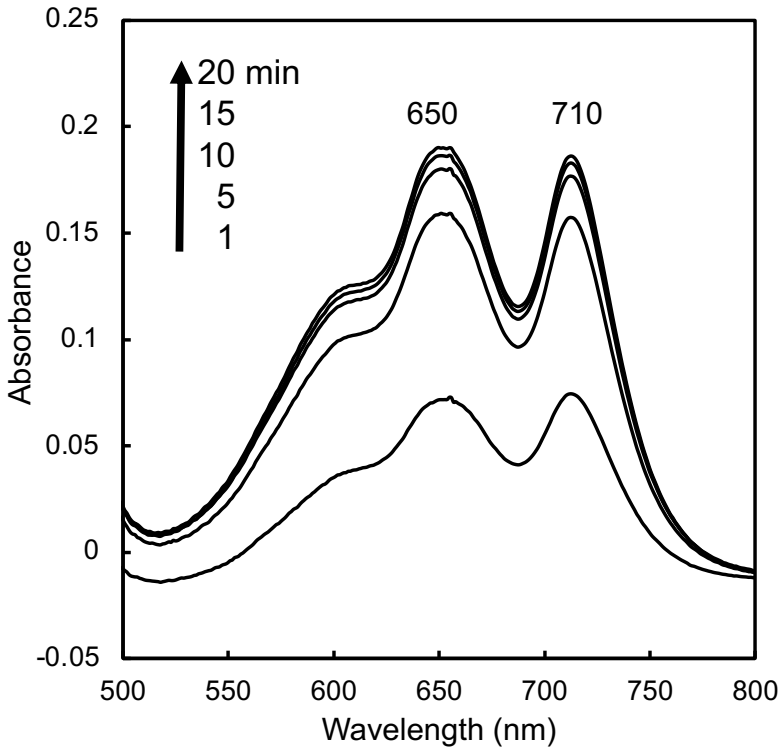

Fig. 2-15. Difference UV-Vis absorption spectral changes of the sample solution containing TEOA, ZnTPPS, and PCV in Bis-tris buffer (pH 7.4) with visible-light irradiation time at 30 ºC.

The difference UV–Vis absorption spectra after visible-light irradiation in a reaction system consisting of TEOA, ZnTPPS, and PCV are shown in Fig. 2-15. Similar to PV and PSV, PCV showed an increase in absorption for the PCV^0 species. This indicates that PCV was also reduced to double electrons by the photosensitization of ZnTPPS.

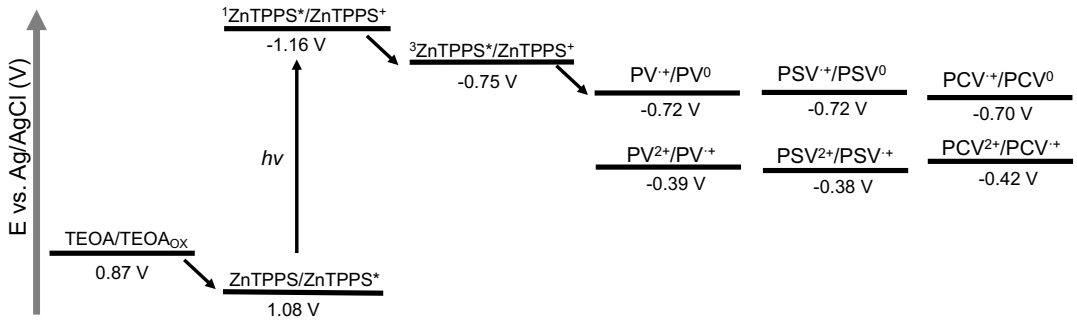

Fig. 2-16. The potential diagram of ZnTPPS and PV derivatives.

2.3.6 Visible-light-induced malate production from CO_2 and pyruvate with ZnTPPS, PV derivatives, and ME

When the sample solution containing TEOA, H_2TPPS, PV, pyruvate, ME, and Mg^{2+} in 5 mL of CO_2-saturated Bis-tris buffer (pH 7.4) was irradiated with a 250 W halogen lamp, oxaloacetate (■) and malate (●) were produced, as shown in Fig. 2-17. The concentrations of malate and oxaloacetate increased with irradiation time, where the former was estimated to be 565 μM after 3 h of irradiation. The conversion yield of pyruvate to malate was 4.7 %. In this system, the H_2TPPS, PSV, and ME turnover numbers (TONs) were estimated to be 4.7, 0.47, and 198 h^{-1}, respectively.

Fig. 2-18 shows the time dependence of oxaloacetate (■) and malate (●) production with the system consisting of CO_2 and pyruvate with TEOA, H_2TPPS, PSV, Mg^{2+}, and ME. When a sample solution containing TEOA, ZnTPPS, PSV, pyruvate, ME, and Mg^{2+} in CO_2-saturated Bis-tris buffer (pH 7.4) was irradiated, oxaloacetate and malate were produced, as shown in Fig. 2-18. In this system, the concentration of oxaloacetate increased during the first hour of irradiation, and then decreased. On the other hand, the concentration of malate increased with decreasing concentration of oxaloacetate. Oxaloacetate is formed as an intermediate, and malate is produced owing to oxaloacetate reduction. The malate concentration after 3 h of irradiation was estimated to be 604 μM. The conversion yield of pyruvate to malate was 5.0 %. In this system, the TONs of H_2TPPS, PSV, and ME were estimated to be 5.0, 0.50, and 216 h^{-1}, respectively. Significantly, the TON of ME was higher than those of H_2TPPS and PSV. Thus, catalytic production of malate from CO_2 and pyruvate proceeded.

The different shapes of the graph of oxaloacetate produced using PV vs. PSV are thought to be due to the difference in ionicity of the phenyl group of the side chain of the PV derivatives. The reaction to produce oxaloacetate from pyruvate and CO_2 is likely to involve the double-electron-reduced PV derivative. In other words, when PSV was used, the formation of oxaloacetate proceeded faster within the first hour than when PV was used owing to the presence of more double-electron-reduced PV derivatives.

In the absence of TEOA, ZnTPPS, PV or PSV, oxaloacetate, and malate were not observed with the system containing pyruvate, Mg^{2+}, and ME in CO_2-saturated Bis-tris buffer (pH 7.4) under visible-light irradiation. When the reaction mixture containing TEOA, ZnTPPS, PV or PSV, pyruvate, Mg^{2+}, and ME in CO_2-saturated Bis-tris (pH 7.4) buffer was reacted under dark conditions, neither oxaloacetate nor malate was produced. Thus, the single- and double-electron-reduced forms of PV and PSV are necessary to form oxaloacetate and malate.

It is presumed that the reduction of oxaloacetate to malate with ME proceeded with a couple of single-electron-reduced PV derivatives. This is because the double-electron-reduced viologen derivatives were less likely to release electrons, while the single-electron-reduced form of these was more likely to release an electron. The reduction potential of oxaloacetate/malate is –0.166 (vs. NHE). The Gibbs free energy for the oxaloacetate reduction with $PSV^{\bullet+}$ oxidation was estimated to be –79 kJ mol^{-1}, thus this process is thermodynamically feasible.

$Oxaloacetate + 2H^+ + 2e^- \rightarrow Malate$	$E_0' = -0.166$ V
$PSV^{2+} + e^- \rightarrow PSV^{\cdot+}$	$E_0' = -0.58$ V
$Oxaloacetate + 2H^+ + 2PSV^{\cdot+} \rightarrow Malate + 2PSV^{2+}$	$\Delta E_0' = -0.41$ V
	$\Delta G^0 = -79$ kJ mol^{-1}

On the other hand, in the system using MV, oxaloacetate and malate were not produced. By the photosensitization of ZnTPPS and H_2TPPS, only the single-electron reduced form of MV was produced.

From these results, it is presumed that CO_2 was introduced as a carboxy group into pyruvate to form oxaloacetate and then reduced to malate with single- or double-electron-reduced PV ($PV^{\cdot+}$ and PV^0, respectively) derivatives. Thus, it is presumed that single-electron-reduced 4,4'-BP is not involved in C–C bond formation. It is considered that C–C bond formation was promoted by the double-electron-reduced PV derivatives. The enol of pyruvate is needed for C–C bond formation based on introducing CO_2 with ME in the presence of natural coenzyme NADPH.[60,61] It is presumed that the double-electron-reduced form of PV is involved

in the keto–enol tautomerism of pyruvate. PSV^0 seems to act like a base and promotes the enolization of pyruvate with ME, while Mg^{2+} stabilizes the enolate intermediate. In addition, it is assumed that PSV^0 activates the C–H bond of pyruvate or CO_2 activation occurs to form oxaloacetate with ME.

From these results, a model for the reaction mechanism of ME is proposed in Fig. 2-19. It is considered that CO_2 was introduced as a carboxy group into pyruvate to form oxaloacetate with PSV^0 and was then reduced to malate with $PSV^{\bullet+}$. By using PSV, visible light efficiently induced C–C bond formation using CO_2 as a feedstock. Therefore, for the visible-light-induced oxaloacetate and malate production system from CO_2 and pyruvate, the reduced form of PV ($PV^{\bullet+}$, PV^0) is essential.

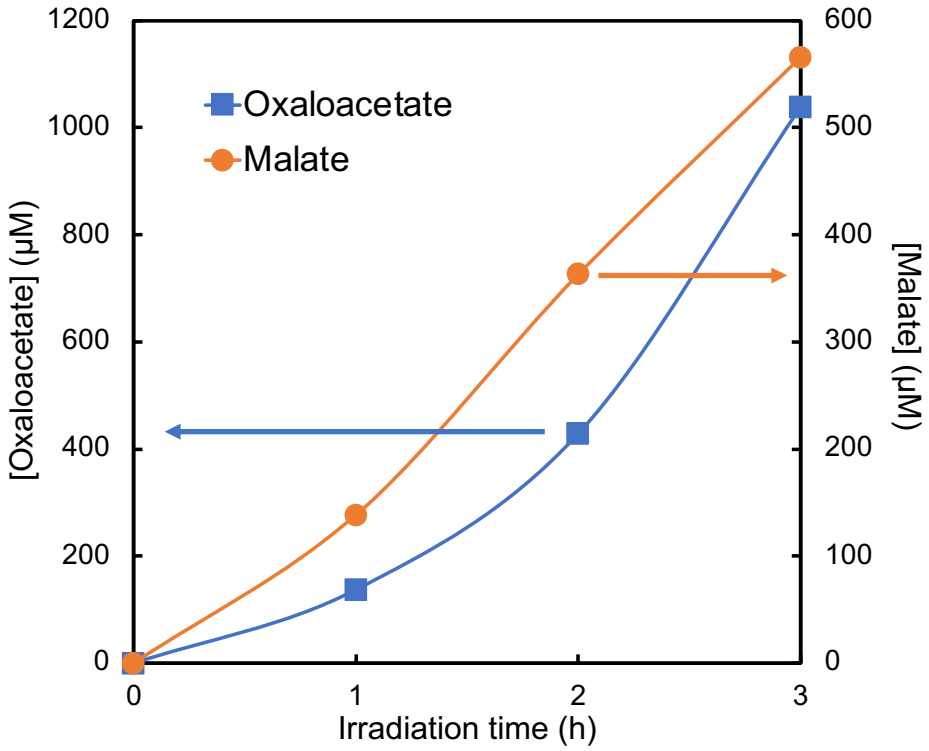

Fig. 2-17. Time dependence of visible-light-induced oxaloacetate (■) and malate (●) production in the solution containing TEOA, H_2TPPS, PV^{2+}, ME, pyruvate, and Mg^{2+} in a CO_2 saturated Bis-tris buffer (pH 7.4).

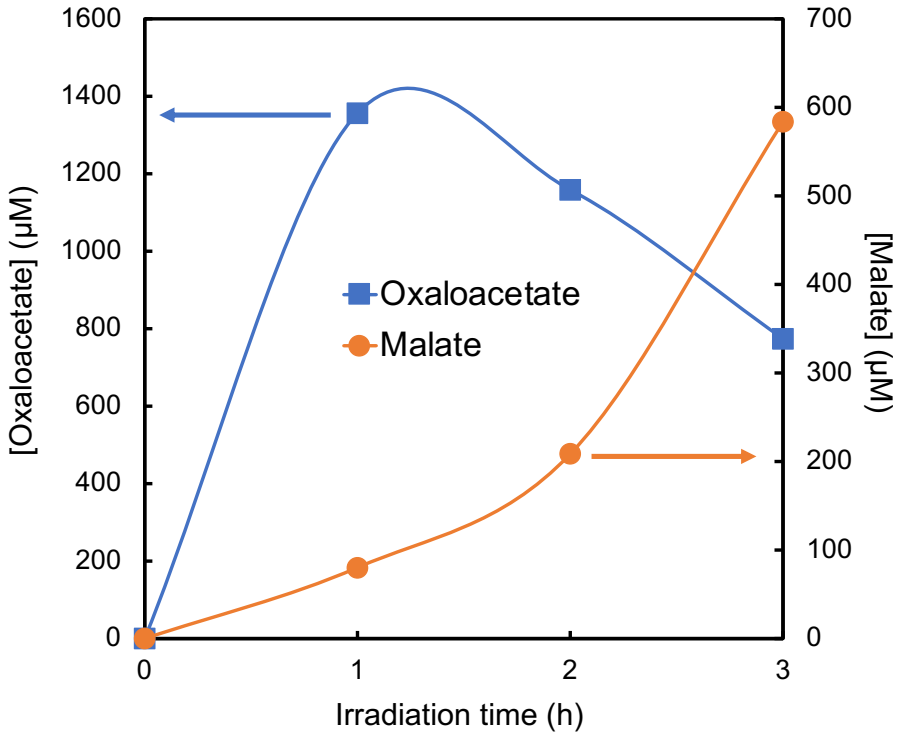

Fig. 2-18. Time dependence of visible-light-induced oxaloacetate (■) and malate (●) production in the solution containing TEOA, H_2TPPS, PSV^{2+}, ME, pyruvate, and Mg^{2+} in a CO_2 saturated Bis-tris buffer (pH 7.4).

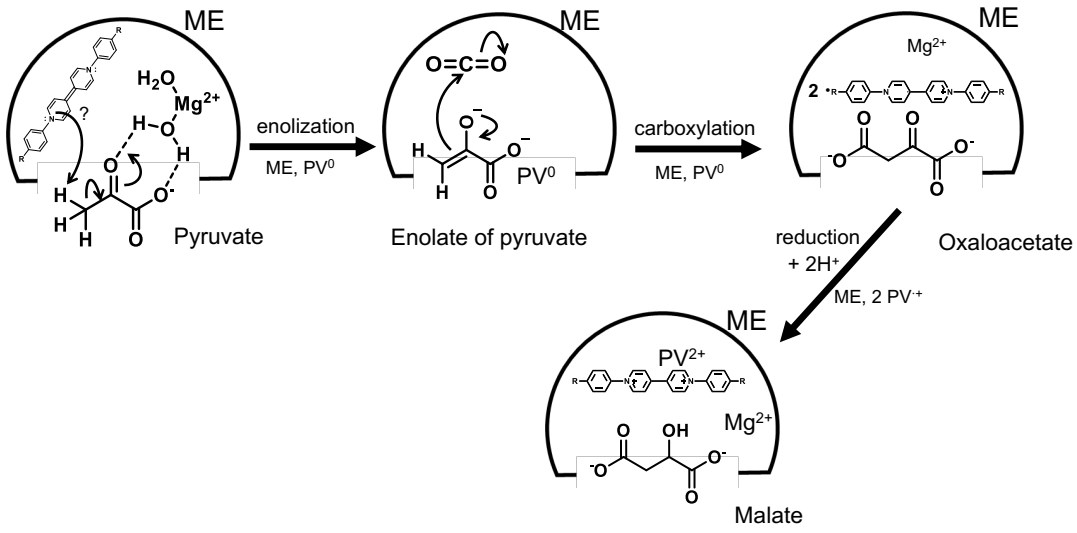

Fig. 2-19. Proposed mechanism for malate production from pyruvate and CO_2 with ME and multi-electron reduced PV derivative.

2.3.7 Function of the PV derivative for the malate oxidation with ME

Malate oxidation to oxaloacetate with ME and PCV^{2+} as an oxidized form of the PV derivative was studied. The time dependence of the reduced form of PCV and NADPH production is shown in Fig. 2-20. In the malate oxidation reaction using PCV^{2+}, the formation of the reduced forms of PCV ($PCV^{\bullet+}$ and PCV^{0}) was not observed owing to the reaction progress.

On the other hand, when $NADP^{+}$ was used as a coenzyme for ME, NADPH, the reduced form of $NADP^{+}$, was produced owing to the reaction progress. These results indicate that the oxidized form of PCV does not function as a cofactor for ME during malate oxidation.

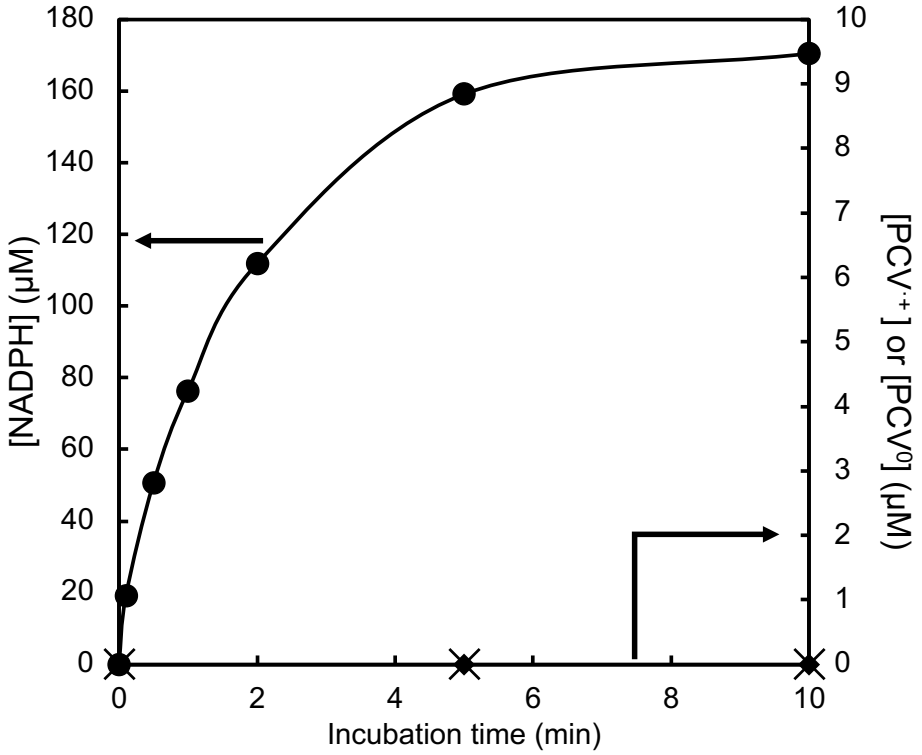

Fig. 2-20. The time dependence of the $PCV^{\cdot+}$ (◆), PCV^{0} (×) and NADPH (●) production. The sample solution including PCV^{2+} or $NADP^{+}$, malate and ME (0.95 μM; 4 U) in HEPES-NaOH buffer (pH 7.4).

2.3.8 Function of multi-electron reduced PV derivative for the oxaloacetate production with ME in the presence of pyruvate and bicarbonate

An enzyme kinetic analysis of the conversion of pyruvate and CO_2 to oxaloacetate was performed according to the following procedure. The sample solution contained pyruvate, bicarbonate as a CO_2 resource, and Mg^{2+} as a cofactor for ME and PCV in a solution of HEPES-NaOH buffer (pH 7.4). The Michaelis constant K_m of sodium bicarbonate for ME in the reaction system of pyruvate and NADPH was estimated to be 420 μM. When the concentration of pyruvate was increased in the reaction system, it was difficult to systematically detect the oxaloacetate using ion chromatography, so the concentration of pyruvate was adjusted to be 1.2 mM. Moreover, the parameters obtained from this analysis were all apparent constants. The kinetic parameters of oxaloacetate production with PCV^0 and ME in the presence of pyruvate and bicarbonate were determined using the Michaelis–Menten equation.

The relationship between the PCV^0 concentration and the initial rate of oxaloacetate produced (v_0) is shown in Fig. 2-21. The v_0 increased in a PCV^0 concentration-dependent manner up to 100 μM. The reaction wherein CO_2 was introduced into pyruvate using PCV^0 (until 100 μM) and ME followed Michaelis–Menten kinetics. In contrast, the v_0 was drastically reduced under the concentration of [PCV^0] > 150 μM in the solution. From these results, it is presumed that the substrate inhibition by PCV^0 (>150 μM) occurred in the oxaloacetate production with ME. Substrate inhibition occurs when the substrate concentration itself inhibits to the reaction. Inhibition models have been suggested by various researchers.[62–65] Among the inhibition models, the best-fitting curve was obtained by using Eq. 2-2, as reported by Haldane.[62]

$$v_0 = \frac{V_{max}[PCV^0]}{[PCV^0]+K_m+\frac{[PCV^0]^2}{K_i}} \quad \text{(Eq. 2-2)}$$

The kinetic parameter K_m, inhibitory constant K_i, maximum velocity (V_{max}), k_{cat}, and k_{cat}/K_m were determined using non-linear regression analysis with characterized

substrate inhibition using Eq. 2-2 of the v_0 and [PCV^0]. The obtained kinetic parameters are listed in Table 2-2. In general, the K_m value of NADPH for ME is reported to be 1.8 to 60 μM.[66,67] There was little difference in the K_m values of PCV^0 and NADPH for ME. Thus, it was suggested that PCV^0 plays the role of coenzyme for ME in the introduction of CO_2 to pyruvate to produce oxaloacetate. Ikeyama et al. previously reported that higher concentrations of the single-electron-reduced 4,4'-bipyridinium salt derivative inhibits biocatalytic activity.[68] There is a possibility that the deactivation of the catalytic activity of ME occurs with >150 μM of PCV^0 in oxaloacetate production. The carboxyl group of PCV^0 is in close proximity to the CO_2 or pyruvate binding site of ME. Therefore, it is predicted that the approach of CO_2 or pyruvate to the binding site in ME was hindered by the carboxyl group of PCV^0 under the higher PCV^0 concentrations.

From the oxaloacetate production with ME and PCV^0 at 100 μM before inhibition, the reduction in pyruvate and bicarbonate concentrations in the reaction was estimated to be 200 μM (1.2 to 1.0 mM). In addition, from the result of

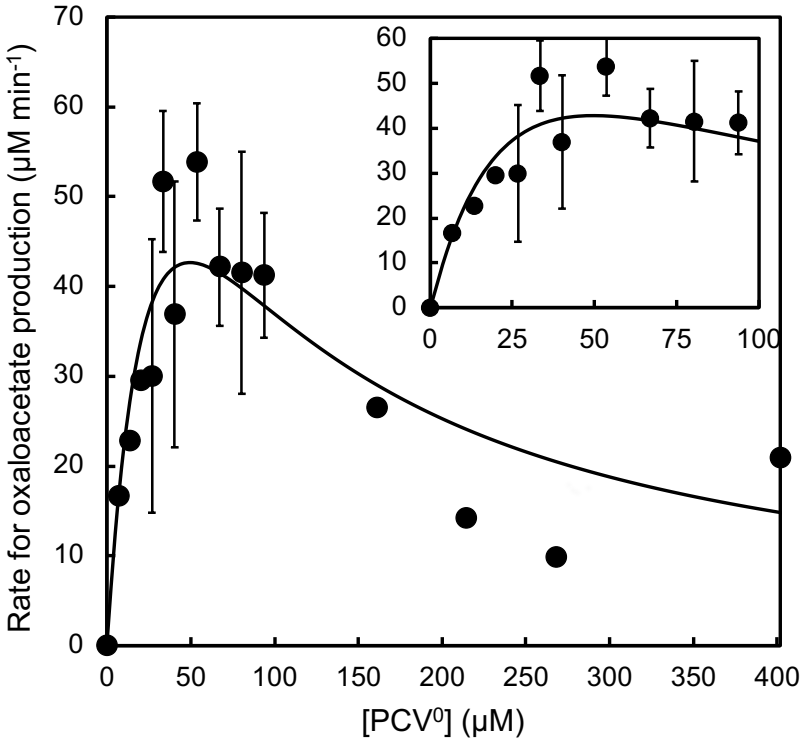

Fig. 2-21. Relationship between the concentration of PCV^0 and the initial rate (v_0) of oxaloacetate production.

bicarbonate concentration dependency in malate production with ME and NADPH, the reaction rate in the presence of 1.0 mM bicarbonate was only 5% lower compared with that of 1.2 mM bicarbonate, indicating that the reduction of bicarbonate concentration of this study had little effect on the reaction rate.

Table 2-2. Kinetic parameters for the reaction of introducing CO_2 to pyruvate with PCV^0 and ME

	V_{max} ($\mu M\ min^{-1}$)	K_m (μM)	K_i (μM)	k_{cat} (min^{-1})	k_{cat}/K_m ($M^{-1}\ min^{-1}$)
PCV^0	108	38	65	113	3.0×10^6

K_m : Micahelis constant, V_{max} : Maximum velocity, k_{cat} : Turnover number, k_{cat}/K_m : Catalytic efficiency. The kinetic parameters V_{max}, K_m and k_{cat} were determined by fitting to inhibition model by Haldane. The molecular weight of ME from chicken liver was estimated to be 5.6×10^4.[49]

In the absence of ME, no oxaloacetate production was observed, and by using PCV^0, no malate production was observed in this reaction system. In other words, the reduction of oxaloacetate to malate, attributed to two-electron and two-proton coupling reduction, did not proceed in the presence of PCV^0 only. The following two processes describe the mechanism for oxaloacetate production owing to the coupling of pyruvate and CO_2 with ME.

1) Tautomerization of the keto-form to the enolate intermediate of pyruvate

2) CO_2 bonded to the enolate intermediate of pyruvate to produce oxaloacetate

As these two processes are unrelated to the reductive reaction, oxaloacetate production should rely only on the catalytic activity of ME in the absence of NADPH. However, no oxaloacetate production with ME was observed in the absence of NADPH. When using PCV^0, no oxaloacetate production with ME was observed without using PCV^0 or $PCV^{\cdot+}$. From these results, PCV^0 acts as the catalyst for oxaloacetate production from pyruvate and CO_2. It was reported that 2,2'-bipyridine acts as a catalyst in the carboxylation process using CO_2, although a metal ion such as Ni or Mn is required.[69] Moreover, the visible-light-driven carboxylation of aryl

halides using a system including a Pd catalyst and Ir-complex-based photoredox catalyst has also been reported.[70] In this reaction, the activated electron mediator produced via the photoredox system acts as a substrate for the catalyst in the carboxylation process. The proposed mechanism for oxaloacetate production from pyruvate and CO_2 is shown in Fig. 2-22. For tautomerization of the keto form to the enolate intermediate of pyruvate to proceed, a base abstraction of the hydrogen-bonded α-carbon of the keto form of pyruvate is necessary. If the amino acid residue as a base in ME can abstract the hydrogen-bonded α-carbon of the enol-form of pyruvate, oxaloacetate will be produced without NADPH. However, no oxaloacetate production was observed. Thus, a coenzyme is needed as a base for this process. Careful scrutiny of the chemical structure of PCV^0 reveals that there are lone pairs on the two nitrogen atoms of PCV^0. Since PCV^0 acts as a base, the hydrogen bonded to the α-carbon of the keto form of pyruvate will be abstracted by PCV^0. No oxaloacetate production with ME was observed when using the oxidized form of PCV. Thus, the lone pairs on the four oxygen atoms of the two carboxy groups of PCV did not act as a base for abstraction of the hydrogen bonded to the α-carbon of the keto form of pyruvate.

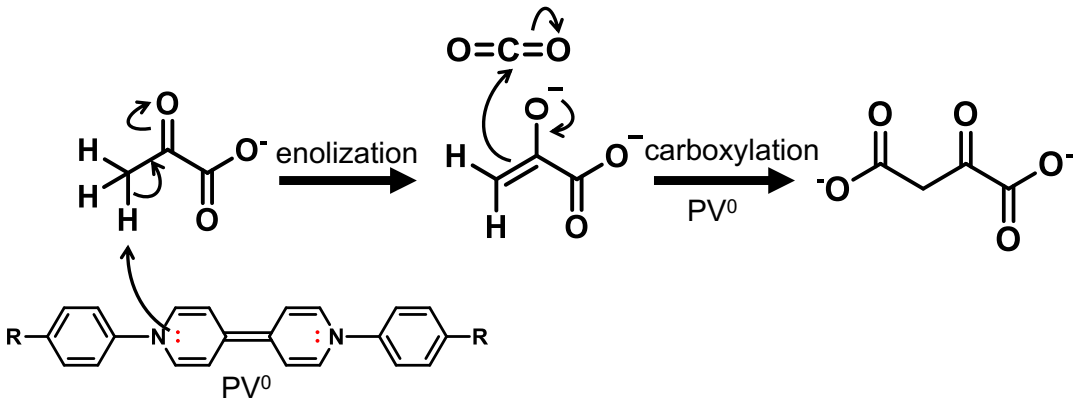

Fig. 2-22. Proposed reaction mechanism for oxaloacetate production from pyruvate and CO_2 in ME.

As shown in the below, the reduction of oxaloacetate by several one-electron-reduced forms of PCV is a thermodynamically feasible reaction because the Gibbs free energy change (ΔG^0) is –87 kJ mol^{-1}.

Oxaloacetate + $2H^+$ + $2e^-$ → Malate	E_0' = -0.166 V
PCV^{2+} + e^- → $PCV^{\cdot+}$	E_0' = -0.62 V
Oxaloacetate + $2H^+$ + $2PCV^{\cdot+}$ → Malate + $2PCV^{2+}$	$\Delta E_0'$ = -0.45 V
	ΔG^0 = -87 kJ mol^{-1}

2.3.9 Oxaloacetate production using 1-methyl-4,4-bipyridiniumu salt with ME in the presence of pyruvate and bicarbonate

Oxaloacetate production with ME was investigated in terms of the lone pairs on the nitrogen atom of 1-methyl-4,4'-bipyridinium iodide. The reaction solution contained pyruvate, bicarbonate, Mg^{2+}, ME, and 1-methyl-4,4'-bipyridinium in a pH 7.4 solution of HEPES-NaOH buffer. The time dependence of oxaloacetate production is shown in Fig. 2-23. The lone electron pair on the nitrogen atom is assumed to act as a base, abstracting the α-hydrogen of the keto form of pyruvate. The enolization of the pyruvate is promoted, and then CO_2 is introduced as a carboxy group into the enolate intermediate of pyruvate.

Furthermore, it is unclear whether CO_2[71] or bicarbonate (HCO_3^-)[72] directly contributes to the carboxylation of pyruvate with ME. Kuo et al. proposed that basic amino-acid lysine residue in ME obtained from the other species abstracts hydrogen bonded to the α-carbon of the keto form of pyruvate during the tautomerization to the enolate intermediate.[61] This report also suggested that a base is needed for this process.

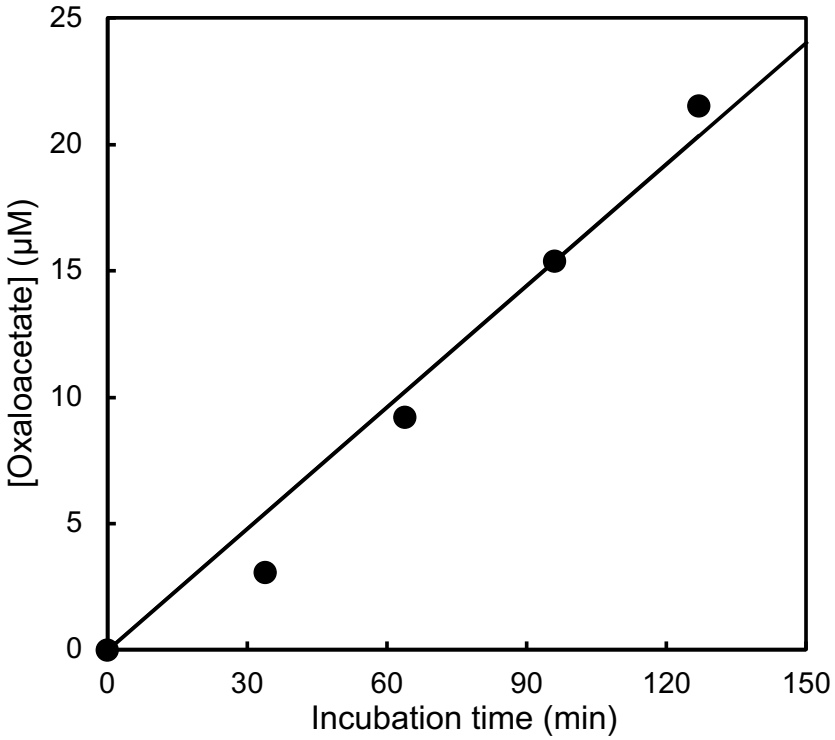

Fig. 2-23. Time dependence of oxaloacetate in the solution containing 1-methyl-4,4'-bipyridinium salt, ME, pyruvate and Mg^{2+} in HEPES-NaOH buffer (pH 7.4).

2.4 Conclusion

In this chapter, the chemical and visible-light-induced reduction properties of PV derivatives with water-soluble Zn porphyrin were investigated. The reduction potentials of the PV derivative are sufficiently negative to reduce two electrons by photosensitization of the water-soluble Zn porphyrin. The electron transfer to PV derivatives from ^{3}ZnTPPS* proceeded. In the PV derivative photoreduction accompanied by the visible-light sensitization of ZnTPPS, double-electron reduction proceeded. Visible-light-induced malate production from pyruvate and CO_2 using ME in the presence of Mg^{2+} as a cofactor for ME, H_2TPPS, PV derivatives, and TEOA was successfully achieved. PSV is an efficient electron mediator in the visible-light-induced photoredox system for C–C bond formation using CO_2 as a feedstock.

In addition, the kinetic parameters of oxaloacetate production based on C–C bond formation between a coupling pyruvate and CO_2 using a water-soluble PV derivative, double-electron-reduced PCV^0, and ME were determined with the analysis of enzymatic kinetics. PCV^0 acts as a base and is involved in oxaloacetate production via C–H bond activation and carboxylation of pyruvate by CO_2.

2.5 References

1. Smart CO_2 Transformation (SCOT) project in EU Seventh Framework Program; http://scotproject.org
2. H. Choe, J. C. Joo, D. H.Cho, M. H. Kim, S. H. Lee, K. D. Jung and Y. H. Kim, "Efficient CO_2-reducing activity of NAD-dependent formate dehydrogenase from *Thiobacillus* sp. KNK65MA for formate production from CO_2 gas", *PLoS One*, 2014, **9**, e103111.
3. J. H. Kim, D. H. Nam and C. B. Park, "Nanobiocatalytic assemblies for artificial photosynthesis", *Curr. Opinion in Biotechnology*, 2014, **28**, 1–9.
4. S. K. Kuk, R. K. Singh, D. H. Nam, R. Singh, J. K. Lee and C. B. Park, "Photoelectrochemical reduction of carbon dioxide to methanol through a highly efficient enzyme cascade", *Angew. Chem. Int. Ed.*, 2017, **56**, 3827–3832.
5. H. Wu, C. Tian, X. Song, C. Liu, D. Yang and Z. Jiang, "Methods for the regeneration of nicotinamide coenzymes", *Green Chem.*, 2013, **15**, 1773–1789.
6. D. Mandler, and I. Willner, "Photochemical fixation of carbon dioxide: enzymic photosynthesis of malic, aspartic, isocitric, and formic acids in artificial media", *J. Chem. Soc., Perkin Trans. 2*, 1988, 997–1003.
7. I. Willner and D. Mandler, "Characterization of palladium-.beta.-cyclodextrin colloids as catalysts in the photosensitized reduction of bicarbonate to formate", *J. Am. Chem. Soc.*, 1989, **111**, 1330–1336.
8. I. Willner, N. Lapidot, A. Riklin, R. Kasher, E. Zahavy and E. Katz, "Electron-transfer communication in glutathione reductase assemblies: Electrocatalytic, photocatalytic, and catalytic systems for the reduction of oxidized glutathione", *J. Am. Chem. Soc.*, 1994, **116**, 1428–1441.
9. I. Willner, A. Riklin and N. Lapidot, "Electron-transfer communication between a redox polymer matrix and an immobilized enzyme: activity of nitrate reductase in a viologen-acrylamide copolymer", *J. Am. Chem. Soc.*, 1990, **112**, 6438–6439.
10. R. K. Yadav, G. H. Oh, N. J. Park, A. Kumar, K. J. Kong and J. O. Baeg, "Highly selective solar-driven methanol from CO_2 by a

photocatalyst/biocatalyst integrated system" *J. Am. Chem. Soc.*, 2014, **136**, 16728–16731.

11. R. K. Yadav, J. O. Baeg, G. H. Oh, N. J. Park, K. J. Kong, J. Kim, D. W. Hwang and S. K. Biswas, "A photocatalyst–enzyme coupled artificial photosynthesis system for solar energy in production of formic acid from CO_2", *J. Am. Chem. Soc.*, 2012, **134**, 11455–11461.
12. W. S. Choi, S. H. Lee, J. W. Ko and C. B. Park, "Human urine-fueled light-driven NADH regeneration for redox bocatalysis", *ChemSusChem*, 2016, **9**, 1559–1564.
13. X. Ji, Y. Kang, T. Fan, Q. Xiong, S. Zhang, W. Tao and H. Zhang, "An antimonene/Cp*Rh(phen)Cl/black phosphorus hybrid nanosheet-based Z-scheme artificial photosynthesis for enhanced photo/bio-catalytic CO_2 reduction", *J. Mater. Chem. A*, **2020**, 8, 323–333.
14. R. Cazelles, J. Drone, F. Fajula and O. Ersen, S. Moldovan, and A. Galarneau, "Reduction of CO_2 to methanol by a polyenzymatic system encapsulated in phospholipids–silica nanocapsules", *New J. Chem.*, 2013, **37**, 3721–3730.
15. X. Ji, Z. Su, P. Wang, G. Ma and S. Zhang, "Tethering of nicotinamide adenine dinucleotide inside hollow nanofibers for high-yield synthesis of methanol from carbon dioxide catalyzed by coencapsulated multienzymes", *ACS Nano*, 2015, **9**, 4600–4610.
16. R. Miyatani and Y.Amao, "Bio-CO_2 fixation with formate dehydrogenase from Yeast and water-soluble zinc porphyrin by visible light", *Biotechnol. Lett.*, 2002, **24**, 1931–1934.
17. R. Miyatani and Y. Amao, "Photochemical synthesis of formic acid from CO_2 with formate dehydrogenase and water-soluble zinc porphyrin", *J. Mol. Catal. B. Enzym.*, 2004, **27**, 121–125.
18. R. Miyatani and Y. Amao, "Visible light-induced formic acid synthesis from HCO_3^- with formate dehydrogenase and water-soluble zinc porphyrin", *J. Jpn. Petrol. Inst.*, 2004, **47**, 27–31.

19. I. Tsujisho, M. Toyoda and Y.Amao, “Photochemical and enzymatic synthesis of formic acid from CO_2 with chlorophyll and dehydrogenase system”, *Catal. Commun.*, 2006, **7**, 173–176.
20. M. Kodaka and Y. Kubota, “Effect of structures of bipyridinium salts on redox potential and its application to CO_2 fixation”, *J. Chem. Soc. Perkin Trans 2*, 1999, 891–894
21. S. Ikeyama and Y. Amao, “A novel electron carrier molecule based on a viologen derivative for visible light-driven CO_2 reduction to formic acid with the system of zinc porphyrin and formate dehydrogenase”, *Sustainable Energy Fuels*, 2017, **1**, 1730–1733.
22. S. Ikeyama and Y. Amao, “The effect of the functional ionic group of the viologen derivative on visible-light driven CO_2 reduction to formic acid with the system consisting of water-soluble zinc porphyrin and formate dehydrogenase”, *Photochem. Photobiol. Sci.*, 2018, **17**, 60–68.
23. Y. Amao and T.Watanabe, “Photochemical and enzymatic synthesis of methanol from HCO_3^- with dehydrogenases and zinc porphyrin”, *Chem. Lett.*, 2004, **33**,1544–1545.
24. Y. Amao and T. Watanabe, “Photochemical and enzymatic methanol synthesis from HCO_3^- by dehydrogenases using water-soluble zinc porphyrin in aqueous media”, *Appl. Catal. B. Enviromental.*, 2009, **86**,109–113.
25. Y. Amao and R. Kataoka, “Methanol production from CO_2 with the hybrid system of biocatalyst and organo-photocatalyst”, *Catal. Today*, 2018, **307**, 243–247.
26. K. J. Shah and T. Imae, “Photoinduced enzymatic conversion of CO_2 gas to solar fuel on functional cellulose nanofiber films”, *J. Mater. Chem. A*, 2017, **5**, 9691–9701.
27. M. Tamura, K. Ito, M. Honda, Y. Nakagawa, H. Sugimoto and K. Tomishige, “Direct copolymerization of CO_2 and diols”, *Sci. Rep.*, 2016, **6**, 24038.
28. M. Tamura, K. Ito, Y. Nakagawa and K. Tomishige, “CeO_2-catalyzed direct synthesis of dialkylureas from CO_2 and amines”, *J. Catal.*, 2016, **343**, 75–85.

29. M. Honda, M. Tamura, Y. Nakagawa and K. Tomishige, "Catalytic CO_2 conversion to organic carbonates with alcohols in combination with dehydration system", *Catal. Sci. Technol.*, 2014, **4**, 2830–2845.
30. J. Takaya and N. Iwasawa, "Synthesis, structure, and catalysis of palladium complexes bearing a group 13 metalloligand: Remarkable effect of an aluminum-metalloligand in hydrosilylation of CO_2", *J. Am. Chem. Soc.*, 2017, **139**, 6074–6077.
31. T. Suga, T. Saitou, J. Takaya and N. Iwasawa, "Mechanistic study of the rhodium-catalyzed carboxylation of simple aromatic compounds with carbon dioxide", *Chem. Sci.*, 2017, **8**, 1454–1462.
32. T. Suga, H. Mizuno, J. Takaya and N. Iwasawa, "Direct carboxylation of simple arenes with CO_2 through a rhodium-catalyzed C–H bond activation", *Chem. Commun.*, 2014, **50**, 14360–14363.
33. M. Hatazawa, K. Nakabayashi, S. Ohkoshi and K. Nozaki, "In situ generation of CoIII–salen complexes for copolymerization of propylene oxide and CO_2", *Chem. Eur. J.*, 2016, **22**, 13677–13681.
34. M. L. Lephoto, K. Nakano, D. Appavoo, B. O. Owaga, K. Nozaki and J. Darkwa, "Pyrazole supported zinc(II) benzoates as catalysts for the ring opening copolymerization of cyclohexene oxide and carbon dioxide", *Catalysts*, 2016, **6**, 17–30.
35. T. Ohkawara, K. Suzuki, K. Nakano, S. Mori and K. Nozaki, "Facile estimation of catalytic activity and selectivities in copolymerization of propylene oxide with carbon dioxide mediated by metal complexes with planar tetradentate ligand", *J. Am. Chem. Soc.*, 2014, **136**, 10728–10735.
36. S. Ochoa, A. H. Mehler and A. Kornberg, "Biosynthesis of dicarboxylic acids by carbon dioxide fixation. I. Isolation and properties of an enzyme from pigeon liver catalyzing the reversible oxidative decarboxylation of L-malic acid", *J. Biol. Chem.*, 1948, **174**, 979–1000.
37. I. Harary, S. R. Korey and S. Ochoa, "Biosynthesis of dicarboxylic acids by carbon dioxide fixation. VII. Equilibrium of malic enzyme reaction", *J. Biol. Chem.*, 1953, **203**, 595–604.

38. B. W. Geer, D. Krochko, M. J. Oliver, V. K. Walker and J. H. Williamson, “A comparative study of the NADP-malic enzymes from Drosophila and chick liver”, *Comp. Biochem. Physiol.*, 1980, **65B**, 25–34.
39. T. Itoh, H. Asada, K. Tobioka, Y. Kodera, A. Matsushima, M. Hiroto, H. Nishimura, T. Kamachi, I. Okura and Y. Inada, “Hydrogen gas evolution and carbon dioxide fixation with visible light by chlorophyllin coupled with polyethylene glycol”, *Bioconjugate Chem.*, 2000, **11**, 8–13.
40. Y. Amao and M. Ishikawa, “Photochemical and enzymatic synthesis of malic acid from pyruvic acid and HCO_3^- with combination system of zinc chlorin-e6 and malic enzyme in aqueous medium”, *J. Jpn. Petrol. Inst.*, 2007, **50**, 272–277.
41. Y. Amao and M. Ishikawa, “Visible light and enzymatic induced synthesis of malic acid from pyruvic acid and HCO_3^- with the combination system of zinc chlorophyll derivative and malic enzyme in water media”, *Catal. Commun*., 2007, **8**, 523–526.
42. Y. Amao, S. Ikeyama, T. Katagiri and K. Fujita, “Development of Dye Molecule-biocatalyst Hybrid System with Visible-light Induced Carbon-carbon Bond formation from CO_2 as a Feedstock”, *Faraday Discuss.*, 2017, **198**, 73–81.
43. E. B. Fleischer and S. K. Cheung, “Mechanisms of reduction of cobaltic porphyrins with various reducing agents”, *J. Am. Chem. Soc.*, 1976, **98**, 8381.
44. Y. Amao and I. Okura, “Effective photoinduced hydrogen evolution with hydrogenase in surfactant micelles”, *J. Mol. Catal. A: Chem.*, 1996, **105**, 125–130.
45. H. Kamogawa and S. Sato, “Redox photochromism of arylviologen crystals”, *Bull. Chem. Soc. Jpn.*, 1994, **64**, 321.
46. M. Leroux, N. Mercier, M. Allain, M. C. Dul, J. Dittmerγ, A. H. Kassibaγ, J. P. Bellat, G. Weber and I. Bezverkhyy, “Porous Coordination Polymer Based on Bipyridinium Carboxylate Linkers with High and Reversible Ammonia Uptake”, *Inorg. Chem.*, 2016, **55**, 8587–8594.
47. V-A. Constantin, “Viologen Stars and Rods: Synthesis, electrochemical Investigations and Polymerization”, *Universität Osnabrück, Doctoral Thesis,* 2012.

48. J-J. Liu, Y-F. Guan, M-J. Lin, C-C. Huang and W-X. Dai, “Luminescent coordination polymer with conjugated lewis acid sites for the detection of organic amines”, *Cryst. Growth Des.*, 2015, **15**, 5040–5046.
49. P. Silpananta and A. G. Goodridge, “Synthesis and degradation of malic enzyme in chick liver”, *J. Biol. Chem.*, 1971, **246**, 5754.
50. R. B. McComb, L. W. Bond, R. W. Burnett, R. C. Keech and G. N. Bowers Jr., “Determination of the molar absorptivity of NADH”, *Clin. Chem.*, 1976, **22**, 141–150.
51. B. A. Beaupre, M. R. Hoag, J. Roman, F. H. Försterling and G. R. Moran, “Metabolic function for human renalase: oxidation of isomeric forms of β-NAD(P)H that are inhibitory to primary metabolism”, *Biochemistry,* 2015, **54**, 795–806.
52. O. Stern and M. Volmer, “The extinction period of fluorescence”, *Phys. Z*, 1919, **20,** 183–188.
53. M. Kaneko, K. Suzuki, E. Ebel and D. Wöhrle, “Specific electron transfer mechanism from the photoexcited tetrasulfonated Zn(II)-tetraphenylporphyrin to methylviologen via self-assembled ionic complex”, *Macromol. Symp.*, 2003, **204**, 71–78.
54. D. Genovese, M. Cingolani, E. Rampazzo, L. Prodi and N. Zaccheroni, “Static quenching upon adduct formation: a treatment without shortcuts and approximations”, *Chem. Soc. Rev.*, 2021, **50**, 8414–8427.
55. M. Kaneko, H. Ueno, S. Masuda, K. Suzuki, H. Okimi, M. Hoshino, L. Lapok and D. Wöhrle, “Quenching of singlet photoexcited state of water soluble phthalocyanines and porphyrins by viologens interacting electrostatically”, *J. Porphyr. Phthalocyanines*, 2005, **9**, 667–680.
56. Y. Amao, Y. Tomonou, Y. Ishikawa and I. Okura, “Photoinduced hydrogen production with water-soluble zinc porphyrin and hydrogenase in nonionic surfactant micellar system”, *Int. J. Hydrogen Energy*, 2002, **27**, 621–625.
57. Y. Amao, R. Abe and S. Shiotani, “Effect of chemical structure of bipyridinium salts as electron carrier on the visible-light induced conversion of CO_2 to formic

acid with the system consisting of water-soluble zinc porphyrin and formate dehydrogenase", *J. Photochem. Photobio. A: Chemistry*, 2015, **313**, 149–153.

58. K. Kalyanasundaram and M. Nerman-Spallart, "Photophysical and redox properties of water-soluble porphyrins in aqueous media", *J. Phys. Chem.*, 1982, **86**, 5163–5169.
59. A. M. Manke, K. Geisel, A. Fetzer and P. Kurz, "A water-soluble tin(iv) porphyrin as a bioinspired photosensitiser for light-driven proton-reduction", *Phys. Chem. Chem. Phys.*, 2014, **16**, 12029–12042.
60. C. B. Grissom and W. W. Cleland, "Isotope effect studies of chicken liver NADP malic enzyme: role of the metal ion and viscosity dependence", *Biochemistry*, 1988, **27**, 2927–2732.
61. C. C. Kuo, K. Y. Lin, Y. J. Hsu, S.Y. Lin, Y. T. Lin, G. G. Chang and W. Y. Chou, "The roles of Tyr^{91} and Lys^{162} in general acid–base catalysis in the pigeon $NADP^+$-dependent malic enzyme", *Biochem. J.*, 2008, **411**, 467–473.
62. J. B. S. Haldane, Enzymes. 1930. London, UK: Longman Green.
63. J. L. Webb, Enzymes and metabolic inhibitors. 1963. Boston: Academic.
64. T. Yano, T. Nakahara, S. Kamiyama and K. Yamada, "Kinetic studies on microbial activities in concentrated solutions. I. Effect of excess sugars on oxygen uptake rate of a cell-free respiratory system", *Agric. Biol. Chem.*, 1966, **30**, 42–48.
65. S. Aiba, M. Shoda and M. Nagatani, "Kinetics of product inhibition in alcohol kinetics", *Biotech. Bioeng.*, 1968, **10**, 845–864.
66. J. Y. Hsieh, S. Y. Li, M. C. Chen, P. C. Yang, H. Y. Chen, N. L. Chan, J. H. Liu, and H. C. Hung, "Structural characteristics of the nonallosteric human cytosolic malic enzyme", *Biochim. Biochim. Acta.*, 2014, **1844**, 1773–1783.
67. P. Gourdon, M. F. Baucher, N. D. Lindley and A. Guyonvarch, "Cloning of the malic enzyme gene from Corynebacterium glutamicum and role of the enzyme in lactate metabolism", *Appl Environ Microbiol.*, 2000, **66**, 2981–2987.
68. S. Ikeyama and Y.Amao, "Abnormal co-enzymatic behavior of a one electron reduced bipyridinium salt with a carbamoyl group on the catalytic activity of

CO_2 reduction by formate dehydrogenase", *New. J. Chem.*, 2018, **42**, 15556–15560.

69. M. Gaydou, T.Moragas, F.Juliá-Hernández and R. Martin, "Site-selective catalytic carboxylation of unsaturated hydrocarbons with CO_2 and water", *J. Am. Chem. Soc.*, 2017, **139**, 12161–12164.
70. K. Shimomaki, K. Murata, R. Martin and N. Iwasawa, "Visible-light-driven carboxylation of aryl halides by the combined use of palladium and photoredox catalysts", *J. Am. Chem. Soc.*, 2017, **139**, 9467–9470.
71. K. Dalziel and J. C. Londesborough, "The mechanisms of reductive carboxylation reactions. carbon dioxide or bicarbonate as substrate of nicotinamide-adenine dinucleotide phosphate-linked isocitrate dehydrogenase and 'malic' enzyme", *Biochem. J.*, 1968, **110**, 223–230.
72. S. Asami, K. Inoue, K. Matsumoto, A. Murauchi and T. Akazawa, "NADP-malic enzyme from maize leaf: Purification and properties". *Arch. Biochem. Biophys.*, 1979, **194**, 503–510.

Chapter 3

Visible-light-driven selective NADH regeneration using a system of photosensitizer and homogeneously polymer-dispersed metal nanoparticles

3.1 Introduction

Enzymes have high catalytic activity and selectivity under ambient conditions and have thus been used in biodegradation reactions, pharmaceuticals, chemical syntheses, and so on.[1] Oxidoreductase is a type of enzyme that accounts for 25% of all known enzymes.[2,3] It mainly depends on a nicotinamide adenine dinucleotide (NAD^+) or its phosphate ($NADP^+$). The oxidized and reduced forms are $NAD(P)^+$ and NAD(P)H, respectively.[4] NAD(P)H is used as a coenzyme for oxidoreductase in various biological reactions. Since NAD(P)H is very expensive and has low stability, an efficient NAD(P)H regeneration system from $NAD(P)^+$ is desired.[5,6] Therefore, NAD(P)H regeneration using biocatalytic, photochemical,[7-9] electrochemical,[10-12] heterogeneous,[5] and homogeneous[13] catalytic methods has been investigated. As examples of catalysts for NADH regeneration, organometallic complexes of rhodium, ruthenium, and iridium have been reported. In particular, rhodium catalyst $[Cp^*Rh(bpy)(H)]^+$ (Cp* = pentamethylcyclopentadienyl, bpy = 2,2'-bipyridyl) has been widely used and studied for the regioselective reduction of $NAD(P)^+$ to NAD(P)H owing to its versatile range of application and regiospecific activity.[14-22]

Compared with these methods, photochemical NADH regeneration from NAD^+ has attracted much attention because solar energy is clean, inexpensive, abundant, and renewable. Using light energy, $NAD(P)^+$ can be reduced simply and directly with a photosensitizer such as a tris(bipyridine)ruthenium(II) complex ($[Ru(bpy)_3]^{2+}$) or a water-soluble porphyrin. However, a single-electron-reduced $NAD(P)^+$ (NAD(P) radical) is formed and immediately undergoes dimerization to a biologically inactive reduction product (4,4'-NAD(P) dimer or 4,6-NAD(P) dimer), as shown in Fig. 3-1. In the non-enzymatic NAD(P)H regeneration, it has been frequently reported that enzymatically inactive NAD(P)H isomers (1,2- and 1,6-NADH) can be formed.[23] A photoredox system for NAD(P)H regeneration typically consists of three main components: a photosensitizer, an electron mediator, and a catalyst.[25-27] An example of the enzymatic reduction of $NAD(P)^+$ to NAD(P)H is the photoredox system with ferredoxin-$NADP^+$ reductase (FNR, EC 1.18.1.2). FNR

catalyzes a reduction of NAD(P)$^+$ to NAD(P)H by coupling with ferredoxin in natural photosynthesis.[28,29] FNR also catalyzes a reduction of NADP$^+$ to NADPH by coupling with 1,1'-dimethyl-4,4'bipyridinium salt (methylviologen, MV) and single-electron-reduced MV (MV_{red}).[30] By using MV as an electron mediator between the photosensitizer and FNR as a catalyst,[30] a light-driven NAD(P)H regeneration system was developed.[25] Although this system shows high selectivity owing to using enzymes, it has drawbacks in terms of durability, cost, and scalability. In addition, MV is highly toxic and is not suitable for green chemistry. As examples of non-enzymatic regioselective photoreduction of NAD(P)$^+$, Rh complexes were used as catalysts for electron and hydride transfer in the presence of a photosensitizer.[31-33] In this way, Rh catalysts are useful for hydride production. One of the Rh catalysts studied, Rh nanoparticles dispersed in polyvinylpyrrolidone (Rh-PVP), has attracted considerable attention owing to its simple preparation method by the reduction of Rh^{3+} ion in alcohol solvent with the polyvinylpyrrolidone.[35-39] The nanoparticles require a dispersant such as a hydrophilic polymer or surfactant for maintaining their small particle sizes. Rh-PVP has catalyzed various reactions, such as the hydrogenation of nitriles and benzoic acid.[40,41]

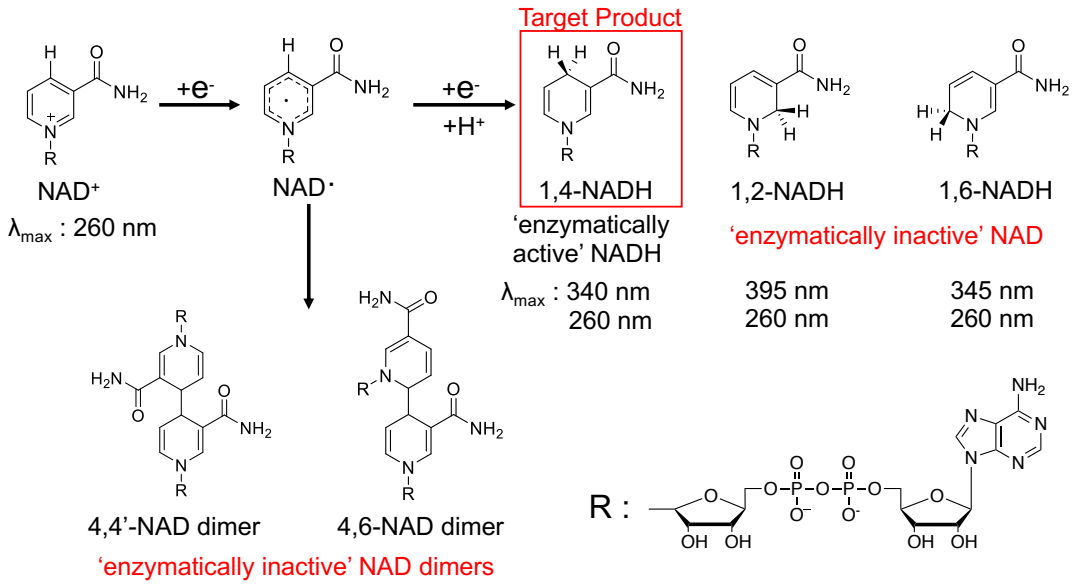

Fig. 3-1. Plausible intermediates and 'enzymatically active/inactive' NAD(P)H isomers to be formed during the reduction of NAD$^+$.

In this study, focusing on the unique catalytic function of Rh catalysts, the regioselective photoreduction of NAD^+ to enzymatically active 1,4-NADH using Rh-PVP in a photoredox system without producing byproducts was investigated. A novel and simple system using homogeneously polymer-dispersed Rh nanoparticles for selective 1,4-NADH regeneration with visible light energy was developed. It is first demonstrated that Rh nanoparticles dispersed in polyvinylpyrrolidone (Rh-PVP) can be used in the visible-light-driven selective NADH regeneration in the presence of an electron donor, a photosensitizer in the aqueous media, as shown in Scheme 3-1. The reduced product of NAD^+ was validated using HPLC analysis and an enzymatic assay. In addition, we explored NAD^+-dependent enzyme-catalyzed pyruvate reduction through visible-light-driven NADH regeneration. Rh-PVP was purchased from Renaissance Energy Research (Osaka, Japan). As a photosensitizer, we used ZnTPPS, which has often been reported as a photosensitizer in the photoredox system and is expected to have a sufficiently high potential for NAD^+ reduction.[42] By using homogeneously dispersed metal particles, the system is expected to be both durable and inexpensive.

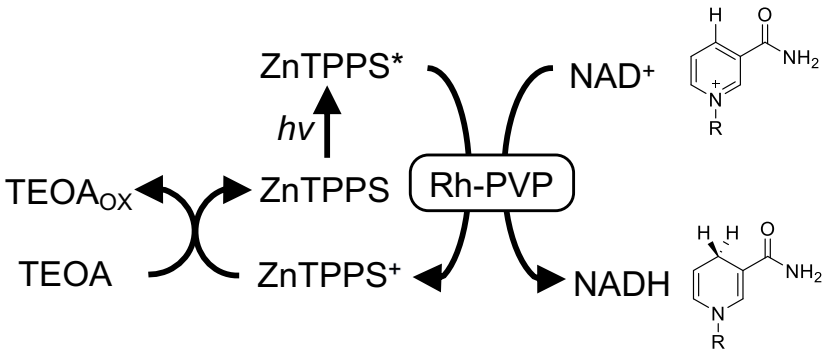

Scheme 3-1. The diagram of visible light-driven NADH regeneration with the system consisted of TEOA an electron donor, ZnTPPS as a photosensitizer, Rh-PVP as a catalyst and NAD^+.

3.2 Experimental

3.2.1 Materials

β-Nicotinamide adenine dinucleotide oxidized form (NAD^+) and L-lactate dehydrogenase from pig heart (LDH, EC 1.1.1.27) were purchased from Oriental Yeast Co., Ltd. (Tokyo, Japan). Tetraphenylporphyrin tetrasulfonic acid (H_2TPPS) was purchased from Dojindo Laboratories (Kumamoto, Japan). Triethanolamine (TEOA), zinc acetate dihydrate, and sodium pyruvate were obtained from FUJIFILM Wako Pure Chemical Corporation (Osaka, Japan). 4-(2-Hydroxyethyl)-1-piperazineethanesulfonic acid (HEPES) was purchased from NACALAI TESQUE, INC. Sodium borohydride was purchased from Tokyo Chemical Industry Co., Ltd. (Tokyo, Japan). Rh nanoparticles dispersed in polyvinylpyrrolidone (Rh-PVP) were purchased from Renaissance Energy Research (Osaka, Japan). All the materials were of analytical grade or the highest grade available and were used as received, without further purification. Ar gas of ultrahigh purity (≧99.9999 %, Grade 1) was supplied by TAIYO NIPPON SANSO CORPORATION (Toyko, Japan). Water was purified using a Milli-Q purification system. Zinc tetraphenylporphyrin tetrasulfonate (ZnTPPS) was synthesized by refluxing H_2TPPS with an approximately 5-fold molar equivalent of zinc acetate dihydrate in 50 mL methanol at 50 °C for 3 h, according to a previously reported method.[43,44]

3.2.2 Transmission electron microscopy (TEM) measurement

Transmission electron microscopy (TEM) was conducted to acquire morphological information about the Rh nanoparticles in the catalyst. The particle size of Rh-PVP was estimated using the TEM Image. For the transmission electron microscopy (TEM) measurements, a drop of the sample solutions was mounted on a carbon-covered copper mesh. The TEM images of Rh-PVP were recorded with a JEM-2100F (JEOL) electron microscope operated at 200 kV.

3.2.3 Visible-light-driven NAD^+ reduction

The visible-light-driven NADH regeneration was carried out as follows. A sample solution containing TEOA (0.20 M), ZnTPPS, Rh-PVP, and NAD^+ in 5 mL of 50 mM HEPES-NaOH buffer (pH 7.4) was deaerated by performing six consecutive freeze–pump–thaw cycles and then flushed with Ar gas for 10 min. The sample solution in the cell equipped with a magnetic stirrer was irradiated with a 250 W halogen lamp (TOSHIBA) with a light intensity of 200 J m^{-2} s^{-1} at 30 °C. The production of 1,4-NADH was determined by the absorption change at 340 nm (ε = 6.3 × 10^3 cm^{-1} M^{-1})[45] using a UV–Vis absorption spectrometer (SHIMADZU, MultiSpec-1500 spectrophotometer).

3.2.4 Determination of the regenerated NADH by HPLC

The reduced products of NAD^+ were analyzed using an HPLC system equipped with a TOSHO ODS column (4.6 × 250 mm, 5 μm particle size; temperature: 30 °C)), a Shimadzu LC-20AD SP pump, and a Shimadzu SPD-20A UV–Vis detector (detected wavelength; 260 nm). Mixed solutions of methanol/100mM potassium phosphate buffer pH 7.1 (1:9 v/v) were used as the eluent.

1,2- and 1,6-NADH were prepared by the reduction of NAD^+ by sodium borohydride. Initially, a 25 mM sodium borohydride solution was prepared in 100 mM potassium phosphate buffer (pH 10.9). A 100 μL of this solution was then added to a freshly prepared volume (2 mL) of 0.5 mM NAD^+ solution in 100 mM potassium phosphate buffer (pH 7.1). The assignments of 1,2- and 1,6-NADH were referenced from a previous report.[43]

3.2.5 Bioactivity assay of reduction product of NAD^+

The enzymatic activity of regenerated NADH was tested as follows. First, a sample containing pyruvate (4.0 mM) and LDH (4.0 U) in 0.4 mL of 50 mM HEPES-NaOH buffer (pH 7.4) was added to a 0.4 mL solution of regenerated NADH in a

quartz UV cell. The absorbance of the solution was monitored using UV–Vis spectroscopy (SHIMADZU, MultiSpec-1500 spectrometer).

3.2.6 Fluorescence quenching behavior of ZnTPPS by Rh-PVP and NAD^+

The quenching of the photoexcited state of ZnTPPS by Rh-PVP was investigated using steady-state fluorescence spectroscopy. The sample solution contained ZnTPPS (1.0 μM) and Rh-PVP in 50 mM HEPES-NaOH buffer (pH 7.4). The concentration of Rh-PVP was varied from 0 to 100 μM. The excitation wavelength was 422 nm owing to the Soret band of ZnTPPS. The fluorescence emission spectrum of ZnTPPS was measured using a fluorescence spectrophotometer (SHIMADZU, RF-5300PC) with a 150 W Xenon lamp as a visible-excitation light source. Excitation and emission band-passes were 5.0 nm. In addition, the quenching of photoexcited state of ZnTPPS by NAD^+ was studied.

3.2.7 Measurement of H_2 production with Rh-PVP

H_2 production was determined using a gas chromatograph (GC-2014, SHIMADZU Corporation) equipped with a TCD detector. An activated charcoal column (column length: 3 mm I.D. × 2 m) was used for detecting the gas. The temperatures of injection, column, and detector were 100.0, 70.0 and 100.0 C, respectively. Ar gas was used as the carrier gas, and the flow rate was 30.0 mL min^{-1}.

3.2.8 Visible-light-driven pyruvate reduction through NADH regeneration

Visible-light-driven pyruvate reduction to malate with TEOA, ZnTPPS, Rh-PVP, NAD^+, and LDH was carried out as follows. A sample solution containing TEOA (0.20 M), ZnTPPS (19 μM), Rh-PVP (0.25 mM), NAD^+ (1.0 mM), sodium pyruvate (2.0 mM), and LDH (20 units) in 5 mL of 50 mM HEPES-NaOH buffer (pH 7.4) was deaerated by repeating freeze–pump–thaw cycles six times and then flushing with Ar gas for 10 min. The sample solution in the cell equipped with a magnetic

stirrer was irradiated with a 250 W halogen lamp (TOSHIBA) with a light intensity of 200 J m^{-2} s^{-1} at 30 °C. UV rays with a wavelength of shorter than 390 nm were blocked with a cut-off filter. The concentration of lactate production in the sample cell was analyzed using an ionic chromatograph system (Metrohm Eco IC; electrical conductivity detector) possessing an ion-exclusion column (Metrohm Metrosep Organic Acid - 250/7.8; column length: 250 × 7.8 mm; composed of a polystyrene/divinylbenzene copolymer with sulfonic acid groups; temperature: 35 °C). Perchloric acid (1.0 mM) and lithium chloride (50 mM) were used as an eluent and regenerant, respectively. The absorption spectrum of the sample solution was also monitored using UV–Vis absorption spectroscopy (SHIMADZU, MultiSpec-1500 spectrophotometer).

3.3 Results and Discussion

3.3.1 Characterization of Rh-PVP

Rh-PVP was purchased from Renaissance Energy Research, and transmission electron microscopy (TEM) was conducted to obtain morphological information about the Rh nanoparticles in the catalyst. The particle size of Rh was well-controlled, as can be seen from the TEM images of Rh-PVP in Fig. 3-2. The average particle size of the Rh nanoparticles was estimated to be ca. 4 nm. The particle size of Rh-PVP was almost identical to that reported by Wako.[46,47]

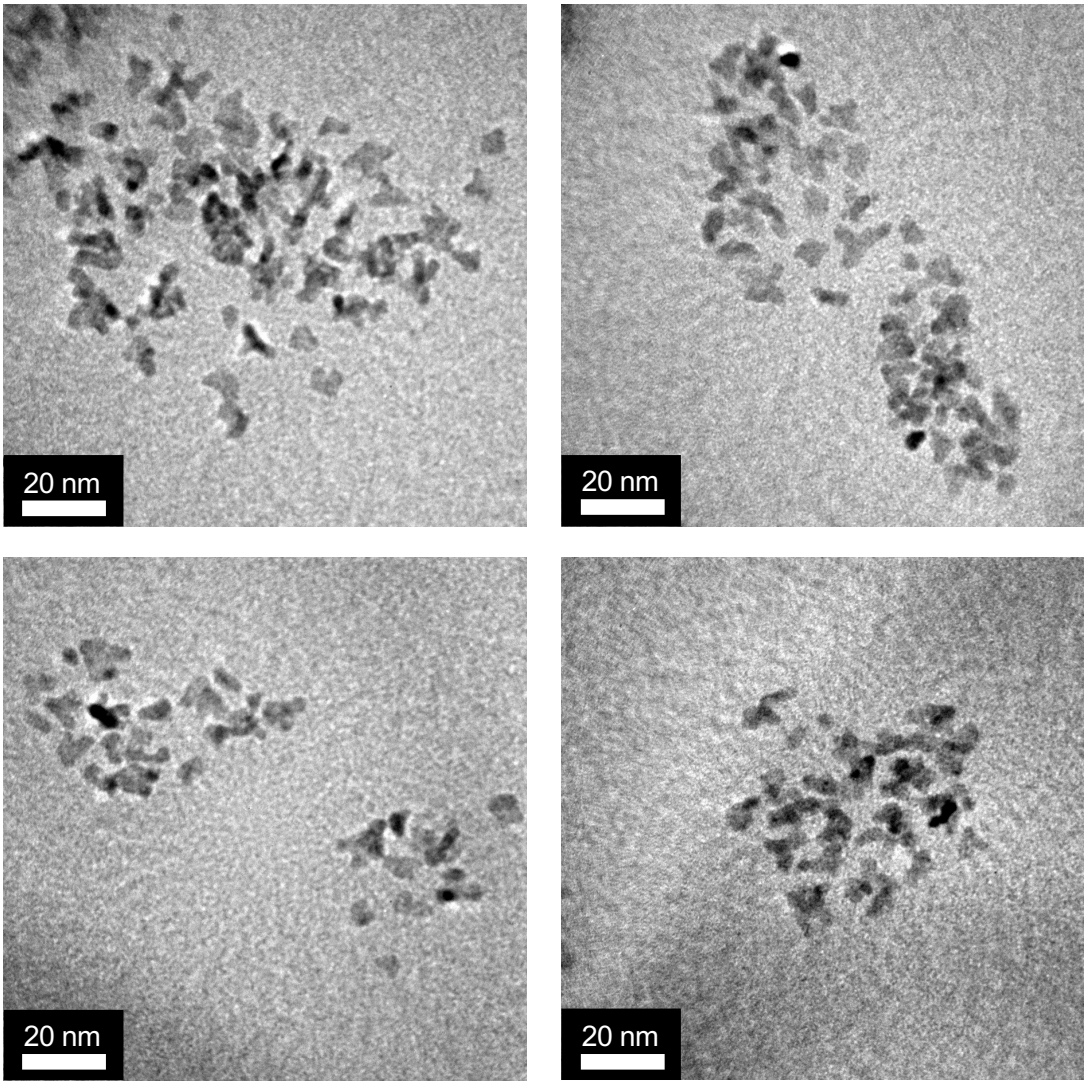

Fig. 3-2. Transmission electron microscopy (TEM) images of Rh-PVP.

The UV–Vis absorption spectra of Rh-PVP in HEPES-NaOH (pH 7.4) buffer are shown in Fig. 3-3. The color of the Rh-PVP solution was dark brown. Rh nanoparticles are known to absorb light in the UV–Vis region with no characteristic band. [48]

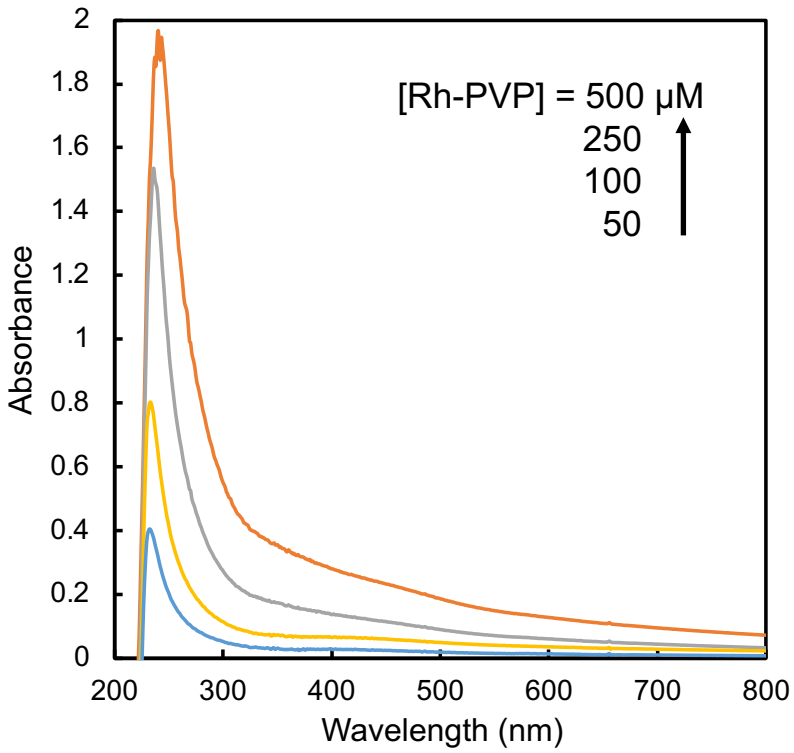

Fig. 3-3. UV-Vis absorption spectra of Rh-PVP in HEPES-NaOH (pH 7.4) buffer.

3.3.2 Visible-light-driven NAD^+ reduction using a ZnTPPS in the presence and absence of Rh-PVP

The reduction of NAD^+ to NADH using a system containing triethanolamine (TEOA) as an electron donor, ZnTPPS as a photosensitizer, Rh-PVP as a catalyst, and NAD^+ was investigated in HEPES-NaOH buffer (pH 7.4). When the system was irradiated with visible light, the absorption band at 300–380 nm increased with irradiation time, as shown in Fig. 3-4(a). Different UV–Vis absorption spectra of the sample solution before irradiation are also shown in Fig. 3-4 (b). The absorption maximum at 340 nm increased and that at 395 nm attributed to 1,2-NADH was not

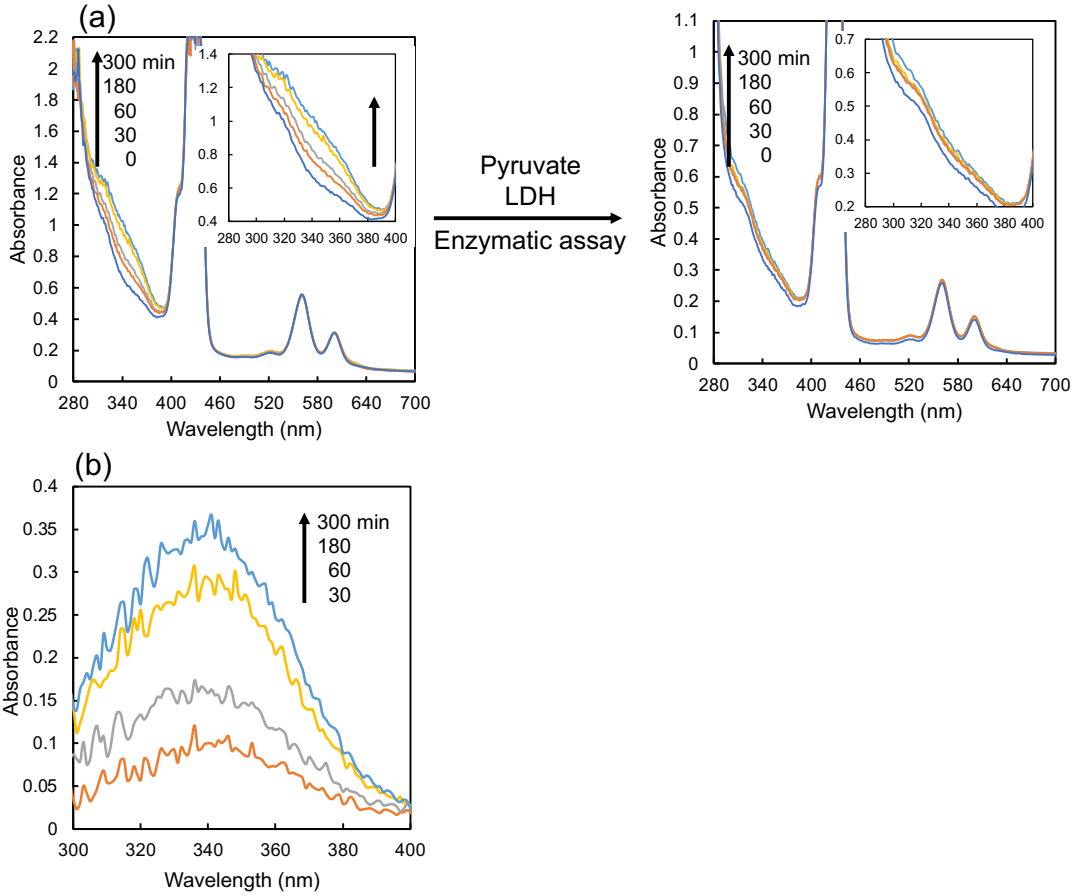

Fig. 3-4. UV-Vis absorption spectral changes during the reduction process with UV-Vis spectroscopy and enzymatic assay. (a) Different UV-Vis absorption spectral changes of sample solution including TEOA, ZnTPPS, Rh-PVP, and NAD^+ with visible-light irradiation time. Baseline is HEPES-NaOH buffer. (b) Baseline was recorded befor irradiation. (c) Different UV-Vis absorption spectral changes of after enzymatic assay. A sample solution including TEOA (0.1 M), ZnTPPS (9.5 μM), Rh-PVP (125 μM), LDH (2 U), and pyruvate (2 mM).

observed. These observations indicated that NAD^+ was reduced to 1,4-, 1,6- NADH or NAD dimer, which give rise to absorption maxima at ≈340 nm. As a control experiment, the visible-light-driven reduction of NAD^+ was performed in the absence of ZnTPPS. Although Rh-PVP has an absorbance band in the visible region, as shown in Fig. 3-5, the absorbance at 300–400 nm did not increase. Therefore, ZnTPPS is essential in the visible-light-driven NADH regeneration system. The photochemical reduction of NAD^+ was also examined in the absence of Rh-PVP and an increase of

absorption around 340 nm was observed, as shown in Fig. 3-5(a). Even in this case, an absorption maximum at 395 nm based on 1,2-NADH was not observed (Fig. 3-5(b)). Therefore, it was confirmed that hydrogen gas was not produced using the TEOA, ZnTPPS, and Rh-PVP system with visible-light irradiation (Fig. 3-6) and NAD^+ hydrogenation did not proceed. These results indicate that NAD^+ was reduced to 1,4-, 1,6-NADH or NAD dimer when the system included ZnTPPS and Rh-PVP or only ZnTPPS.

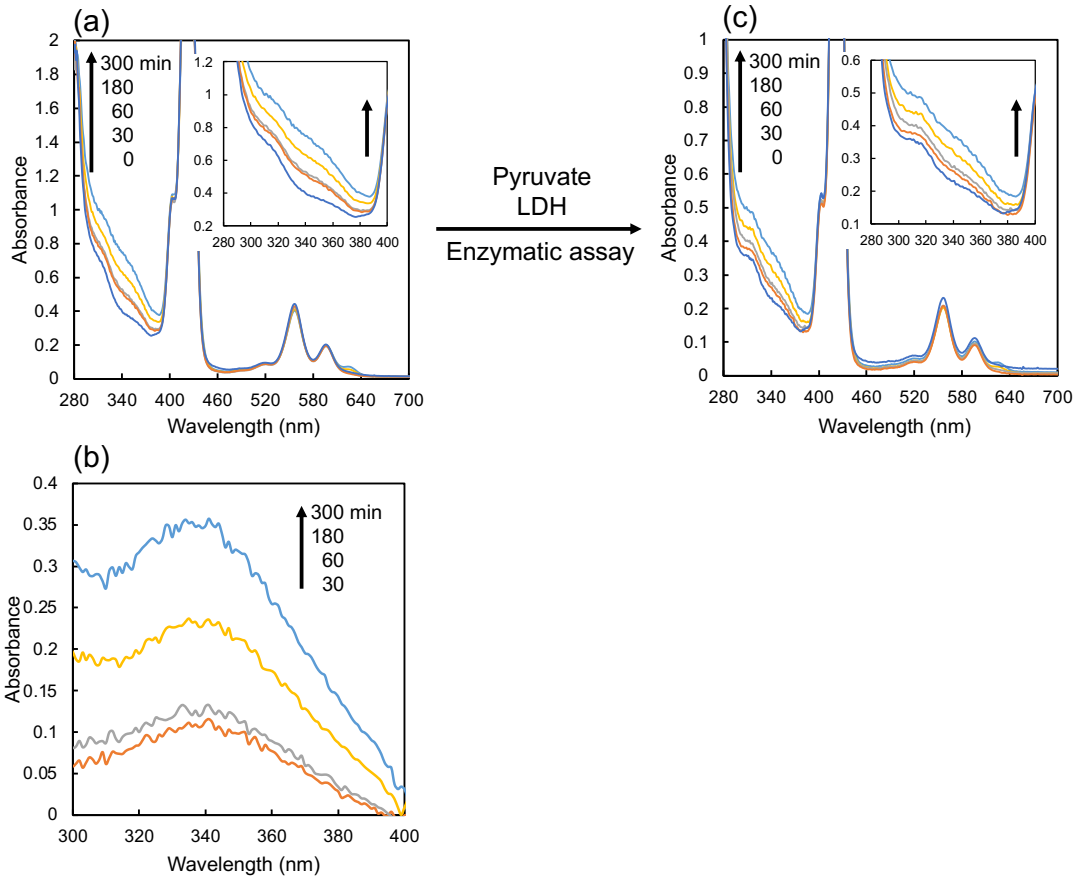

Fig. 3-5. UV-Vis absorption spectral changes during the reduction process with UV-Vis spectroscopy and enzymatic assay. (a) Different UV-Vis absorption spectral changes of sample solution including TEOA, ZnTPPS, and NAD^+ with visible-light irradiation time. Baseline is HEPES-NaOH buffer. (b) Baseline was recorded before irradiation. (c) Different UV-Vis absorption spectral changes of after enzymatic assay. A sample solution consisted of TEOA (0.1 M), ZnTPPS (9.5 μM), LDH (2 U), and pyruvate (2 mM).

In addition, the reaction was also performed without deaeration in the presence of Rh-PVP. The absorption band with the maximum at ≈340 nm also increased in the presence of oxygen.

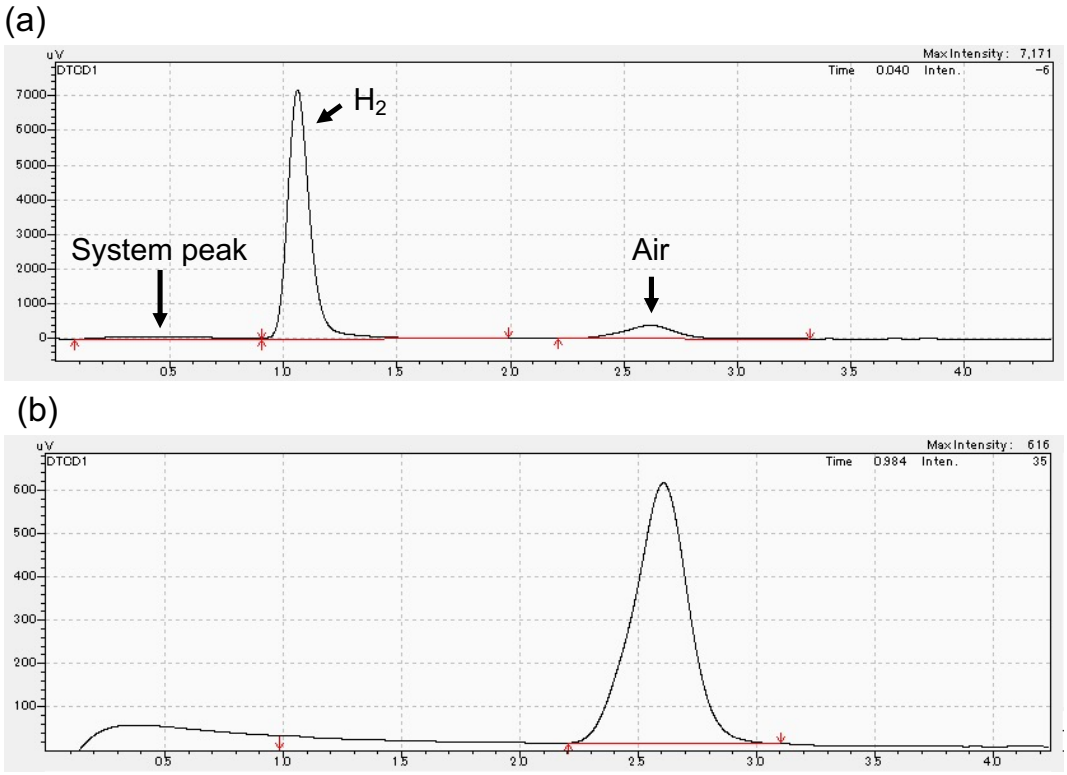

Fig. 3-6. The gas chromatogram of H_2 gas and Air (a), and analysis of the gas phase in the system of TEOA, ZnTPPS, and Rh-PVP after 3 h irradiation (b).

3.3.3 Determination of the reduction product of NAD^+ using HPLC

To determine whether the NAD^+ reduction product is 1,4-NADH, 1,6-NADH, or NAD dimer, the reduction product of NAD^+ was validated by carried out an HPLC assay. The NAD^+ reduction products were analyzed using HPLC to determine the 1,2-, 1,4-, and 1,6-NADH contents. Fig. 3-7 shows the analytical HPLC chromatograms for these NADH isomers.

Fig. 3-7(a) illustrates the chromatographic separation of the products obtained when NAD^+ is reduced by sodium borohydride. The reduction of NAD^+ by

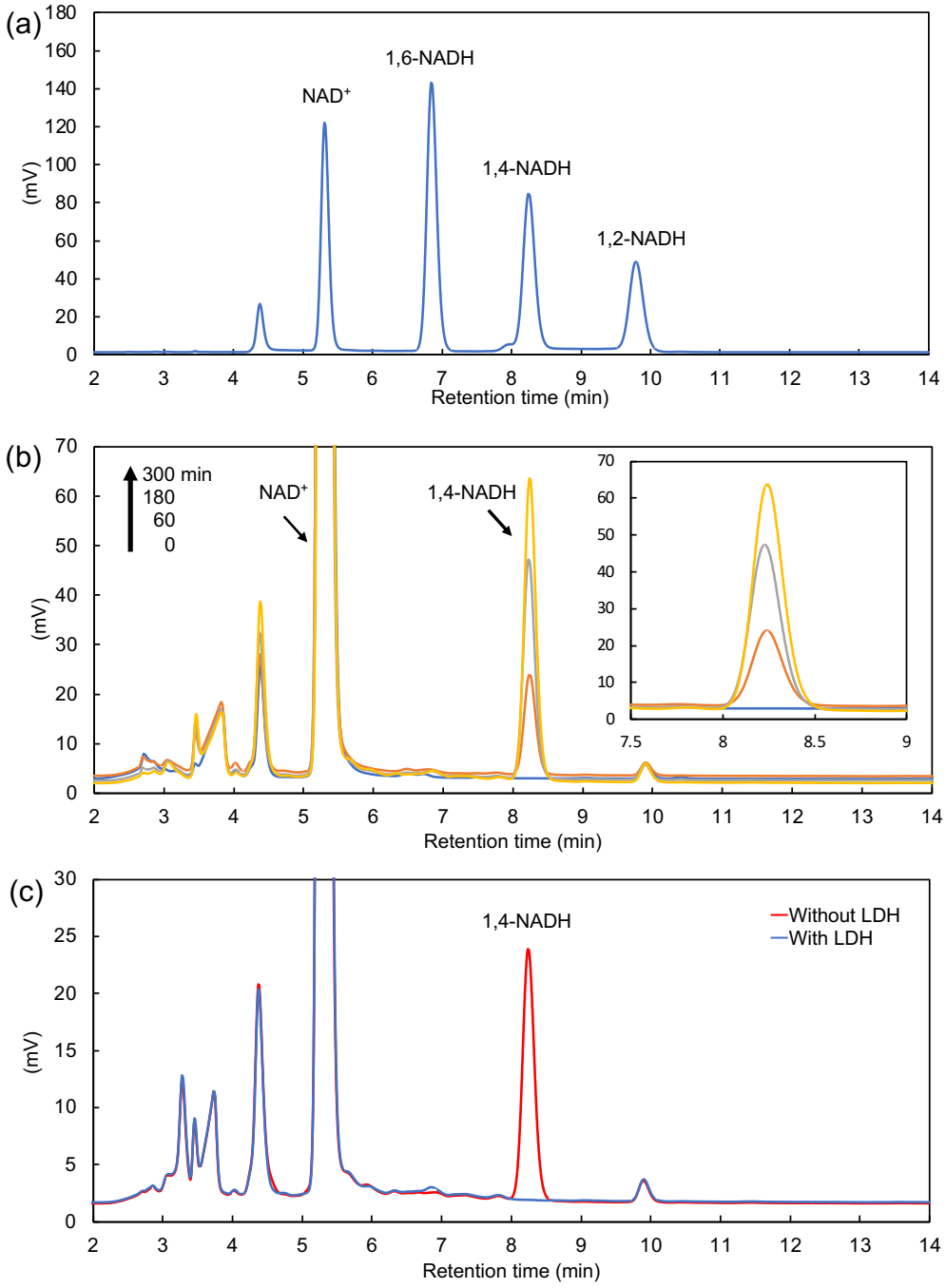

Fig. 3-7. Analytical HPLC chromatograms. (a) After the reduction of NAD^+ with sodium borohydride. (b) Visible-light-driven NAD^+ reduction with the system including TEOA, ZnTPPS, Rh-PVP, and NAD^+. (c) Enzymatic assay for visible-light-driven NAD^+ reduction after 300 min irradiation. A sample solution including TEOA (0.1 M), ZnTPPS (9.5 μM), Rh-PVP (125 μM), pyruvate (2 mM) and LDH (2 U, — or 0 U, —).

borohydride ($E°$ = –1.24 V vs. SHE) yields three products: 1,6-, 1,4-, and 1,2-NADH. The retention times of 1,6-, 1,4-, and 1,2-NADH were 6.8, 8.3, and 9.8 min, respectively. The attributions of 1,2- and 1,6-NADH were made according to a previous report.[45]

Fig. 3-7(b) shows the analytical HPLC chromatograph for each irradiation time of the sample solution of the visible-light-driven NAD^+ reduction using the system constituting TEOA, ZnTPPS, and Rh-PVP. The intensity of the 1,4-NADH peak noticeably increased with irradiation time. By adding LDH and pyruvate to the solution after light irradiation, the intensity of the 1,4-NADH signal decreased, as shown in Fig.3-7(c). On the other hand, changes to the intensities of the 1,2- or 1,6-NADH peaks were not detected.

3.3.4 Bioactivity assay of reduction product of NAD^+

To determine whether the NAD^+ reduction product is 1,4-NADH or NAD dimer, an enzymatic assay was carried out. The enzymatic activity of the reduction product of NAD^+ was validated using an NAD^+-dependent enzyme, lactate dehydrogenase (LDH, EC 1.1.1.27), which catalyzes the reaction given in Eq. 3-1.

$$\text{Pyruvate} + \text{1,4-NADH} \rightarrow \text{L-Lactate} + NAD^+ \quad \text{(Eq. 3-1)}$$

LDH catalyzes the pyruvate reduction to L-lactate with 1,4-NADH oxidation to NAD^+. By adding pyruvate as a substrate along with LDH in 0.4 mL of HEPES-NaOH buffer (pH 7.4) to a 0.4 mL NAD^+ photoreduction solution, the final concentration was adjusted to 2.0 mM of pyruvate and 2 U of LDH. When a system composed of TEOA, ZnTPPS, and Rh-PVP was irradiated with visible light, the absorption maximum at 340 nm of the NAD reduction solution decreased after adding LDH and pyruvate, as shown in Fig. 3-8. The figure shows the different UV–Vis absorption spectral changes of the NAD^+ photoreduction solution in the presence and absence of LDH and pyruvate after different irradiation periods. The difference in the decrease in absorbance at 340 nm indicated the amount of 1,4-NADH production. By measuring the enzymatic-assay solution using ionic chromatography, the concentration of L-lactate production approximately corresponded to the change in absorbance owing to 1,4-NADH consumption. As shown in Fig. 3-4 (c), the

absorption spectra for each irradiation time nearly overlaps the absorption spectra acquired before irradiation. This implied that the reduction product of NAD^+ with Rh-PVP has comparable bioactivity to 1,4-NADH and is competent in assisting the enzymatic synthesis of L-lactate from pyruvate.

On the other hand, in the system consisting of TEOA and ZnTPPS in the absence of Rh-PVP, the absorption at 300–380 nm remained nearly unchanged before

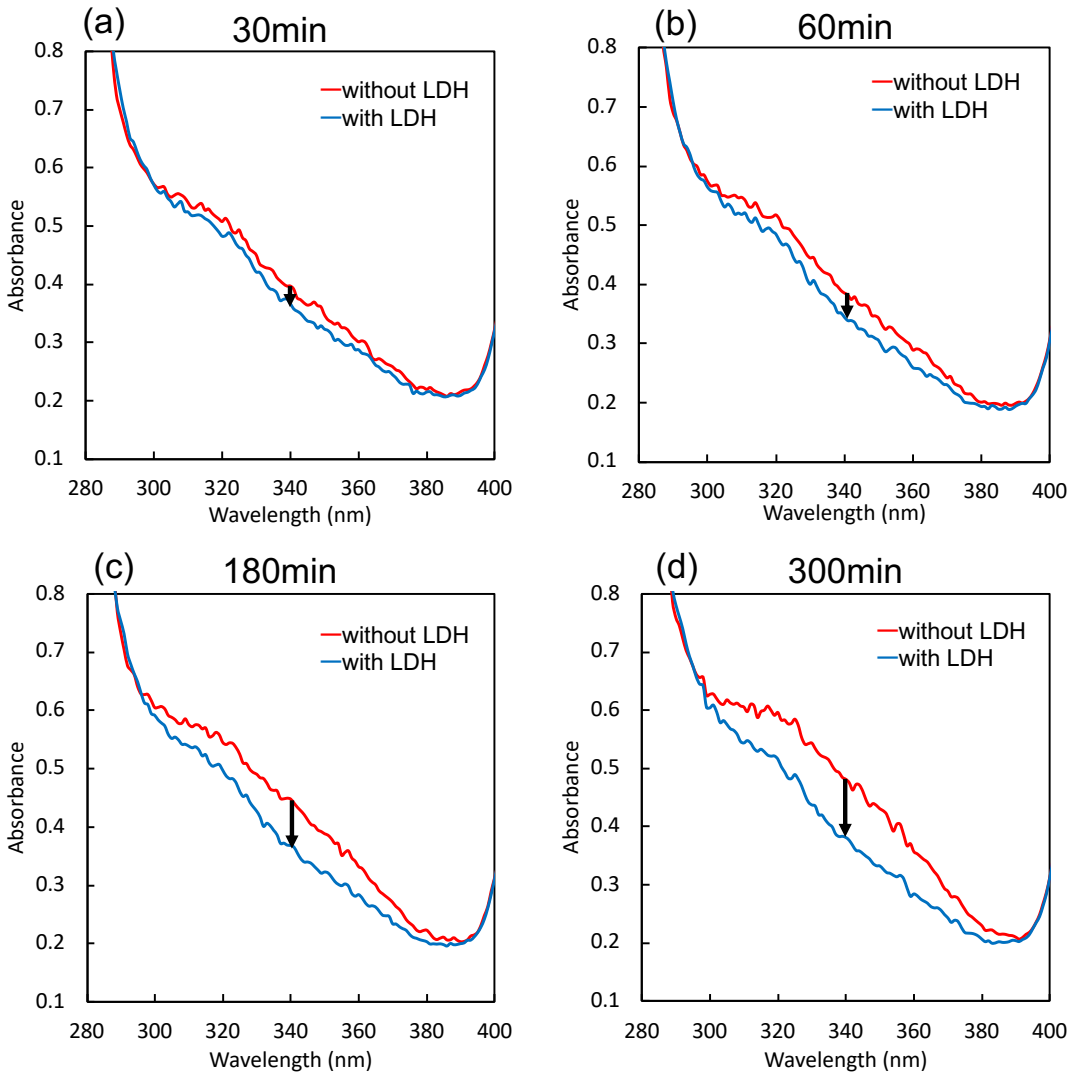

Fig. 3-8. Difference UV-Vis absorption spectral changes of before and after enzymatic assay. A sample solution contained TEOA (0.1 M), ZnTPPS (9.5 μM), Rh-PVP (125 μM), LDH (2 U), and pyruvate (2 mM). (a) 30 min irradiation, (b) 60 min irradiation, (c) 180 min irradiation, (d) 300 min irradiation.

adding LDH and pyruvate, as shown in Fig. 3-5 (c). When the enzymatic assay solution without Rh-PVP was measured using ionic chromatography, no L-lactate production was detected, indicating that the most reduced product of NAD^+ with ZnTPPS was NAD dimer. By photosensitization of ZnTPPS, NAD^+ received one electron and was reduced to NAD radical. NAD radical immediately coupled with another NAD radical to form the NAD dimer with an absorption coefficient of 6650 M^{-1} cm^{-1} at 340 nm. The concentration of NAD dimer after 5 h of irradiation was 41 μM.

When the reaction was performed without being deaerated in the presence of Rh-PVP, the absorption at 300–380 nm was nearly unchanged before adding LDH and pyruvate. By photosensitization of ZnTPPS, NAD^+ was reduced to NAD radical, which immediately coupled with another to form the NAD dimer. Thus, NADH regeneration did not proceed in the presence of oxygen, and deaeration is essential for the system.

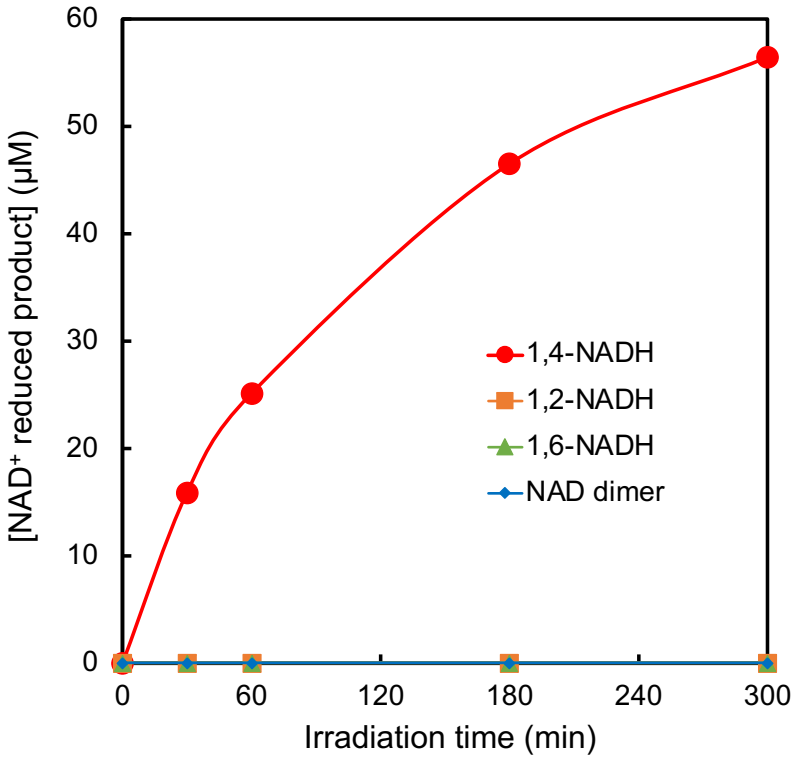

Fig. 3-9. Time course of 1,4-NADH production with the system of TEOA, ZnTPPS, Rh-PVP, and NAD^+ in HEPES-NaOH buffer under continuous irradiation.

The results of HPLC and enzymatic assay indicated that the reduction product of NAD^+ with the system of TEOA, ZnTPPS, and Rh-PVP was only 1,4-NADH. On this basis, the concentration of the reduction product of NAD^+ with visible-light irradiation was determined. The time course of product concentration in the NAD^+ reduction is shown in Fig. 3-9. The concentration of regenerated 1,4-NADH after 5 h of irradiation was 56 μM, and the conversion yield was estimated to be 5.6 %.

3.3.5 The analysis of quenching behavior of ZnTPPS

The electron transfer from the photoexcited state of ZnTPPS (1.0 μM) to Rh-PVP (0–500 μM) was investigated by measuring the fluorescence intensity at 606 and 656 nm by exciting the ZnTPPS signal at 422 nm. The fluorescence spectral changes of ZnTPPS with various concentrations of Rh-PVP is shown in Fig. 3-10. The fluorescence maximum of the ZnTPPS at 606 nm and 656 nm decreased by adding Rh-PVP and with increasing Rh-PVP concentration. The fluorescence of

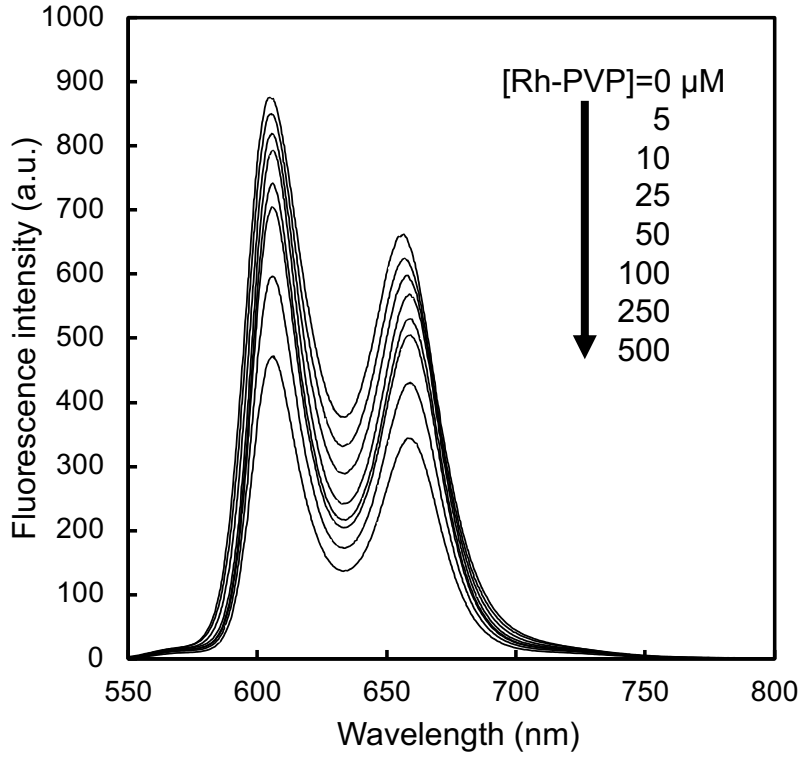

Fig. 3-10. Fluorescence spectra changes of ZnTPPS with Rh-PVP.

ZnTPPS was quenched by Rh-PVP. The relative fluorescence intensity (I_0/I, where I_0 is the intensity in the absence of Rh-PVP) plotted against Rh-PVP concentration shows a non-linear relationship (Fig. 3-1), which was rationalized in terms of the existence of multiple quenching sites. These multiple populations were analyzed using a modified form of the Stern–Volmer equation following Eq. 3-2,[49]

$$\frac{I_0}{I} = \left(\sum \frac{f_n}{1 + K_{SVn}[Q]} \right)^{-1} \quad \text{(Eq. 3-2)}$$

where f_n is the fractional contributions to each quencher accessible site, K_{SVn} is the quenching constant for each site, and Q is the quencher. The best-fit curve obtained when n = 2 is shown in Fig. 3-11. Using a modified form of the Stern–Volmer equation, the K_{SV1} and K_{SV2} values were estimated to be 1.3×10^{-3} and 8.7×10^{-4} μM^{-1}, respectively, and the f_1 and f_2 values were estimated to be 0.898 and 0.102, respectively. The K_{SV} value of MV, widely used as an electron mediator, is 0.12 μM,

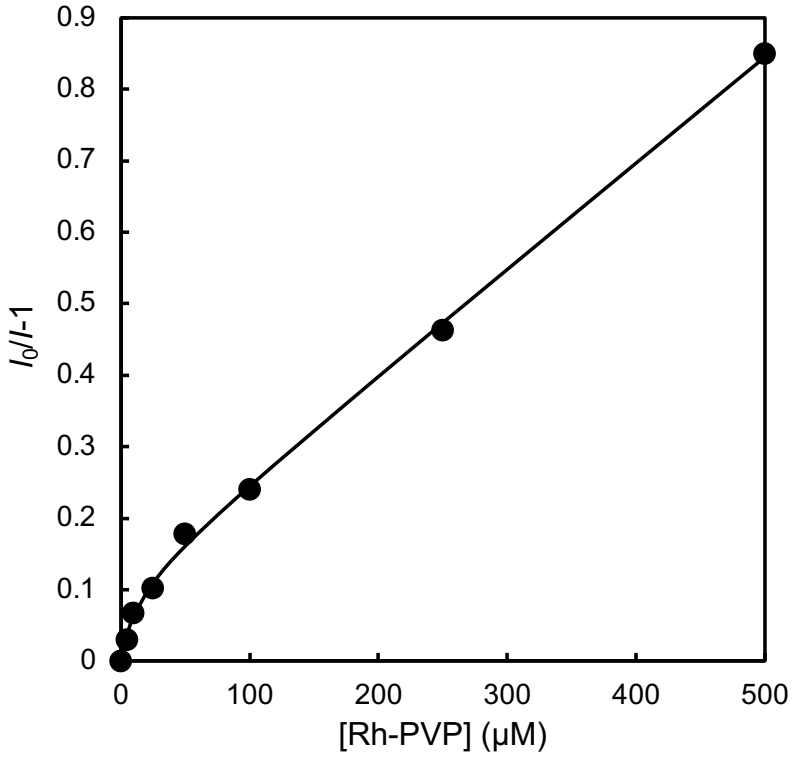

Fig. 3-11. Modified Stern-Volmer plot for the fluorescence quenching of ZnTPPS by Rh-PVP. The excitation and fluorescence wavelength were 422 and 606 nm, respectively.

as estimated in Chapter 2. The K_{SV} values of Rh-PVP are much lower than those of MV. Thus, the Rh-PVP interacts more weakly with ZnTPPS than MV does.

The UV–Vis absorption spectral changes of ZnTPPS (1.0 μM) with addition of Rh-PVP (0-50 μM) is also shown in Fig. 3-12. The absorbance maximum of the ZnTPPS at 422 nm decreased and shifted to the longer wavelength side by adding Rh-PVP, as shown in Fig. 3-12, indicating that ZnTPPS interacted with Rh-PVP and formed a complex.

These results signified static quenching owing to the interaction between ZnTPPS and Rh-PVP without energy transfer. Therefore, the electron transfer from the photoexcited singlet state of ZnTPPS (^{1}ZnTPPS*) to Rh-PVP did not occur, and the photoexcited triplet state of ZnTPPS (^{3}ZnTPPS*) to Rh-PVP proceeded.

On the other hand, no fluorescence quenching by NAD^+ was observed, as shown in Fig. 3-13. Thus, we presumed that the electron transfer from the photoexcited triplet state of ZnTPPS (^{3}ZnTPPS*) to Rh-PVP or NAD^+ occurred.

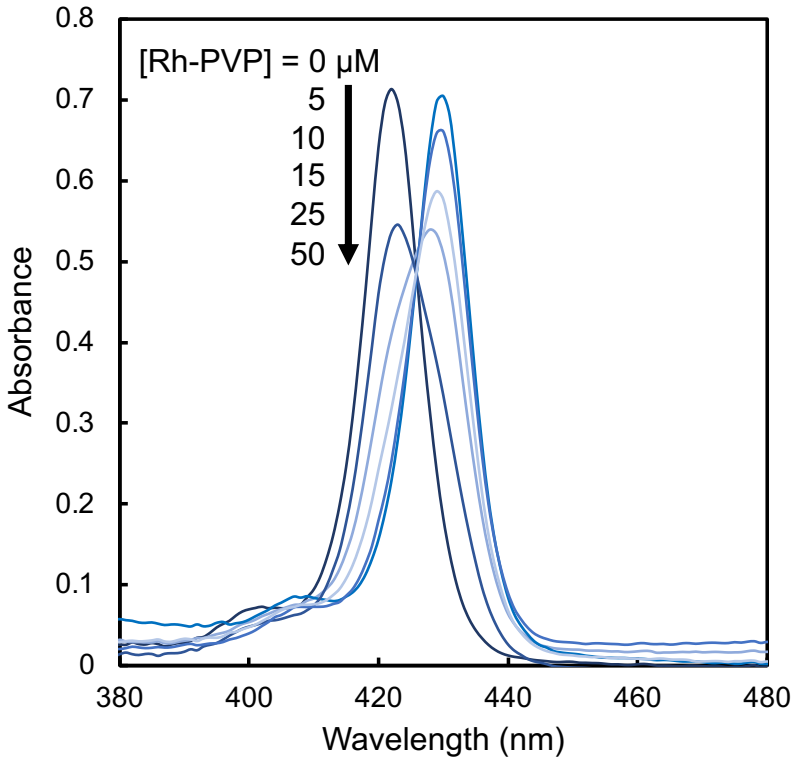

Fig. 3-12. UV-Vis absorption spectral changes of ZnTPPS with addition of Rh-PVP. The sample solution contained ZnTPPS (1.0 μM) and Rh-PVP in HEPES-NaOH buffer (pH 7.4).

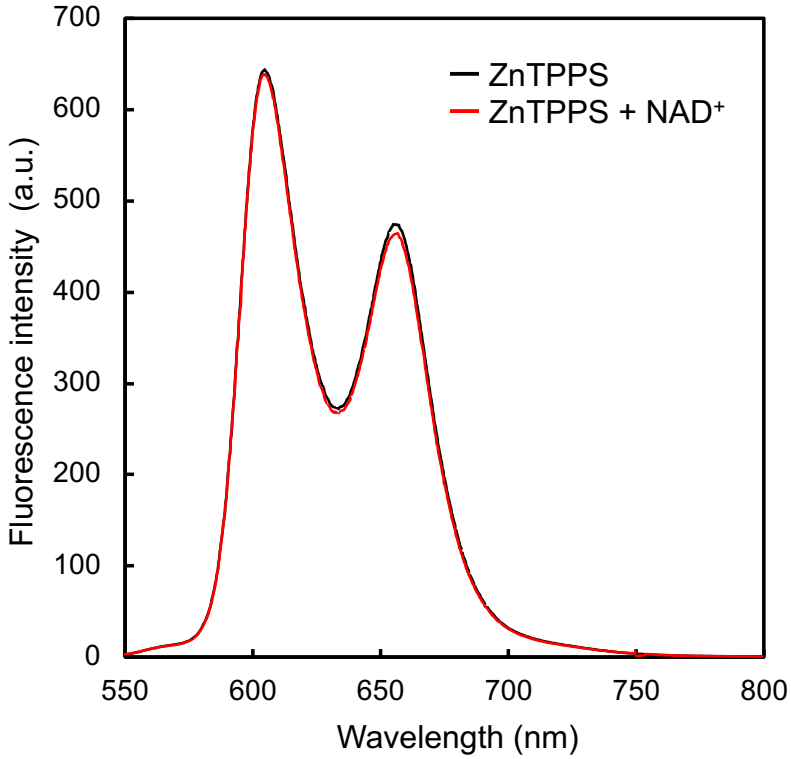

Fig. 3-13. Fluorescence spectra of ZnTPPS (1.0 uM) in the presence and absence of NAD^+ (250μM, —red) in HEPES-NaOH buffer (pH 7.4). The excitation wavelength is 422 nm.

3.3.6 Visible-light-driven pyruvate reduction through NADH regeneration

Scheme 3-2 shows the visible-light-driven pyruvate reduction to lactate with LDH using an NADH regeneration system consisting of TEOA, ZnTPPS, Rh-PVP, NAD^+, and pyruvate. When the sample solution consisting of TEOA, ZnTPPS, Rh-PVP, NAD^+, LDH, and pyruvate in 50 mM HEPES-NaOH buffer (pH 7.4) was irradiated with visible light at 30 °C, lactate was produced, as shown in Fig. 3-14 (●red). The signal intensity of lactate increased with the irradiation time and that of pyruvate decreased (Fig. 3-15). The concentration of lactate produced was estimated to be 305 mM after 5 h of irradiation, and the conversion yield of pyruvate at this time was 15 %. At this point, the absorption band centered at 300–380 nm did not change, as shown Fig. 3-15. This indicated that NAD^+ was reduced to 1,4-NADH

selectively, and the generated 1,4-NADH from NAD^+ was immediately used for pyruvate reduction as a coenzyme for LDH. Hence, the amount of lactate production was expected to correspond to the amount of NADH production. Thus, we estimated the TON and turnover frequency (TOF) of Rh-PVP from the amount of lactate production. In this system, the TOFs of ZnTPPS and Rh-PVP after 1 h of irradiation were estimated to be 5.4 and 0.41 h^{-1}, respectively. The TONs of ZnTPPS and Rh-PVP after 5 h of irradiation were estimated to be 16 and 1.2, respectively. Thus, the catalytic production of NADH proceeded in the system of TEOA, ZnTPPS, Rh-PVP, and NAD^+.

A control experiment performed in the absence of NAD^+ and LDH showed little formation of lactate. The oxidation potential of TEOA was estimated to be 0.87 V (vs. Ag/AgCl),[50] and the redox potential of ^{3}ZnTPPS* (E ($ZnTPPS^+/^3ZnTPPS^*$)) was reported to be –0.75 V (vs. Ag/AgCl).[51] The oxidation potential of ZnTPPS was estimated to be 1.08 V (vs. Ag/AgCl).[51] The reduction potential of pyruvate to lactate was –0.38 V (vs. Ag/ AgCl). The energy diagram for the visible-light-driven pyruvate reduction is shown in Fig. 3-17. Therefore, the direct pyruvate reduction to lactate with the system in the absence of NAD^+ also proceeded. In addition, a visible-light-driven pyruvate reduction system consisting of TEOA, ZnTPPS, MV as an electron mediator, and Pt-PVP was previously reported.[52] In this system, the PVP-dispersed metal nanoparticles catalyzed pyruvate reduction to lactate in the presence of MV. Thus, it is considered that a similar process occurred for the Rh nanoparticles. The

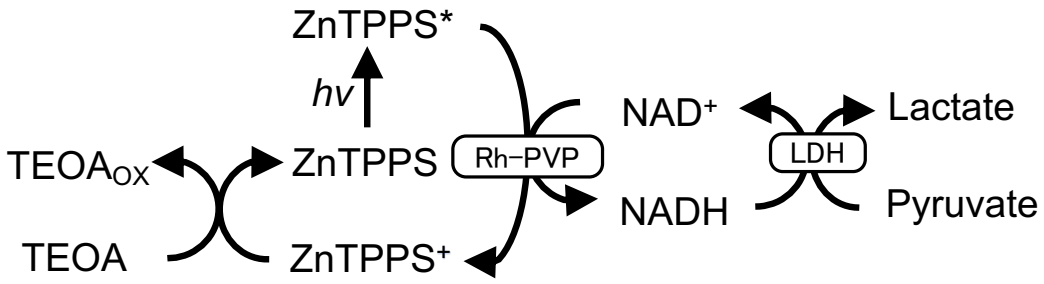

Scheme 3-2. Visible-light-driven pyruvate reduction to lactate using a NADH regeneration system consisting of TEOA, ZnTPPS, Rh-PVP, NAD, LDH, and pyruvate.

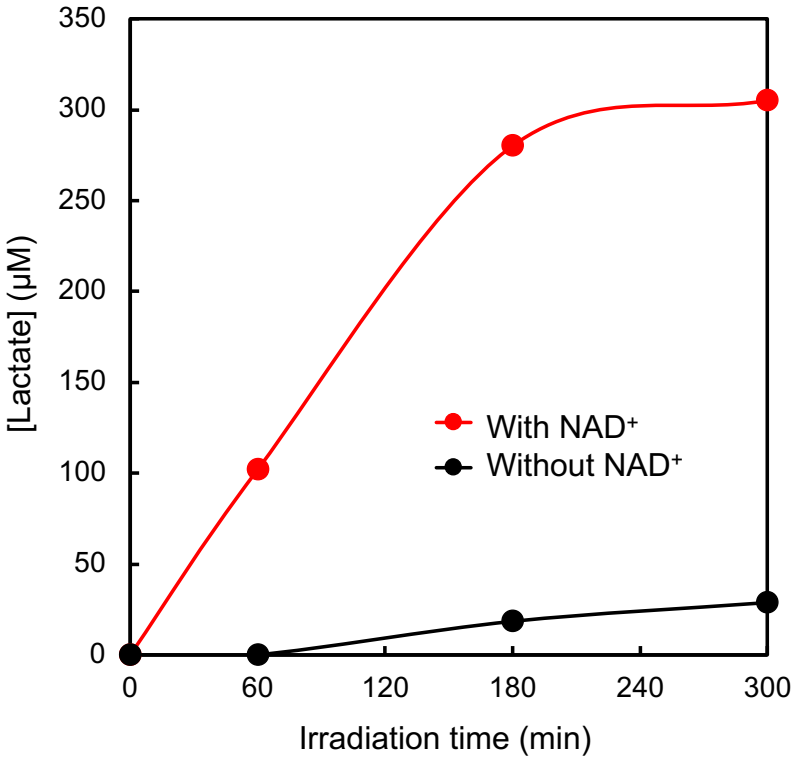

Fig. 3-14. Time course of lactate production with the system of TEOA, ZnTPPS, Rh-PVP, LDH, and pyruvate in HEPES-NaOH buffer under continuous irradiation. (●red) in the presence of NAD^+, (●black) in the absence of NAD^+.

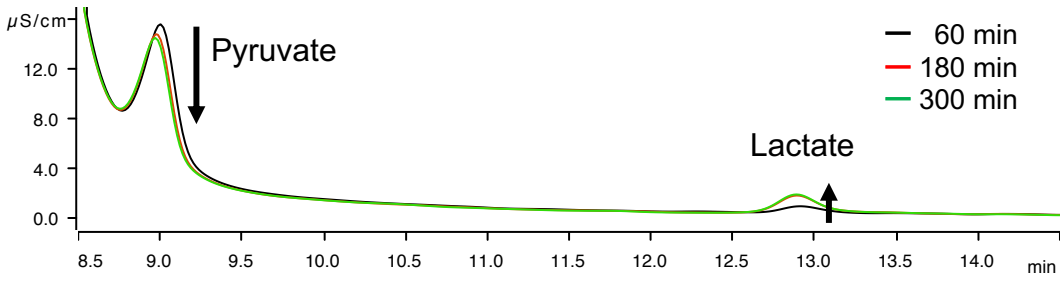

Fig. 3-15. The chromatogram for visible-light-driven pyruvate reduction with the system consisted of TEOA, ZnTPPS, Rh-PVP, NAD^+, LDH, and pyruvate.

concentration of L-lactate with LDH was at least 10-fold the concentration of L-lactate without LDH. Thus, L-lactate production using a system of NAD^+ and LDH proceeded owing to enzymatically pyruvate reduction.

As a control experiment, the sample solution containing TEOA, Rh-PVP, NAD^+, LDH, and pyruvate in the absence of ZnTPPS was irradiated; no L-lactate was produced. Therefore, the enzymatic reaction proceeded with ZnTPPS and Rh-PVP under visible-light irradiation. In the system without Rh-PVP, while the UV–Vis absorption band at 300–380 nm increased, lactate was not produced. This means that NAD^+ was not reduced to the enzyme-active 1,4-NADH but to a NAD dimer (NAD_2) by photosensitization of ZnTPPS. When the reaction mixture containing TEOA, ZnTPPS, Rh-PVP, NAD^+, LDH, and pyruvate in the HEPES-NaOH buffer (pH 7.4) was allowed to react in the dark, the intensity of the absorption band at 300–380 nm did not increase, and L-lactate was not produced. These results support the hypothesis that Rh-PVP catalyzed the reaction of selective NAD^+ reduction to enzyme-active 1,4-NADH with the photosensitization of ZnTPPS.

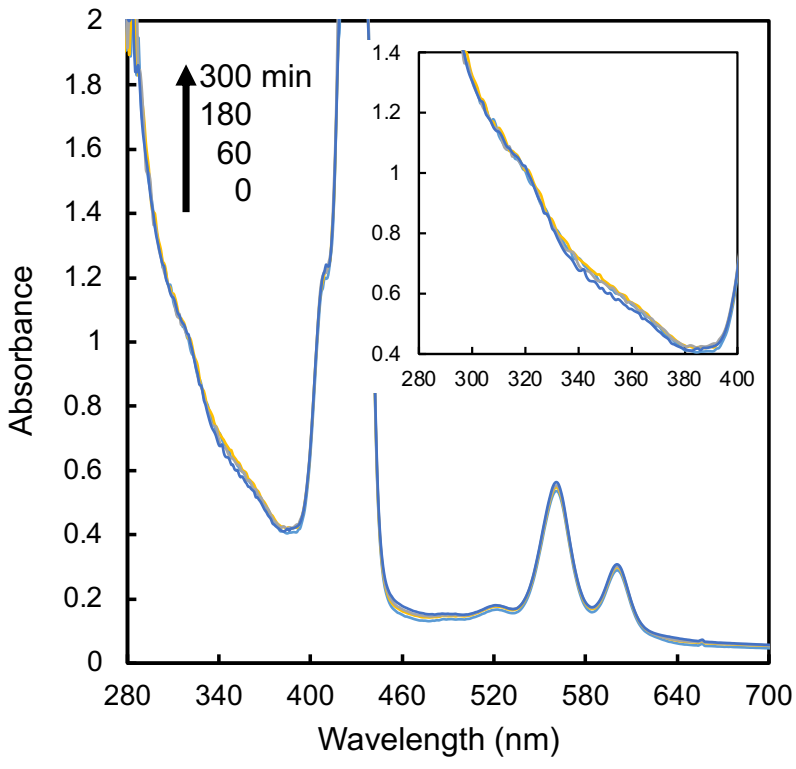

Fig. 3-16. The UV-Vis absorption spectral changes of the reaction mixture for visible-light-driven pyruvate reduction. The system consisted of TEOA, ZnTPPS, Rh-PVP, NAD^+, LDH, and pyruvate.

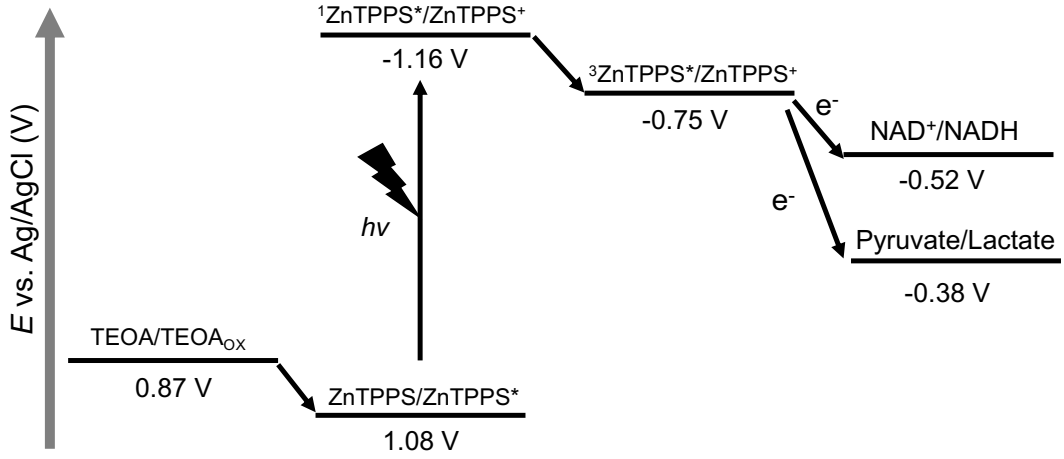

Fig. 3-17. The energy diagram for visible-light-driven pyruvate reduction with the system of TEOA, ZnTPPS.

3.3.7 Proposed mechanism for regioselective NAD^+ reduction with Rh-PVP

Two possible mechanisms for NADH regeneration are proposed in Fig. 3-18. The reduced proton (hydride or H atom) from the aqueous solution at the surface of Rh-PVP can interact with NAD^+. First, NAD^+ is adsorbed onto the surface of Rh-PVP by the carbonyl of the amide, similar to the Rh complex.[11-13,53] The first possible mechanism is shown in Fig. 3-18 (a). A proton in the aqueous solution received an electron from the photoexcited state of ZnTPPS and adsorbed onto the surface of Rh-PVP as a H atom. Furthermore, a H atom received an electron from the photoexcited state of ZnTPPS and could attack the C4 position of nicotinamide as a hydride species, forming 1,4-NADH directly. The hydride transfer step is the key to avoiding formation of the NAD radical intermediate and NAD dimer. This mechanism is similar to the reduction of NAD^+ using sodium borohydride in the sense that the hydride transfer is also the key to avoiding the radical intermediate. The induced electronic effect of the bound carbonyl group at the surface of Rh-PVP may also render the C4 position of nicotinamide more electrophilic toward hydride transfer. In the system using the Rh complex for NADH regeneration, the role of the amide carbonyl at the 3-position of nicotinamide may prevent the occurrence of other

regioselective transition-metal-hydride reactions that afford 1,4-NADH.[51] This selective hydride transfer process is further affected by the induced electron-withdrawing effect of the bound amide group on C4.

Another possible mechanism is shown in Fig. 3-18 (b). A proton in the aqueous solution received an electron from the photoexcited state of ZnTPPS and adsorbed onto the surface of Rh-PVP as a H atom. The interaction of NAD^+ with an absorbed H atom on the surface of Rh-PVP coupled with an electron transferred from ZnTPPS in the photoexcited state. In the previous reports of electrochemical NAD^+ reduction, the adsorbed H atom played a critical role in NADH regeneration.[55-57] The absence of 1,2-, 1,6-NADH and NAD dimer rules out a simple uncoupled sequence of electron and proton transfer.

In the two possible mechanisms, the key step is the adsorption of NAD^+ by the carbonyl of the amide. The adsorption with carbonyl on the surface of Rh-PVP arranges the C4 position of nicotinamide closer to the adsorbed hydrogen (hydride or H atom) on the Rh-PVP surface owing to steric hindrance with the side chain of NAD^+ and PVP. This may help prevent the formation 1,2- or 1,4-NADH.

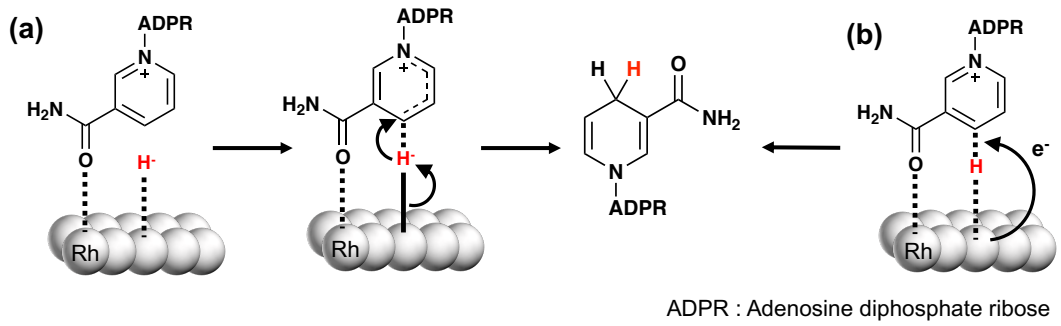

Fig. 3-18. Plausible mechanism of NADH regeneration using Rh-PVP by (a) hydride transfer or (b) adsorbed H/electron transfer.

3.4 Conclusion

Enzymes have high catalytic activities and selectivities in ambient conditions. NADH is widely used as a cofactor in enzymatic redox reactions. In general, the supply of NADH is a major challenge owing to its high cost and low stability. Recently, photochemical NADH regeneration has attracted much attention because solar energy is clean, inexpensive, abundant, and renewable. However, it has been frequently reported that enzymatically inactive byproducts (i.e., 1,2- or 1,6-NADH, and NAD dimer) can be formed in the direct NAD photoreduction.

In this section, the catalytic activity of Rh-PVP for NADH regeneration was investigated. The regioselective reduction of NAD^+ to enzymatically active NADH, (i.e., 1,4-NADH) has been successfully achieved using a system consisting of TEOA as an electron donor, ZnTPPS as a photosensitizer, and Rh-PVP as a catalyst. The reduction product of NAD^+ was solely 1,4-NADH, which validated the enzymatic assay and HPLC analysis.

The fluorescence quenching by Rh-PVP or NAD^+ was also investigated. The fluorescence maximum of ZnTPPS at 606 and 656 nm decreased with the increase in Rh-PVP concentration. The quenching behavior was analyzed using a modified form of the Stern–Volmer equation. From the analysis, we concluded that static quenching proceeded without electron transfer, and an electron transfer from the photoexcited triplet state of ZnTPPS occurred.

In addition, the photochemical conversion system comprising the NADH regeneration system and NAD^+-dependent lactate dehydrogenase was constructed. By using this photoredox system, up to 15 % reduction conversion of pyruvate was achieved after irradiation for 5 h. In this system, the TOFs of ZnTPPS and Rh-PVP after 1 h of irradiation were estimated to be 5.4 and 0.41 h^{-1}, respectively. The TONs of ZnTPPS and Rh-PVP after 5 h of irradiation were estimated to be 16 and 1.2, respectively. NADH regeneration mechanisms were also proposed.

This work provides a platform for using rhodium nanoparticles as highly efficient homogeneous catalysts for regioselective NADH regeneration, which is a key technology in the design of biological solar energy conversion and energy storage devices as well as in artificial photosynthesis.

3.5 References

1. U. T. Bornscheuer, G. W. Huisman, R. J. Kazlauskas, S. Lutz, J. C. Moore and K. Robins, "Engineering the third wave of biocatalysis", *Nature*, 2012, **485**, 185–194.
2. A. T. Martínez, F. J. Ruiz-Dueñas, S. Camarero, A. Serrano, D. Linde, H. Lund, J. Vind. M. Tovborg, O. M. Herold-Majumdar, M. Hofrichter, C. Liers, R. Ullrich, K. Scheibner, G. Sannia, A. Piscitelli, C. Pezzella, M. E. Sener, S. Kılıç, W. J. H. van Berkel. V. Guallar, M. F. Lucas, R. Zuhse, R. Ludwig, F. Hollmann, E. Fernández-Fueyo, E. Record, C. B. Faulds, M. Tortajada, I. Winckelmann, J.-A. Rasmussen. M. Gelo-Pujic, A. Gutiérrez, J. C. del Río, J. Rencoret and M. Alcalde, "Oxidoreductases on their way to industrial biotransformations", *Biotechnol. Adv.*, 2017, **35**, 815–831.
3. L. S. Vidal, C. L. Kelly, P. M. Mordaka and J. T. Heap, "Review of NAD(P)H-dependent oxidoreductases: Properties, engineering and application", *Biochim. Biophys. Acta, Proteins Proteomics*, 2018, **1866**, 327–347.
4. J. K. B. Cahn, C. A. Werlang, A. Baumschlager, S. Brinkmann-Chen, S. L. Mayo and F. H. Arnold, "A General Tool for Engineering the NAD/NADP Cofactor Preference of Oxidoreductases", *ACS Synth. Biol.*, 2017, **6**, 326–333.
5. X. Wang, T. Saba, H. H. P. Yiu, R. F. Howe, J. A. Anderson and J. Shi, "Cofactor NAD(P)H Regeneration Inspired by Heterogeneous Pathways", *Chem*, 2017, **2**, 621–654.
6. H. Wu, C. Tian, X. Song, C. Liu, D. Yanga and Z. Jiang, "Methods for the regeneration of nicotinamidecoenzymes", *Green Chem.*, 2013, **15**, 1773–1789.
7. Y. Zhang, Y. Zhao, R. Li and J. Liu, "Bioinspired NADH Regeneration Based on Conjugated Photocatalytic Systems", *Sol. RRL*, 2021, **5**, 2000339.
8. J. Kiwi, "Photochemical generation of reduced β-nicotinamide-adenine dinucleotide (induced by visible light)", *J. Photochemistry*, 1981, **16**, 193–202.
9. R. Wienkamp and E. Steckhan, "Selective Generation of NADH by Visible Light", *Angew. Chem. Int. Ed.*, 1983, **22**, 497.

10. S. Immanuel, R. Sivasubramanian, R. Gul and M. A. Dar, “Recent Progress and Perspectives on Electrochemical Regeneration of Reduced Nicotinamide Adenine Dinucleotide (NADH)”, *Chem. - Asian J.*, 2020, **15**, 4256–4270.
11. F. Hollmann, I. W. C. E. Arends and K. Buehler, “Biocatalytic Redox Reactions for Organic Synthesis: Nonconventional Regeneration Methods”, *ChemCatChem*, 2010, **2**, 762–782.
12. C. S. Morrison, W. B. Armiger, D. R. Dodds, J. S. Dordick and M. A. G. Koffas, “Improved strategies for electrochemical 1,4-NAD(P)H_2 regeneration: A new era of bioreactors for industrial biocatalysis”, *Biotechnol. Adv.*, 2018, **36**, 120–131
13. S. Fukuzumi, Y.-M. Lee and W. Nam, “Catalytic recycling of NAD(P)H”, *J. Inorg. Biochem.*, 2019, **199**, 110777.
14. R. Ruppert, S. Herrmann and E. Steckhan, “Efficient indirect electrochemical in-situ regeneration of nadh:electrochemically driven enzymatic reduction of pyruvate catalyzed by d-ldh”, *Tetrahedron Lett.*, 1987, **28**, 6583–6586.
15. E. Steckhan, S. Herrmann, R. Ruppert, J. Tho¨mmes and C. Wandrey, “Continuous Generation of NADH from NAD⊕ and Formate Using a Homogeneous Catalyst with Enhanced Molecular Weight in a Membrane Reactor”, *Angew. Chem., Int. Ed. Engl.*, 1990, **29**, 388–390.
16. H. C. Lo, O. Buriez, J. B. Kerr and R. H. Fish, “Regioselective Reduction of NAD^+ Models with $[Cp^*Rh(bpy)H]^+$: Structure-Activity Relationships and Mechanistic Aspects in the Formation of the 1,4-NADH Derivatives”, *Angew. Chem., Int. Ed.*, 1999, **38**, 1429–1432.
17. H. C. Lo, C. Leiva, O. Buriez, J. B. Kerr, M. M. Olmstead and R. H. Fish, “Bioorganometallic chemistry. 13. Regioselective reduction of NAD^+ models, 1-benzylnicotinamde triflate and beta-nicotinamide ribose-5'-methyl phosphate, with in situ generated $[CpRh(Bpy)H]^+$: structure-activity relationships, kinetics, and mechanistic aspects in the formation of the 1,4-NADH derivatives”, *Inorg. Chem.*, 2001, **40**, 6705–6716.
18. C. L. Pitman, O. N. L. Finster and A. J. M. Miller, “Cyclopentadiene-mediated hydride transfer from rhodium complexes”, *Chem. Commun.*, 2016, **52**, 9105–9108.

19. R. Ruppert, S. Herrmann and E. Steckhan, “Very efficient reduction of NAD(P)$^+$ with formate catalysed by cationic rhodium complexes”, *J. Chem. Soc., Chem. Commun.*, 1988, 1150–1151.
20. J. Canivet, G. Süss-Fink and P. Štěpnička, “Water-Soluble Phenanthroline Complexes of Rhodium, Iridium and Ruthenium for the Regeneration of NADH in the Enzymatic Reduction of Ketones”, *Eur. J. Inorg. Chem.*, 2007, **2007**, 4736–4742.
21. D. Sivanesan and S. Yoon, “Functionalized bipyridyl rhodium complex capable of electrode attachment for regeneration of NADH”, *Polyhedron*, 2013, **57**, 52–56.
22. F. Hildebrand, C. Kohlmann, A. Franz and S. Lütz, “Synthesis, Characterization and Application of New Rhodium Complexes for Indirect Electrochemical Cofactor Regeneration”, *Adv. Synth. Catal*., 2008, **350**, 909–918.
23. T. Saba, J. Li, J. W. H. Burnett, R. F. Howe, P. N. Kechagiopoulos and X. Wang, “NADH Regeneration: A Case Study of Pt-Catalyzed NAD$^+$ Reduction with H_2”, *ACS Catal.*, 2021, **11**, 283–289.
24. J. W. H. Burnett, R. F. Howe and X. Wang, “Cofactor NAD(P)H Regeneration: How Selective Are the Reactions?”, *Trends Chem.*, 2020, **2**, 488–492.
25. D. Mandler and I. Willner, “Solar Light Induced Formation of Chiral 2-Butanol in an Enzyme-Catalyzed Chemical System”, *J. Am. Chem. Soc.*, 1984, **106**, 5352–5353.
26. I. Willner and D. Mandler, “Enzyme catalyzed biotransformations through photochemical regeneration of nicotinamide cofactors”, *Enzyme Microb. Technol.*, 1989, **11**, 467–483.
27. M. Grätzel, “Artificial photosynthesis: water cleavage into hydrogen and oxygen by visible light”, *Acc. Chem. Res.*, 1981, **14**, 376–384.
28. G. Kurisu, M. Kusunoki, E. Katoh, T. Yamazaki, K. Teshima, Y Onda, Y. Kimata-Ariga and T. Hase, “Structure of the electron transfer complex between ferredoxin and ferredoxin-NADP$^+$ reductase”, *Nat. Struct. Mol. Biol.*, 2001, **8,** 117–121.

29. P. A. Karplus, M. J. Daniels and J. R. Herriott, “Atomic Structure of Ferredoxin-$NADP^+$ Reductase: Prototype for a Structurally Novel Flavoenzyme Family”, *Science*, 1991, **251**, 60–66.
30. M. Ito and T. Kuwana, “Spectroelectrochemical study of indirect reduction of triphosphopyridine nucleotide: I. Methyl viologen, ferredoxin-TPN-reductase and TPN”, *J. Electroanal. Chem. Interfacial Electrochem*, 1971, **32**, 415–425.
31. Y. Wang, J. Sun, H. Zhang, Z. Zhao and W. Liu, “Tetra(4-carboxyphenyl)porphyrin for efficient cofactor regeneration under visible light and its immobilization”, *Catal. Sci. Technol.*, 2018, **8**, 2578–2587.
32. Y. Wang, Z. Zhao, R. Zhou and W. Liu, “Optimization of a photoregeneration system for NADH using pristine TiO_2 as a catalyst”, *J. Mol. Cat., B Enzym.*, 2016, **133**, S188–S193.
33. F. Gu. Y. Wang, Z. Meng, W. Liu and L. Qiu, “A coupled photocatalytic/enzymatic system for sustainable conversion of CO_2 to formate”, *Catal. Commun.*, 2020, **136**, 105903.
34. H. Hirai and J. Macromol. “Formation and Catalytic Functionality of Synthetic Polymer-Noble Metal Colloid”, *Sci., Chem.*, 1979, **13**, 633–649.
35. H. Hirai, Y. Nakao and N. Toshima, “Preparation of Colloidal Transition Metals in Polymers by Reduction with Alcohols or Ethers”, *J. Marcromol. Sci. Chem. A Chem.*, 1979, **13**, 727–750.
36. H. Hirai, Y. Nakao and N. Toshima, “Preparation of Colloidal Rhodium in Poly(vinyl Alcohol) by Reduction with Methanol”, *J. Marcromol. Sci. Chem. A*, 1978, **12**, 1117–1141.
37. Y. Huang, J. Chen, H. Chen, R. Li, Y. Li, L. Min and X. Li, “Enantioselective hydrogenation of ethyl pyruvate catalyzed by PVP-stabilized rhodium nanoclusters”, *J. Mol. Catal. A: Chem.*, 2001, **170**, 143–146.
38. J.-L. Pellegatta, C. Blandy, V. Collière, R. Choukroun, B. Chaudret, P. Cheng and K. Philippot, “Catalytic investigation of rhodium nanoparticles in hydrogenation of benzene and phenylacetylene”, *J. Mol. Catal. A: Chem.*, 2002, **178**, 55–61.

39. 37. T. Ashida, K. Miura, T. Nomoto, S. Yagi, H. Sumida, G. Kutluk, K. Soda, H. Namatame and M. Taniguchi, “Synthesis and characterization of Rh(PVP) nanoparticles studied by XPS and NEXAFS”, *Surf. Sci.*, 2007, **601**, 3898–3901.
40. C. Chaudhari, H. Imatome, Y. Nishida, K. Sato and K. Nagaoka, “Recyclable Rh-PVP nanoparticles catalyzed hydrogenation of benzoic acid derivatives and quinolines under solvent-free conditions”, *Catal. Commun*., 2019, **126**, 55–60.
41. Y. Nishida, C. Chaudhari, H. Imatome, K. Sato and K. Nagaoka, “Selective Hydrogenation of Nitriles to Secondary Imines over Rh-PVP Catalyst under Mild Conditions”, *Chem. Lett.*, 2018, **47**, 938–940.
42. Y. Amao, “Solar Fuel Production Based on the Artificial Photosynthesis System”, *ChemCatChem*, 2011, **3**, 458–474.
43. E. B. Fleischer and S. K. Cheung, “Mechanisms of Reduction of Cobaltic Porphyrins with Various Reducing Agents”, *J. Am. Chem. Soc.*, 1976, **98**, 8381–8387.
44. Y. Amao and I. Okura, “Effective photoinduced hydrogen evolution with hydrogenase in surfactant micelles”, *J. Mol. Catal. A: Chem.*, 1996, **105**, 125–130.
45. B. A. Beaupre, M. R. Hoag, J. Roman, F. H. Försterling and G. R. Moran, “Metabolic function for human renalase: oxidation of isomeric forms of β-NAD(P)H that are inhibitory to primary metabolism”, *Biochemistry,* 2015, **54**, 795–806.
46. Wako Organic Square No.47, p10.
47. Wako Organic Square No.54, p5 (DECEMBER,2015).
48. J. A. Creighton and D. G. Eadon, “Ultraviolet–visible absorption spectra of the colloidal metallic elements”, *J. Chem. Soc., Faraday Trans.*, 1991, **87**, 3881–3891.
49. J. N. Demas, B. A. DeGraff and P. B. Coleman, “Oxygen Sensors Based on Luminescence Quenching”, *Anal. Chem.*, 1999, **71**, 793A–800A.
50. A. M. Manke, K. Geisel, A. Fetzer and P. Kurz, “A water-soluble tin(IV) porphyrin as a bioinspired photosensitiser for light-driven proton-reduction”, *Phys. Chem. Chem. Phys.*, 2014, **16**, 12029–12042.

51. K. Kalyanasundaram and M. Neumann-Spallart, “Photophysical and redox properties of water-soluble porphyrins in aqueous media”, *J. Phys. Chem.*, 1982, **86**, 5163–5169.
52. Y. Kita and Y. Amao, “Visible-light driven redox system of water-soluble zinc porphyrin and platinum nanoparticles for selective reduction of pyruvate to lactate”, *New J. Chem.*, 2021, **45**, 11461–11465.
53. V. Ganesan, D. Sivanesan and S. Yoon, “Correlation between the Structure and Catalytic Activity of [Cp*Rh(Substituted Bipyridine)] Complexes for NADH Regeneration”, *Inorg. Chem.*, 2017, **56**, 1366–1374.
54. R. T. Hembre and S. McQueen, “Hydrogenase Enzyme Reactivity Modeling with a Transition-Metal Dihydrogen Complex”, *J. Am. Chem. Soc.*, 1994, **116**, 2141–2142.
55. I. Ali, T. Khan and S. Omanovic, “Direct electrochemical regeneration of the cofactor NADH on bare Ti, Ni, Co and Cd electrodes: The influence of electrode potential and electrode material”, *J. Mol. Catal. A: Chem.*, 2014, **387**, 86–91.
56. I. Ali, A. Gill and S. Omanovic, “Direct electrochemical regeneration of the enzymatic cofactor 1,4-NADH employing nano-patterned glassy carbon/Pt and glassy carbon/Ni electrodes”, *Chem. Eng. J.*, 2012, **188**, 173–180.
57. N. Ullah, I. Ali and S. Omanovic, “Direct electrocatalytic reduction of coenzyme NAD^+ to enzymatically-active 1,4-NADH employing an iridium/ruthenium-oxide electrode”, *Mat. Chem. Phys.*, 2015, **149-150**, 413–417.

Chapter 4

Application of visible-light-driven NADH regeneration system to enzymatic reactions

4.1 Introduction

In Chapter 2, a visible-light-driven C–C bond formation system for CO_2 and pyruvate with ME was designed using PV derivatives as an artificial coenzyme. Although PV derivatives were useful coenzymes for ME, the application of PV derivatives to other enzymes was limited. Therefore, the natural coenzyme NADH and NAD^+ reduction to NADH was focused upon. In general, in visible-light-driven enzymatic redox reactions, the NAD^+/NADH redox cycles with FNR or metal complexes as catalysts are widely used.[1,2] As a novel and simple photoredox system, a system that could accomplish regioselective NAD^+ reduction to NADH with Rh-PVP was constructed for use in various enzymatic reactions by harnessing visible-light energy (Chapter 3).

This chapter explores visible-light-driven enzymatic reactions using the NADH regeneration system. In particular, biocatalytic C–C bond formation with CO_2 was attempted. First, the effect of the electron donor on NADH regeneration, and the optimal concentrations of an electron donor and ZnTPPS, Rh-PVP were determined. Next, the catalytic activity of Rh-PVP was compared with that of $[Cp^*Rh(bpy)(H_2O)]^{2+}$, a widely used catalyst for NADH regeneration. Photochemical NAD^+ reduction was also tested in the presence of TiO_2 as a photosensitizer. In addition, the dependence of NADH regeneration on the wavelength of photo-irradiation was studied.

By using the optimized NADH regeneration system, enzymatic reactions using visible-light energy were performed. The various enzymatic reactions with NAD^+-dependent dehydrogenases are shown in Fig. 4-1. As models of enantioselective synthesis, the NADH regeneration system with visible-light energy was applied in the enzymatic reduction of pyruvate to L-lactate using LDH as well as the acetoacetate reduction to D-3-hydroxybutyrate using D-3-hydroxybutyrate dehydrogenase (HBDH). As a model of C–C bond formation from CO_2, a regioselective NAD^+ reduction system was applied to pyruvate carboxylation with CO_2 to L-malate with malate dehydrogenase (decarboxylating; MDH).

In addition, to improve the catalytic activity of ME in the pyruvate carboxylation with CO_2, the effect of metal ions on the ME was studied. In general,

ME requires the divalent metal ion.[3-7] Therefore, the catalytic activity of ME was studied using various metal ions, including trivalent metal ions.

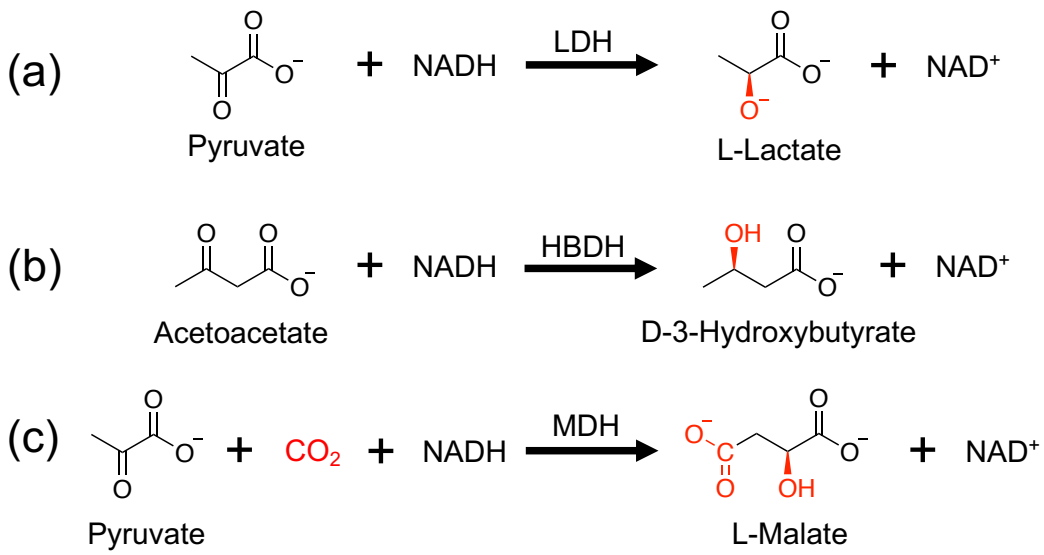

Fig. 4-1. Enzymatic reactions with the (a) L-lactate (LDH), (b) D-3-hydroxybutyrate (HBDH), and (c) malate dehydrogenase (decarboxylating) (MDH).

4.2 Experimental

4.2.1 Materials

β-Nicotinamide adenine dinucleotide oxidized form (NAD^+), β-nicotinamide adenine dinucleotide phosphate oxidized form ($NADP^+$), β-nicotinamide adenine dinucleotide phosphate reduced form (NADPH), and L-lactate dehydrogenase from pig heart (LDH, EC 1.1.1.27) were purchased from Oriental Yeast Co., Ltd. (Tokyo, Japan). Triethanolamine (TEOA), sodium pyruvate, sodium hydrogen carbonate, methanol, diethyl ether, copper(II) sulfate pentahydrate, $MgCl_2•6H_2O$, $MnCl_2$, $ZnCl_2$, $CoCl_2•6H_2O$, $CaCl_2•2H_2O$, $AlCl_3•6H_2O$, and $FeCl_3•6H_2O$ were obtained from FUJIFILM Wako Pure Chemical Corporation (Osaka, Japan). 4-(2-Hydroxyethyl)-1-piperazineethanesulfonic acid (HEPES) was purchased from NACALAI TESQUE, INC. (Pentamethylcyclopentadienyl) rhodium(III) dichloride dimer ($[Cp^*RhCl_2]_2$) and 2,2'-bipyridyl, D-3-hydroxybutyrate dehydrogenase from *Pseudomonas sp.* (HBDH, EC 1.1.1.30) and lithium acetoacetate were purchased from Tokyo Chemical Industry Co., Ltd. (Tokyo, Japan). Zn(II) meso-tetra(4-sulfonatophenyl) porphine tetrasodium salt (ZnTPPS) was purchased from Frontier Scientific, Inc. Thermostable malate dehydrogenase (Decarboxylating) (MDH, EC 1.1.1.38) was obtained from Thermostable Enzyme Laboratory Co., Ltd. (Kobe, Japan). Malic dehydrogenase (oxalacetate-decarboxylating) from chicken liver (ME, EC 1.1.1.40) was obtained from Sigma-Aldrich. Rh nanoparticles dispersed in polyvinylpyrrolidone (Rh-PVP) was purchased from Renaissance Energy Research (Osaka, Japan). TiO_2 nanoparticle powder (P25) was purchased from Degussa Co., Ltd. All the materials were of analytical grade or the highest grade available and were used as received, without further purification. Ar gas of ultrahigh purity (≧99.9999 %, Grade 1) was supplied by TAIYO NIPPON SANSO CORPORATION (Toyko, Japan). Water was purified using a Milli-Q purification system.

4.2.2 Synthesis of $[Cp^*Rh(bpy)(H_2O)]^{2+}$

The synthesis route of pentamethylcyclopentadienyl(2,2′-bipyridyl) rhodium(III) chloride ([Cp*Rh(bpy)Cl]Cl) is summarized in Scheme 4-1. [Cp*Rh(bpy)Cl]Cl was synthesized according to the published procedure.[8-10] First, $[Cp^*RhCl_2]_2$ (61.8 mg, 0.1 mmol) was added to methanol (4 mL). Second, 2,2′-bipyridine (31.2 mg, 0.2 mmol) was introduced into the above suspension, and an orange homogeneous solution immediately formed. Third, diethyl ether was added dropwise into the solution at 4 °C until orange [Cp*Rh(bpy)Cl]Cl particles precipitated, which were subsequently filtered and dried in a vacuum oven for 3 h at room temperature. Finally, [Cp*Rh(bpy)Cl]Cl was added to HEPES-NaOH buffer and readily hydrolyzed to $[Cp^*Rh(bpy)(H_2O)]^{2+}$.

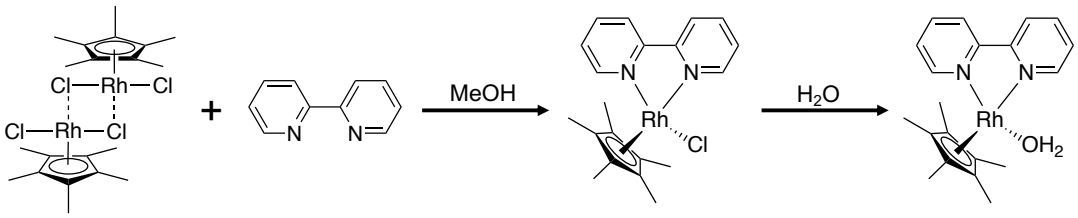

Scheme 4-1. Synthesis scheme of $[Cp^*Rh(bpy)(H_2O)]^{2+}$.

4.2.3 Visible-light-driven NAD^+ reduction

The visible-light-driven NADH regeneration was carried out as follows. A sample solution containing TEOA (0.20 M), ZnTPPS, Rh-PVP, and NAD^+ in 5 mL of 50 mM HEPES-NaOH buffer (pH 7.4) was deaerated by performing six consecutive freeze–pump–thaw cycles and then flushed with Ar gas for 10 min. The sample solution in the cell equipped with a magnetic stirrer was irradiated with a 250 W halogen lamp (TOSHIBA) with a light intensity of 200 J m^{-2} s^{-1} at 30 °C. The outline of the experimental setup for NAD^+ reduction is shown in Fig. 2-3. The production of 1,4-NADH was determined based on the absorption change at 340 nm ($\varepsilon = 6.22 \times 10^3$ cm^{-1} M^{-1})[11,12] using UV–Vis absorption spectroscopy (SHIMADZU, MultiSpec-1500 spectrophotometer).

The enzymatic activity of regenerated NADH was tested as follows. First, a sample containing pyruvate (4.0 mM) and LDH (4.0 U) in 0.4 mL of 50 mM HEPES-NaOH buffer (pH 7.4) was added to 0.4 mL of regenerated NADH in a UV cell. The absorbance of the solution was monitored using UV–Vis absorption spectroscopy.

4.2.4 Photochemical NAD^+ reduction using TiO_2 as a photosensitizer

The photochemical NAD^+ reduction with TiO_2 as a photosensitizer was carried out as follows. First, 7.5 mg of TiO_2 powder was added to 50 mM HEPES-NaOH buffer (pH 7.4) including TEOA in a cell, and then the solution was magnetically stirred for 10 min followed by sonication for 10 min. Next, NAD^+ and Rh-PVP were added. The sample solution containing TEOA (0.20 M), TiO_2 (1.5 mg mL^{-1}), Rh-PVP (50 μM), and NAD^+ (1.0 mM) in 5 mL of 50 mM HEPES-NaOH buffer (pH 7.4) was deaerated over six consecutive freeze–pump–thaw cycles and flushed with Ar gas for 10 min. The sample solution in the cell was stirred and irradiated continuously by a 400 W Xe lamp (SX-UI500XQ, USHIO) at ambient temperature. The light intensity on the surface of the test cell was 80 mW cm^{-2}, measured with a laser power meter (model AN/2; Ophir Optronics, Inc).

The cell solution was periodically sampled and centrifuged for 15 min (KURABO, FR-200). Then, 0.4 mL of supernatant was added to 1.2 mL of HEPES-NaOH buffer (pH 7.4). The absorbance of the solution was measured using UV–Vis absorption spectroscopy (SHIMADZU, MultiSpec-1500 spectrometer). The enzymatic activity of the reduction product of NAD^+ was also tested. The production of 1,4-NADH was determined by the absorption change at 340 nm ($\varepsilon = 6.22 \times 10^3$ cm^{-1} M^{-1}).[11,12]

4.2.5 Irradiation wavelength dependence of NADH regeneration

The apparent quantum yield was calculated using the following equation:

Φ [%] = Amount of NADH production (μmol) × 2 / Irradiated photon (μmol)

Measurements to determine the irradiation wavelength dependence of NADH regeneration were performed under monochromatic irradiation emitted from a Xe lamp (Asahi Spectra Co. Ltd., MAX-303) equipped with bandpass filters (central wavelength: 400, 420, 500, 560, 600, and 700 nm; full-width at half maximum: 10 nm) and a variable neutral density filter. Monochromatic photon fluxes at each wavelength were measured using a photo power meter (Hioki E. E. Co., 3664) equipped with a Si photodiode sensor (Hioki E. E. Co., 9742). The sample solution contained TEOA (200 mM), ZnTPPS (4.6 μM), Rh-PVP (50 μM), and NAD^+ (1.0 mM).

4.2.6 Photochemical conversion using the NADH regeneration system and enzyme

Visible-light-driven conversion was carried out by combining the NADH regeneration system with the enzymes lactate (LDH), 3-hydroxybutyrate (HBDH), and malate (decarboxylating; MDH). The sample solution in the cell equipped with a magnetic stirrer was irradiated with a 250 W halogen lamp (TOSHIBA) with a light intensity of 200 J m^{-2} s^{-1} at 30 °C. The irradiance spectrum of the halogen lamp is shown in Fig. 4-2. UV rays with wavelengths shorter than 390 nm were blocked with a cut-off filter. The concentration of lactate produced in the sample cell was analyzed using an ionic chromatograph (Metrohm Eco IC; electrical conductivity detector) equipped with an ion-exclusion column (Metrohm Metrosep Organic Acid - 250/7.8; column length: 250 × 7.8 mm; composed of a polystyrene/divinylbenzene copolymer with sulfonic acid groups; temperature: 35 °C). Perchloric acid (1.0 mM) and lithium chloride (50 mM) were used as an eluent and regenerant, respectively.

Pyruvate reduction to L-lactate with LDH

Visible-light-driven pyruvate reduction to L-lactate using TEOA, ZnTPPS, Rh-PVP, NAD^+ and LDH was carried out as follows. A sample solution containing TEOA (0.20 M), ZnTPPS (4.9 μM), Rh-PVP (50 μM), NAD^+ (1.0 mM), sodium pyruvate (2.0 mM), and LDH (20 U) in 5 mL of 50 mM HEPES-NaOH buffer (pH 7.4) was deaerated over six freeze–pump–thaw cycles and flushed with Ar gas for 10 min.

D- or L-lactate synthesis was determined using high-performance liquid chromatography (HPLC). The products were analyzed using an HPLC system containing a Shodex ORpak CRX-853 column (8.0 × 50 mm, 6.0 mm particle size), Shimadzu LC-20AD SP pump, and a Shimadzu SPD-20A UV–Vis detector (detection wavelength: 230 nm). An aqueous solution of 4.0 mM $CuSO_4$ was used as the eluent.

Acetoacetate reduction to 3-hydroxybutyrate with HBDH

Visible-light-driven pyruvate reduction to malate with TEOA, ZnTPPS, Rh-PVP, NAD^+, and LDH was carried out as follows. A sample solution containing TEOA (0.20 M), ZnTPPS (4.6 μM), Rh-PVP (50 μM), NAD^+ (1.0 mM), lithium acetate (100 μM), and HBDH (8.5 U) in 5 mL of 50 mM HEPES-NaOH buffer (pH 7.4) was deaerated by performing six freeze–pump–thaw cycles and then flushed with Ar gas for 10 min.

Malate production from pyruvate and CO_2 with MDH

Visible-light-driven pyruvate reduction to malate with TEOA, ZnTPPS, Rh-PVP, NAD^+, and LDH was carried out as follows. A sample solution containing

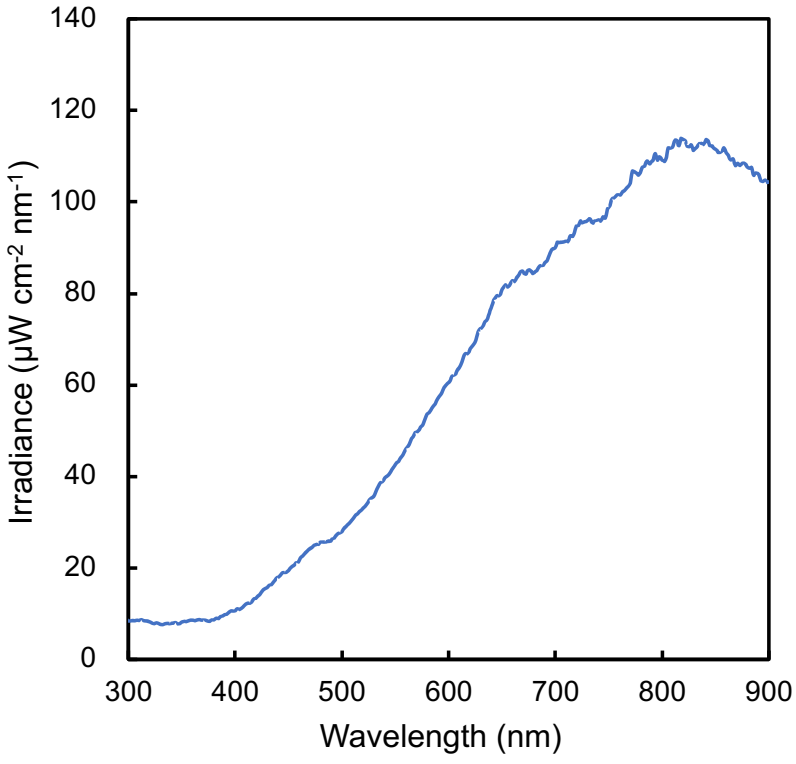

Fig. 4-2. Irradiance spectrum of halogen lamp.

TEOA (0.20 M), ZnTPPS (4.6 μM), Rh-PVP (50 μM), NAD^+ (1.0 mM), sodium pyruvate (10 mM), $NaHCO_3$ (100 mM), $MgCl_2$ (10 mM), and MDH (0.7 U) in 5 mL of 500 mM HEPES-NaOH buffer (pH 7.4) was deaerated over the course of six freeze–pump–thaw cycles and then flushed with Ar gas for 10 min.

4.2.7 Effect of the divalent or trivalent metal ion on MDH

The ME-catalyzed carboxylation of pyruvate with CO_2 to produce malate was investigated under the addition of various metal ions. A sample solution containing NADPH (160 mM), ME (0.95 μM; 2U), sodium pyruvate (10 mM), sodium bicarbonate (10 mM), and metal (Mg^{2+}, Mn^{2+}, Zn^{2+}, Co^{2+}, Ca^{2+}, Fe^{3+} or Al^{3+}) chloride (10 μM) in HEPES-NaOH buffer (pH 7.4) was reacted for 10 min at 30 °C. The apparent malate concentration, as the equivalent of the reduced concentration of NADPH during the reaction, was estimated from the absorbance change at 340 nm in the UV–Vis spectra (SHIMADZU, MultiSpec-1500). The molar absorption coefficient of NADPH was ε_{340} = 6200 M^{-1} cm^{-1}.[11,12] The initial apparent rate of malate production (v_{malate}) was estimated from the gradient of the NADPH consumption up to 10 min of incubation.

In addition, the ME-catalyzed pyruvate production from malate was investigated under the addition of various metal ions. A sample solution consisting of $NADP^+$ (320 μM), sodium L-malate (2 mM), ME (0.95 μM; 2 U), and metal (Mg^{2+}, Mn^{2+}, Zn^{2+}, Co^{2+}, Ca^{2+}, Fe^{3+} or Al^{3+}) chloride (10 μM) in HEPES-NaOH buffer (pH 7.4) was reacted for 10 min at 30 °C. The apparent pyruvate concentration, as the equivalent of the concentration of NADPH produced during the reaction, was also estimated from the absorbance change at 340 nm using UV–Vis absorption spectroscopy. The molar absorption coefficient of NADPH was ε_{340} = 6200 M^{-1} cm^{-1}.[12] The initial apparent rate of pyruvate production ($v_{pyruvatee}$) was estimated from the gradient of the NADPH production up to 10 min of incubation.

4.3 Results and discussion

4.3.1 Optimization of a NADH regeneration system consisting of an electron donor, ZnTPPS, and Rh-PVP

Effect of the electron donor on NADH regeneration

Electron donors are necessary for the stability of many photosensitizers in common photoredox systems.[13] Hydrogen is an attractive electron donor owing to its strong reducibility. Although hydrogen is clean and abundant, it is easily leaked.[14] 2-Mercaptoethanol also has strong reducibility, but it is toxic and expensive. Considering facile handling, environmental compatibility, and low cost, several types of electron donor were selected, including EDTA, TEOA, DEOA, NTA, TEA, and L-ascorbate. Their chemical structures are shown in Fig. 4-3. NADH production after 300 min of irradiation with different electron donors is shown in Fig. 4-4. A sample solution consisted of an electron donor (200 mM), ZnTPPS (4.6 μM), Rh-PVP (50 μM), and NAD^+ (1.0 mM) in the pH 7.4 HEPS-NaOH buffer. When using either EDTA or TEOA, the NADH production after 300 min irradiation was estimated to be 51 and 49 μM, respectively. Using DEOA, NTA, and TEA, NADH production

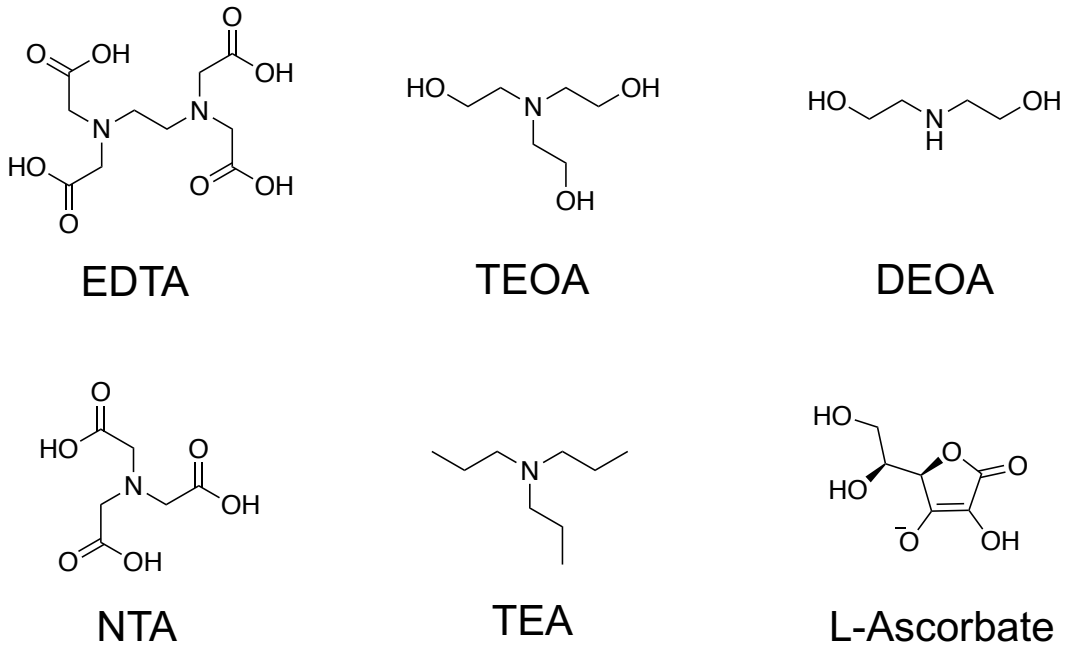

Fig. 4-3. The chemical structure of electron donors.

was lower than by using EFTA and TEOA. On the other hand, by using L-ascorbate, a low amount of NADH was measured. The nitrogen atom of these electron donors might easily coordinate with water-soluble porphyrin through non-covalent interactions to achieve intramolecular transfer of electrons.[15] Although the NADH yield when EDTA was used was slightly higher than that for TEOA, ZnTPPS decomposed with increasing irradiation time in the case of EDTA. In addition, EDTA is expected to chelate, forming a metal-ion complex, which is a cofactor for enzymes. Thus, TEOA was selected as the electron donor for the visible-light-driven NADH regeneration.

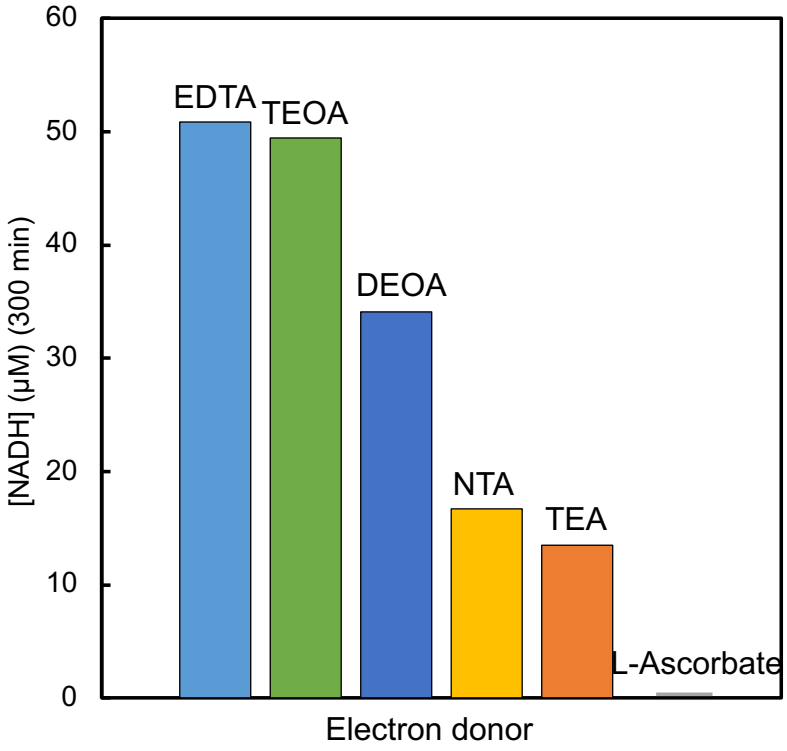

Fig. 4-4. The concentration of NADH after 300 min irradiation with different electron mediators.

Effect of the concentration of TEOA as an electron donor

Fig. 4-5 shows the effect of the concentration of TEOA on NADH reduction. A sample solution consisted of TEOA (0-400 mM), ZnTPPS (4.6 μM), Rh-PVP (50 μM), and NAD^+ (1.0 mM). Fig. 4-5 shows the NADH concentration after 300 min

irradiation with visible light. When the concentration TEOA was increased to 200 mM, the NADH concentration after 300 min irradiation reached 49 μM. When the TEOA concentration was further increased (>200 mM), NADH production decreased. The role of the electron donor is to transfer the electrons to the ground-state acceptor and prevent the recombination of charges. Thus, the efficiency of photo-generated electron utilization is low when the concentration of an electron donor is low. Therefore, NADH production was low at a lower TEOA concentration. On the other hand, a large amount of photo-generated electrons associated with a higher TEOA concentration will cause the reoxidation of NADH.[16,17] Thus, the optimal concentration of TEOA for NADH regeneration was estimated to be 200 mM.

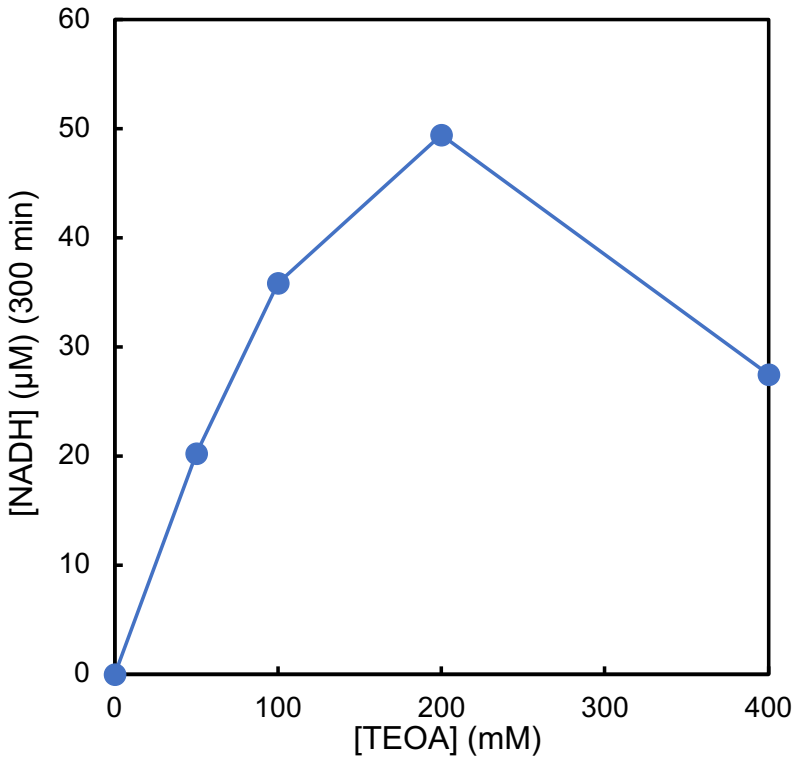

Fig. 4-5. Effect of the TEOA concentration on the NADH yield after 300 min irradiation

Effects of the concentration of ZnTPPS as a photosensitizer and of the Rh-PVP as a catalyst

Fig. 4-6 shows the effect of the ZnTPPS concentration on the NADH yield after 30 min of irradiation with visible light. The sample solution contained TEOA (200 mM), ZnTPPS (0-19 μM), Rh-PVP (250 μM), and NAD^+ (1.0 mM) in pH 7.4 HEPES-NaOH buffer. When the concentration of ZnTPPS was increased to 10 μM, that of NADH reached 17 μM after 30 min of irradiation. When the concentration of ZnTPPS was further increased from 10 to 19 μM, the concentration of NADH production after 30 min of irradiation remained almost unchanged. The TONs corresponding to 4.6, 9.2, and 19 μM ZnTPPS for NADH production were estimated as 2.9, 1.8, and 0.93, respectively. Considering the concentration of NADH production and the TONs of ZnTPPS, a ZnTPPS concentration of 4.6 μM was used.

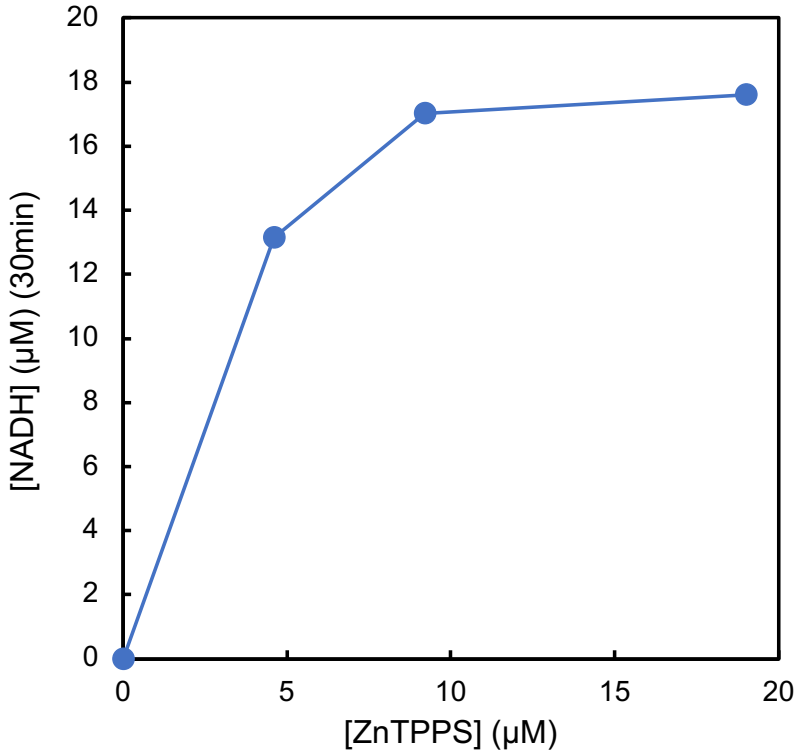

Fig. 4-6. Effect on the ZnTPPS concentration on the NADH yield after 30 min irradiation. A sample solution consists of TEOA (200 mM), ZnTPPS, Rh-PVP (250 μM), and NAD^+ (1.0 mM) in pH 7.4 HEPES-NaOH buffer.

Fig. 4-7 shows the effect of the ZnTPPS concentration on the NADH yield after 30 min of irradiation with visible light. The sample solution contained TEOA (200 mM), ZnTPPS (19 μM), Rh-PVP (0-250 μM), and NAD^+ (1 mM) in pH 7.4 HEPES-NaOH buffer. When the Rh-PVP concentration was 20 μM, the concentration of NADH was 17 μM after 30 min of irradiation. When the Rh-PVP concentration was further increased (>50 μM), NADH production decreased. This is because there is an excess of Rh-PVP relative to ZnTPPS, which reduces the ratio of two electron transfers to Rh-PVP.

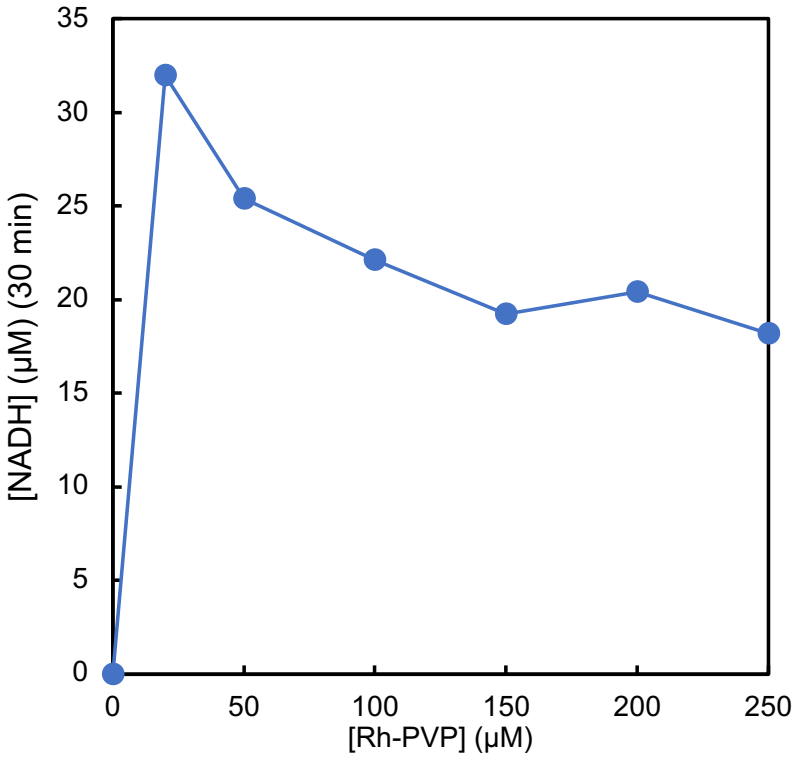

Fig. 4-7. Effect on the Rh-PVP concentration on the NADH yield after 30 min irradiation. A sample solution contained TEOA (200 mM), ZnTPPS (19 μM), Rh-PVP, and NAD^+ (1.0 mM) in pH 7.4 HEPES-NaOH buffer.

The effect of the Rh-PVP concentration on the NADH yield was reinvestigated when the ZnTPPS concentration was 4.6 μM (Fig. 4-8). When the Rh-PVP concentration was low (<50 μM), that of NADH remained almost unchanged. On the other hand, when the Rh-PVP concentration was increased (>50 μM), NADH

production decreased. At higher concentrations of photosensitizer, the electron could potentially be transferred to NAD^+ directly rather than to the catalysts.

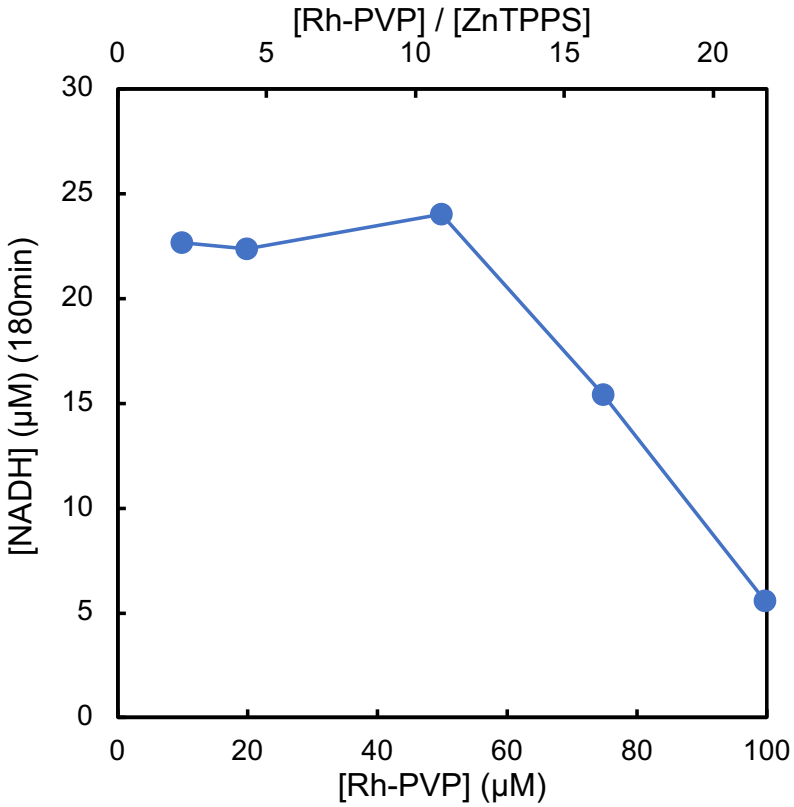

Fig. 4-8. Effect on the Rh-PVP concentration on the NADH yield after 180 min irradiation. A sample solution contained TEOA (200 mM), ZnTPPS (19 μM), Rh-PVP, and NAD^+ (1.0 mM) in pH 7.4 HEPES-NaOH buffer.

Next, the effect of ZnTPPS concentration on NADH yield was reinvestigated when the Rh-PVP concentration was 50 μM (Fig. 4-9). When the concentration of ZnTPPS was increased to 19 μM, that of NADH after 180 min of irradiation reached 38 μM. When the concentration of ZnTPPS was further increased, that of NADH remained almost unchanged. The TONs of ZnTPPS for NADH production were 2.0, 5.2, 2.4, 2.0 and 0.95 at 2.3, 4.6, 9.2, 19, and 37 μM ZnTPPS, respectively. The TON of ZnTPPS for NADH production was highest when the ZnTPPS concentration was 4.6 μM.

For the photochemical conversion system, considering the concentration of NADH production and TONs of ZnTPPS and Rh-PVP, concentrations of 4.6 and 50 μM were used for ZnTPPS and Rh-PVP, respectively.

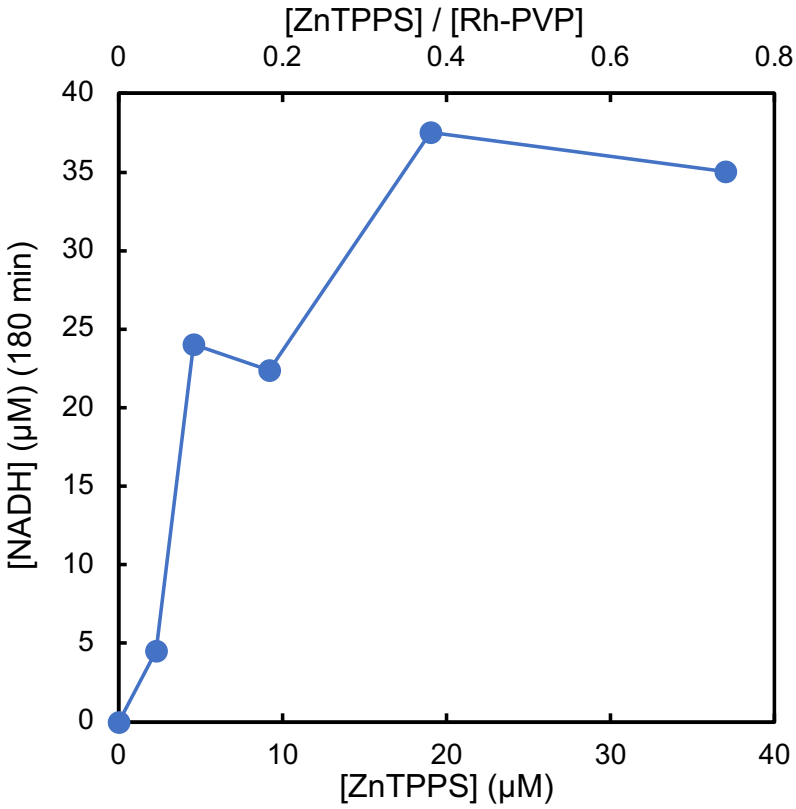

Fig. 4-9. Effect on the ZnTPPS concentration on the NADH yield after 30 min irradiation. A sample solution contained TEOA (200 mM), ZnTPPS (2.3-37 μM), Rh-PVP (50 μM), and NAD^+ (1.0 mM) in pH 7.4 HEPES-NaOH buffer.

4.3.2 Comparison of Rh-PVP and $[Cp^*Rh(bpy)(H_2O)]^{2+}$ in photochemical NADH regeneration

Here, the catalytic activity for NADH regeneration using visible light was compared between Rh-PVP and $[Cp^*Rh(bpy)(H_2O)]^{2+}$, where the latter is a widely used catalyst for NAD^+ reduction. The sample solution contained TEOA (200 mM), ZnTPPS (4.6 μM), Rh-PVP or $[Cp^*Rh(bpy)(H_2O)]^{2+}$ (50 μM), and NAD^+ (1.0 mM) in HEPES-NaOH buffer (pH 7.4) and was irradiated with visible light. Fig. 4-10

shows the time dependence of the concentration of NADH with Rh-PVP or $[Cp^*Rh(bpy)(H_2O)]^{2+}$. When either Rh-PVP or $[Cp^*Rh(bpy)(H_2O)]^{2+}$ was used, the concentration of NADH increased with irradiation time. For Rh-PVP and $[Cp^*Rh(bpy)(H_2O)]^{2+}$, the NADH concentrations after 300 min of irradiation were estimated to be 49 and 79 μM, respectively. The TONs of Rh-PVP and $[Cp^*Rh(bpy)(H_2O)]^{2+}$ after 300 min of irradiation were estimated to be 0.99 and 1.6, respectively, and their TOFs were estimated to be 0.48 and 0.41, respectively. Based on these results, Rh-PVP possesses ≈85 % of the catalytic activity of $[Cp^*Rh(bpy)(H_2O)]^{2+}$ under the current conditions.

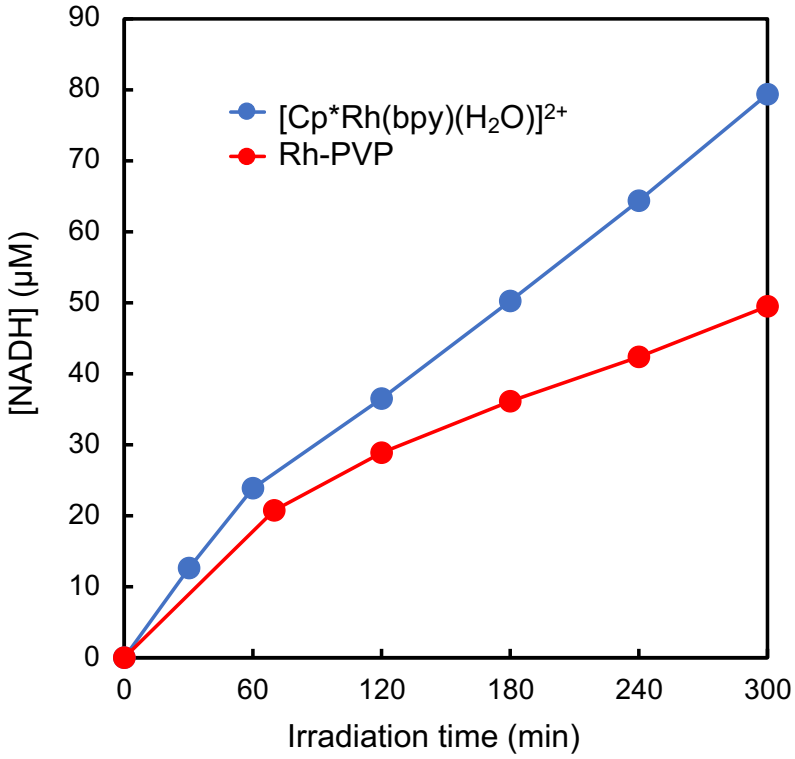

Fig. 4-10. Time dependence of concentration of NADH production with Rh-PVP or $[Cp^*Rh(bpy)(H_2O)]^{2+}$.

In addition, the catalytic activity of Rh-PVP was also tested with TiO_2 as a photosensitizer in place of ZnTPPS. The sample solution, consisting of TEOA, TiO_2, Rh-PVP, and NAD^+, was irradiated with a Xe lamp. The absorbance of the sample solution at 340 nm increased with irradiation time; thus, NADH production also

proceeded with TiO_2 instead of ZnTPPS. The concentrations of NADH after 120 min of irradiation were estimated to be 74 μM without Rh catalyst, 131 μM with Rh-PVP, and 200 μM with $[Cp^*Rh(bpy)(H_2O)]^{2+}$, as shown in Fig. 4-11. On the other hand, the NAD dimer was also produced; the concentrations of NAD dimer were estimated to be 81 μM without Rh catalyst, 31 μM with Rh-PVP, and 200 μM with $[Cp^*Rh(bpy)(H_2O)]^{2+}$. Thus, the selectivities for NADH production were estimated to be 48% without Rh catalyst, 81% with Rh-PVP, and 86% with $[Cp^*Rh(bpy)(H_2O)]^{2+}$. NADH production using Rh-PVP was higher than without Rh-PVP, and NAD dimer production was suppressed using Rh-PVP. Rh-PVP also acted as a catalyst for regioselective NAD^+ reduction to NADH in the presence of TiO_2. In addition, the selectivity of NADH in the presence of Rh-PVP was also higher than in the absence of Rh-PVP. Compared with the results of Rh-PVP and

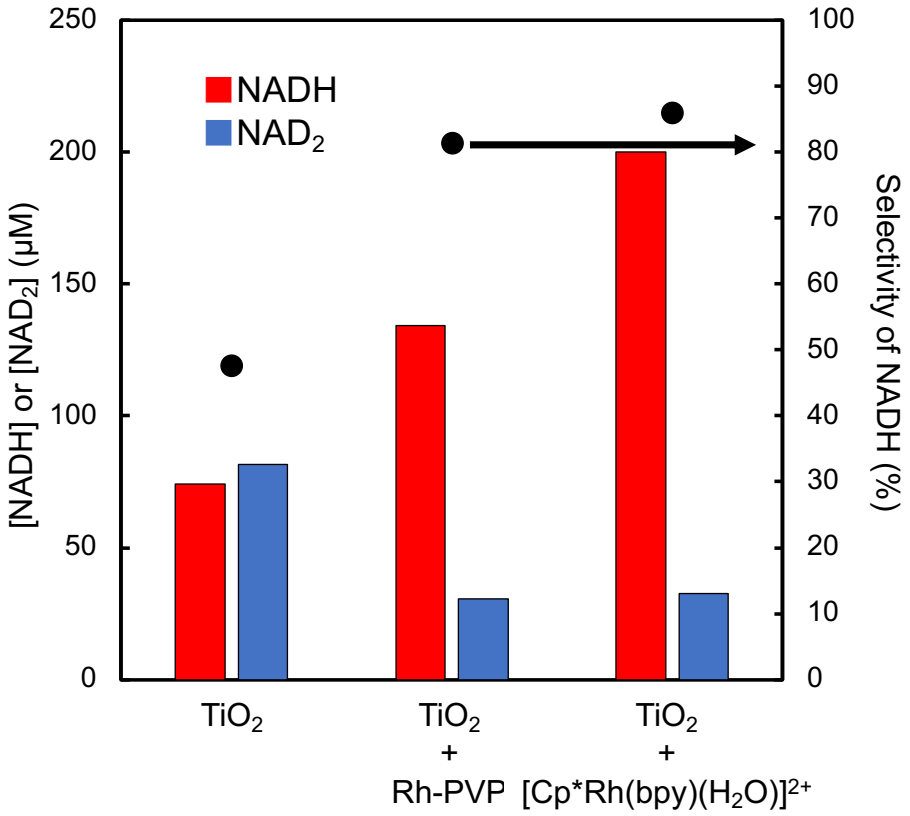

Fig. 4-11. The concentration of NADH or NAD dimer production and selectivity of NADH after 120 min irradiation with TiO_2 as a photosensitizer under various catalysts.

$[Cp^*Rh(bpy)(H_2O)]^{2+}$, no significant difference was observed in the regioselectivity of the NAD^+ reduction.

From these results, Rh-PVP can be considered a highly efficient homogeneous catalyst for selective NADH regeneration.

4.3.3 Irradiation wavelength dependence of NADH regeneration

The irradiation wavelength dependence of NADH regeneration was measured under monochromatic irradiation at 400, 420, 500, 560, 600, and 700 nm. The sample solution consisted of TEOA (200 mM), ZnTPPS (4.6 μM), Rh-PVP (50 μM), and NAD^+ (1.0 mM). NADH regeneration was proceeded by irradiation at 400, 420, 560, and 600 nm, as shown in Fig. 4-12. The amount of NADH production depended on the wavelength of the irradiated light. The apparent quantum efficiencies for NADH regeneration at 400, 420, 560, and 600 nm were 0.00016, 0.0012, 0.00016, and 0.00017 %, respectively. On the other hand, no NADH

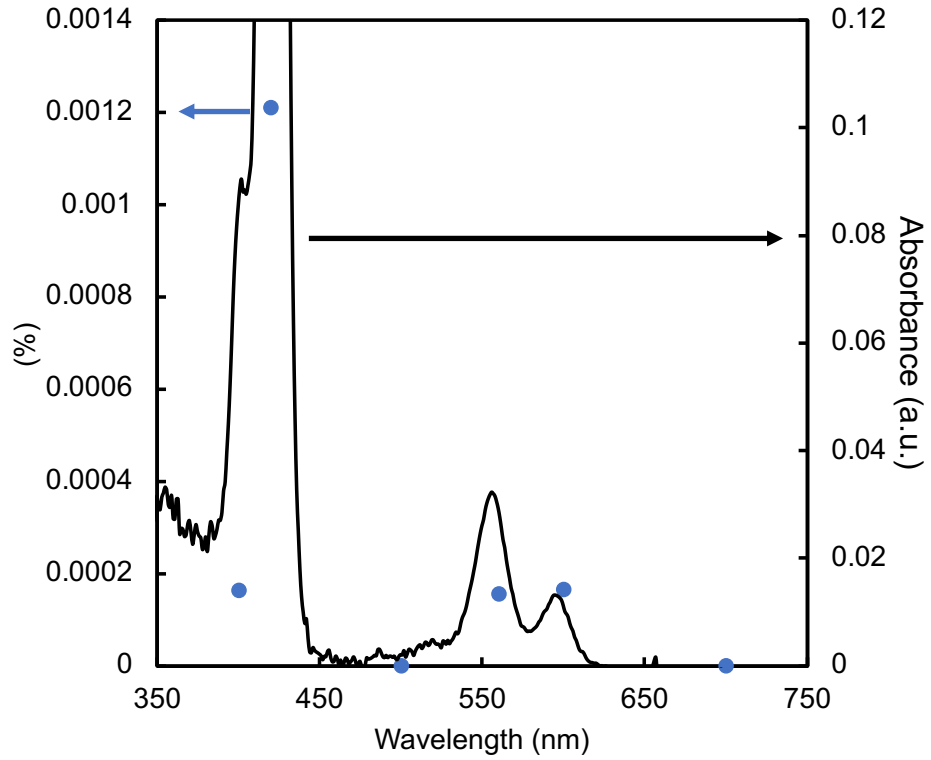

Fig. 4-12. Irradiation wavelength dependence of NADH regeneration.

regeneration was detected after irradiation at 500 and 700 nm, indicating that ZnTPPS absorbs photons with a Soret band and Q band.

4.3.4 Photochemical conversion using the combined NADH regeneration system and enzyme

Pyruvate reduction to L-lactate with LDH

As a model of an enantioselective synthesis, L-lactate production from pyruvate was attempted using the NADH regeneration system. Scheme 4-2 shows the visible-light-driven pyruvate reduction to L-lactate with LDH using an NADH regeneration system including TEOA, ZnTPPS, Rh-PVP, NAD^+, and pyruvate. The sample solution including TEOA, ZnTPPS, Rh-PVP, NAD^+, LDH, and pyruvate in HEPES-NaOH buffer (pH 7.4) was irradiated with visible light at 30 °C, producing L-lactate (Fig. 4-13). The concentration of L-lactate produced was estimated to be 94 μM after 7 h of irradiation, and the conversion yield of pyruvate after 7 h of irradiation was 4.7%. In this system, the TOF and TON of Rh-PVP after 7 h of irradiation were estimated to be 0.38 h^{-1} and 1.9, respectively. The TOF and TON of ZnTPPS after 7 h of irradiation were estimated to be 4.1 h^{-1} and 20, respectively. Thus, the catalytic production of L-lactate proceeded using the NADH regeneration system combined with visible-light energy. A control experiment performed in the absence of NAD^+ and LDH showed no production of L-lactate. As a control experiment, the sample solution including TEOA, Rh-PVP, NAD^+, LDH, and pyruvate was irradiated

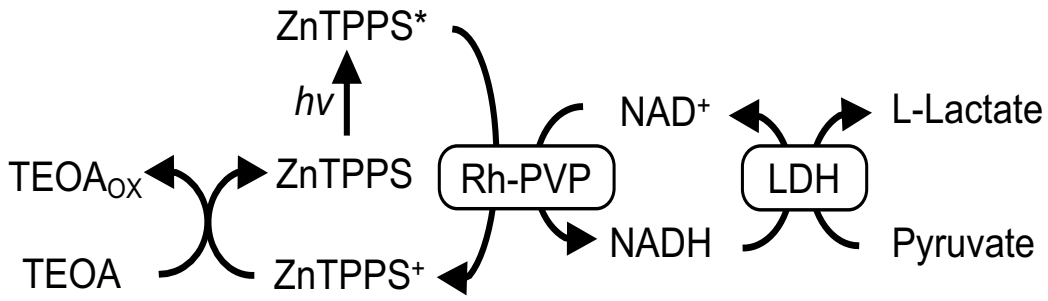

Scheme 4-2. Visible-light-driven pyruvate reduction to L-lactate using a NADH regeneration system including TEOA, ZnTPPS, Rh-PVP, NAD, LDH, and pyruvate.

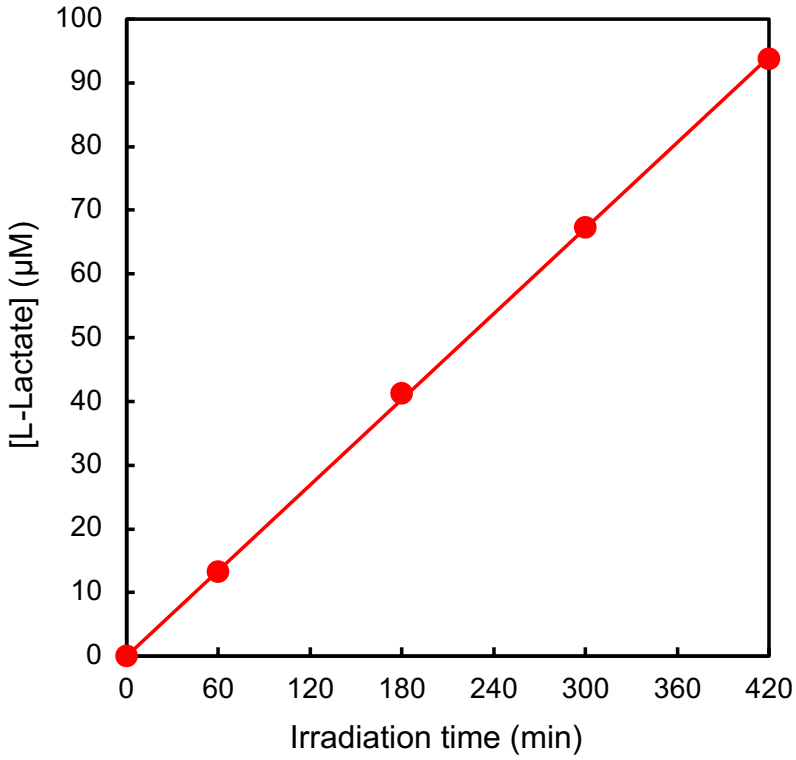

Fig. 4-13. Time course of L-lactate production with the system of TEOA, ZnTPPS, Rh-PVP, LDH, and pyruvate in HEPES-NaOH buffer (pH 7.4) under continuous irradiation.

without ZnTPPS, and no L-lactate was produced. In the system without Rh-PVP, while the UV–Vis absorption band at 300-380 nm increased, lactate was not produced. When the reaction mixture containing TEOA, ZnTPPS, Rh-PVP, NAD^+, LDH, and pyruvate in the HEPES-NaOH buffer (pH 7.4) was allowed to react in the dark, the intensity of the absorption band at 300–380 nm did not increase, and L-lactate was not produced.

The chirality of the lactate synthesized from pyruvate using the system of TEOA, ZnTPPS, Rh-PVP, NAD^+ and LDH with visible-light irradiation was confirmed. A chart showing the HPLC data acquired for the sample solution is shown in Fig. 4-14(a). The chromatogram of the standard sample of DL-lactate is also shown in Fig. 4-14(b). In the chromatogram, the signal peaks attributed to L- and D-lactate appear at retention times of 5.5 and 6.8 min, respectively. After irradiation, the peak

arising from L-lactate was detected and increased with irradiation time. On the other hand, the signal of D-lactate was not detected.

Therefore, the enantioselective synthesis of L-lactate has been successfully achieved using the NADH regeneration system and visible-light energy.

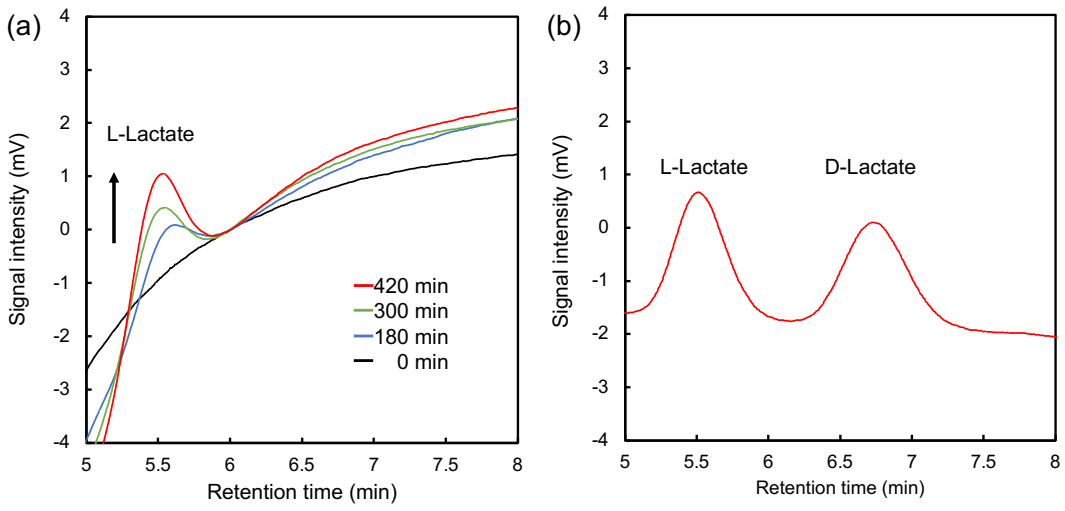

Fig. 4-14 .(a) The chromatogram of HPLC of the sample solution including TEOA, ZnTPPS, Rh-PVP, NAD^+, LDH, and pyruvate. (b) The chromatogram of standard sample of DL-lactate.

Acetoacetate reduction to 3-hydroxybutyrate with HBDH

As a model of an enantioselective synthesis, 3-hydroxybutyrate production from acetoacetate was also attempted using the NADH regeneration system. Scheme 4-3 shows the visible-light-driven acetoacetate reduction to 3-hydroxybutyrate with

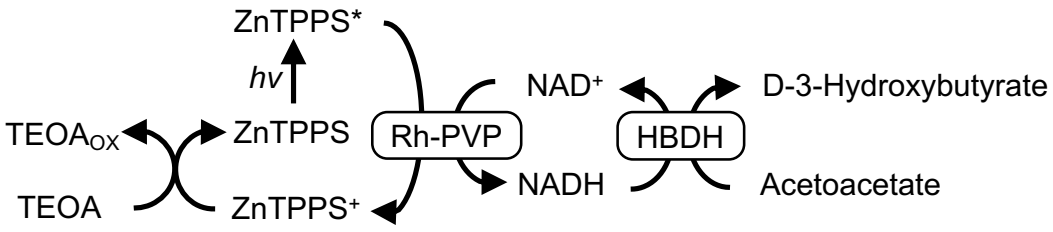

Scheme 4-3. Visible-light-driven acetoacetate reduction to D-3-hydroxybutyrate using a NADH regeneration system including TEOA, ZnTPPS, Rh-PVP, NAD, HBDH, and acetoacetate.

HBDH using an NADH regeneration system consisting of TEOA, ZnTPPS, Rh-PVP, NAD^+, and acetoacetate. When the sample solution was irradiated with visible light at 30 °C, D-3-hydroxybutyrate was produced, as shown in Fig. 4-15. The concentration of D-3-hydroxybutyrate production was estimated to be 42 μM after 5 h of irradiation, and the conversion yield of pyruvate after 4 h of irradiation was 42%. In this system, the TOF and TON of Rh-PVP after 5 of h irradiation were estimated to be 0.17 h^{-1} and 0.84, respectively. Each TOF and TON of ZnTPPS after 5 h of irradiation were estimated to be 1.8 h^{-1} and 9.1, respectively. A control experiment performed in the absence of NAD^+ and HBDH showed no production of D-3-hydroxybutyrate. No D-3-hydroxybutyrate was produced in the control experiment, which involved a sample solution including TEOA, Rh-PVP, NAD^+, HBDH, and acetoacetate without ZnTPPS. In the system without Rh-PVP, while the UV–Vis absorption band at 300–380 nm increased, lactate was not produced. When the reaction mixture containing TEOA, ZnTPPS, Rh-PVP, NAD^+, HBDH, and D-3-

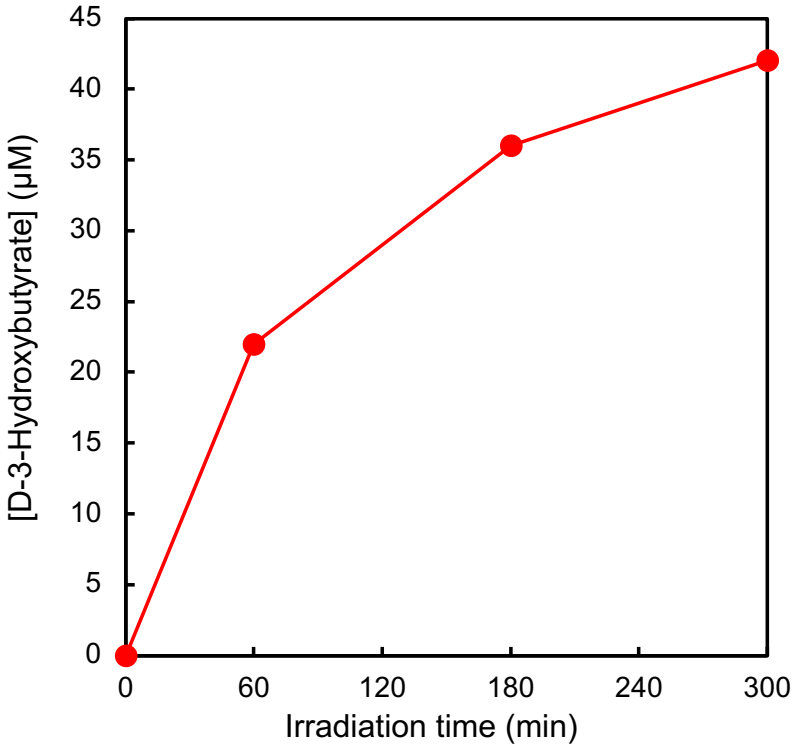

Fig. 4-15. Time course of D-3-hydroxybutyrate production with the system of TEOA, ZnTPPS, Rh-PVP, HBDH, and acetoacetate in HEPES-NaOH buffer (pH 7.4) under continuous irradiation.

hydroxybutyrate in the HEPES-NaOH buffer (pH 7.4) was allowed to react in the dark, the intensity of the absorption band at 300–380 nm did not increase, and D-3-hydroxybutyrate was not produced.

Therefore, the enantioselective synthesis of D-3-hydroxybutyrate has been successfully achieved using the NADH regeneration system and visible-light energy.

Malate production from pyruvate and CO_2 with MDH

As a model of C–C bond formation from CO_2 as a C1 feedstock, L-malate production from pyruvate and CO_2 was attempted using the NADH regeneration system. Scheme 4-4 shows the visible-light-driven malate production from pyruvate and CO_2 with LDH using an NADH regeneration system consisting of TEOA, ZnTPPS, Rh-PVP, NAD^+, MDH, pyruvate, HCO_3^-, and Mg^{2+}. When a sample solution of the regeneration system in HEPES-NaOH buffer (pH 7.4) was irradiated with visible light at 30 °C, malate was produced, as shown in Fig. 4-16. The concentration of malate was estimated to be 18 μM after 5 h of irradiation. In this system, the TOF and TON of Rh-PVP after 5 h of irradiation were estimated to be 0.072 h^{-1} and 0.36, respectively, and those for ZnTPPS after 5 h of irradiation were estimated to be 0.78 h^{-1} and 3.6, respectively. A control experiment performed in the absence of NAD^+ and MDH showed no formation of malate. As a control experiment, when the sample solution consisting of TEOA, Rh-PVP, NAD^+, MDH, pyruvate, HCO_3^-, and Mg^{2+} was irradiated without ZnTPPS, no malate was produced. When the reaction mixture was allowed to react in the dark, the intensity of the absorption band at 300–380 nm did not increase, and malate was not produced.

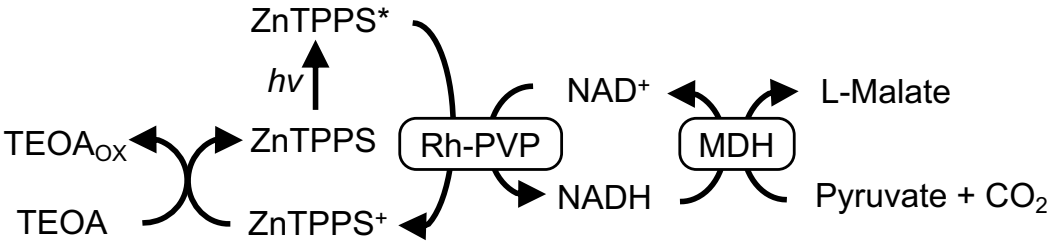

Scheme 4-4. Visible-light-driven malate production using a NADH regeneration system including TEOA, ZnTPPS, Rh-PVP, NAD, MDH, pyruvate, and CO_2.

Therefore, C–C bond formation to produce malate from CO_2 and pyruvate was successfully achieved using the NADH regeneration system and visible light energy.

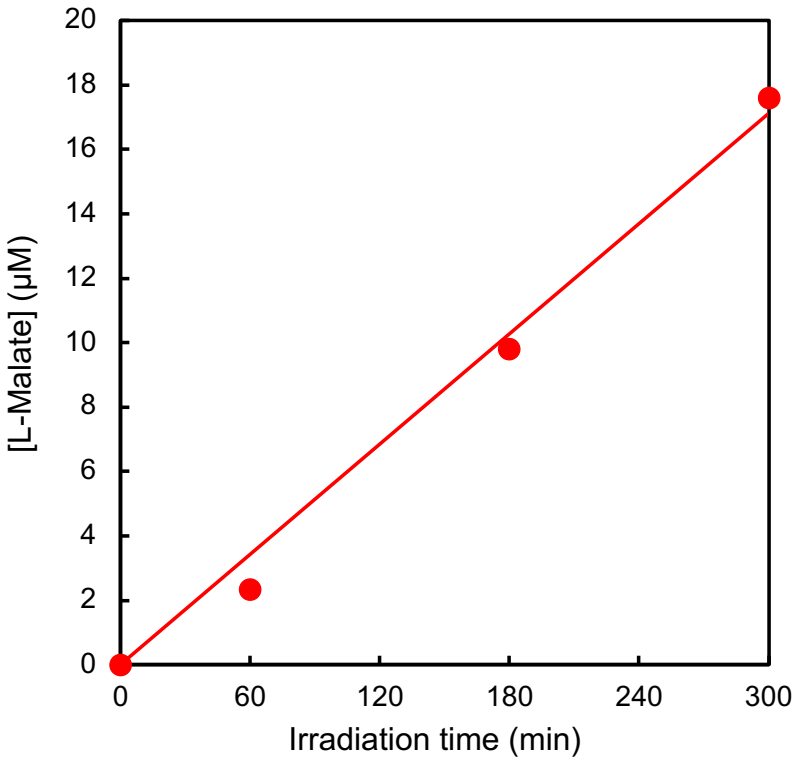

Fig. 4-16. Time course of malate production with the system of TEOA, ZnTPPS, Rh-PVP, MDH, Mg^{2+}, pyruvate, and CO_2 in HEPES-NaOH buffer (pH 7.4) under continuous irradiation.

4.3.5 Effect of the divalent or trivalent metal ion on ME

Effect of metal ions on the catalytic activity of ME in the malate production from pyruvate and CO_2

To improve the catalytic activity of ME in the pyruvate carboxylation with CO_2, the effect of metal ions on the ME was studied. In general, ME requires a divalent metal ion.[3-7] Therefore, the catalytic activity of ME combined with various metal ions, including trivalent metal ions, was studied.

Fig. 4-17(a) shows the time dependence of the produced $NADP^+$ concentration in the ME-catalyzed carboxylation of pyruvate with CO_2 to produce

malate in the presence of NADPH under the addition of various metal ions. The $NADP^+$ concentration increased linearly with increasing incubation time for all in all cases (using metal-ion concentrations of 10 μM). Fig. 4-17(b) shows the initial rate of ME-catalyzed malate production (v_{malate}). The results show that the ME-catalyzed carboxylation was accelerated by adding Mn^{2+}, Fe^{3+}, or Al^{3+}, in particular. On the contrary, the ME-catalyzed carboxylation was inhibited by adding Co^{2+}, Zn^{2+}, or Ca^{2+} compared to the absence of metal ions.

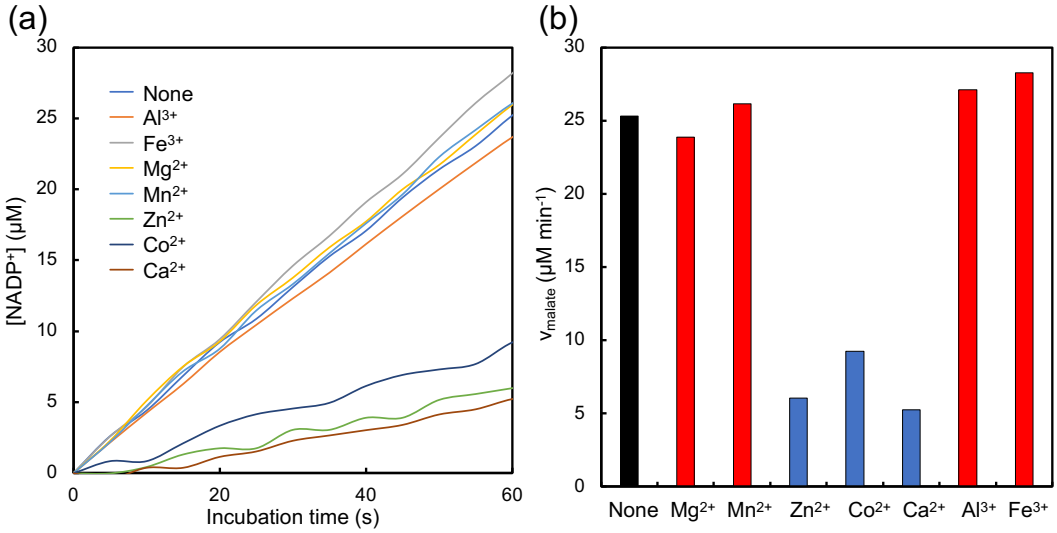

Fig. 4-17. (a) The time dependence of $NADP^+$ concentration in the ME-catalyzed carboxylation of pyruvate with CO_2 to produce malate in the presence of NADPH under various metal ion addition. (b) The apparent rates for ME-catalyzed malate production with addition of various metal ions.

Fig. 4-18(a) shows the time dependence of the NADPH concentration in the ME-catalyzed decarboxylation of malate into pyruvate and CO_2 in the presence of $NADP^+$ under the addition of various metal ions. The NADPH concentration increased linearly with increasing incubation time for all metal-ion additions (10 μM). Fig. 4-18(b) shows the initial rate of ME-catalyzed pyruvate production ($v_{pyruvate}$). However, no drastic acceleration of the ME-catalyzed decarboxylation was observed

upon adding any metal ions. The ME-catalyzed decarboxylation was also inhibited by adding Zn^{2+}, Co^{2+}, or Ca^{2+} compared to omitting the metal ions.

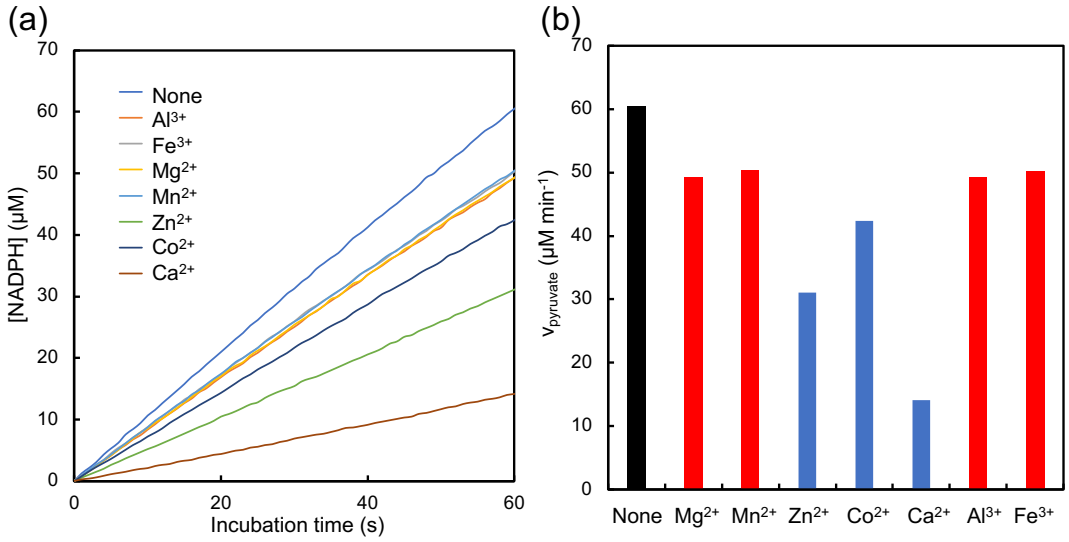

Fig. 4-18. (a) The time dependence of NADPH concentration in the ME-catalyzed decarboxylation of malate into pyruvate and CO_2 in the presence of $NADP^+$ under various metal ion addition. (b) The initial apparent rates for ME-catalyzed malate production with addition of various metal ions.

These results indicated that both ME-catalyzed malate and pyruvate production were greatly inhibited by adding the divalent metal ions Co^{2+}, Zn^{2+}, and Ca^{2+}. It was found that malate production was promoted by adding a trivalent metal ion such as Al^{3+} or Fe^{3+}. The values of v_{malate} without divalent metal ions and with the addition of Al^{3+} and Fe^{3+} were estimated to be 25, 27, and 28 μM min^{-1}, respectively. Fig. 4-19 shows v_{malate} under various concentrations of Fe^{3+}, Al^{3+}, and Mg^{2+}. The v_{malate} increased as the Al^{3+} concentration increased in the reaction system. Al^{3+} concentrations of up to 1.0 mM were sufficiently dissolved in the reaction solution, and v_{malate} increased up to 31μM min^{-1}. By contrast, for the addition of Fe^{3+}, v_{malate} acceleration was not observed with increasing Fe^{3+} concentration. As high concentrations of Fe^{3+} remain undissolved in the reaction solution, it was impossible to measure the absorption changes by spectroscopy after adding 1.0 mM of Fe^{3+}.

As a control test, both malate and pyruvate production in the presence of NADPH or $NADP^+$ were measured upon adding any metal ion in the absence of ME, and the reactions did not proceed. In other words, ME is essential for the carboxylation of pyruvate with CO_2 or the decarboxylation of malate. In addition, no carboxylation of pyruvate with ME was observed in the absence of sodium bicarbonate.

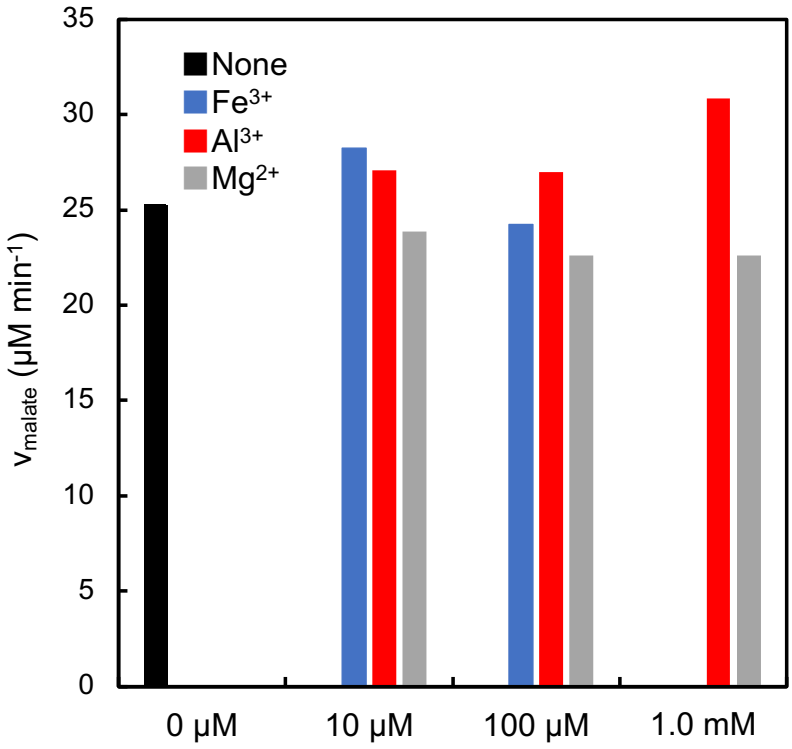

Fig. 4-19. The apparent rates for ME-catalyzed malate production (v_{malate}). The sample solution contained NADPH, pyruvate, bicarbonate, and ME in the presence of various concentrations of metal ions.

Relationship between the radius of the metal ion and the reaction rate

The relationship between the metal-ion radius and the apparent initial rate of ME-catalyzed carboxylation of pyruvate with CO_2 and decarboxylation of malate is shown in Fig. 4-20. At first glance, the relationship between the radius and v_{malate} or $v_{pyruvate}$ did not appear to affect the malate or pyruvate reactions, respectively. When

the radius of the metal ion was increased, the ME-catalyzed carboxylation of pyruvate with CO_2 and the decarboxylation of malate tended to be suppressed.

The mechanism of oxaloacetate production from pyruvate and CO_2 with ME was previously described.[18,19] First, a base abstracts an α-hydrogen of pyruvate to form an enolate. The enolate intermediate or generated carbanion intermediate then interacts with CO_2 to produce oxaloacetate. In this step, it is assumed that the metal ion stabilizes the intermediate in ME as a Lewis acid. Thus, it is assumed that the abstraction of α-hydrogen of keto-pyruvate to produce the enolate or carbanion intermediate is accelerated or decelerated by forming a complex of pyruvate with the metal ion.

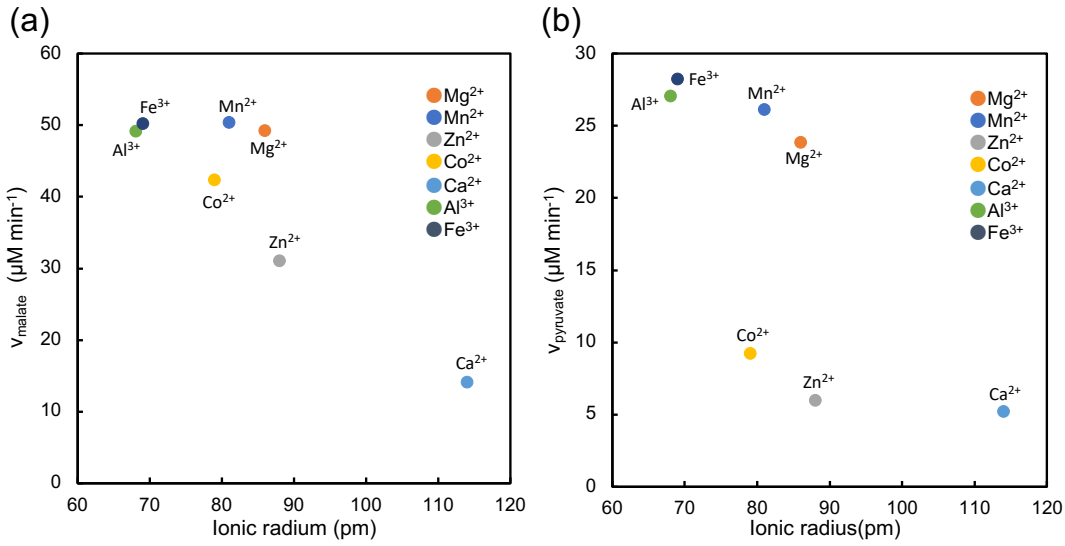

Fig. 4-20. The relationship between the metal ion radius and the apparent intial rate for ME-catalyzed malate (v_{malate}) (a) and pyruvate ($v_{pyruvate}$) (b) production.

4.4 Conclusion

This chapter described several visible-light-driven enzymatic reactions using the NADH regeneration system. In particular, biocatalytic C–C bond formation with CO_2 was attempted.

Choosing the optimal type and concentration of the electron donor, ZnTPPS, and Rh-PVP are vital to achieving a high regeneration rate. Optimal ranges for the concentrations of TEOA and the ratio of ZnTPPS to Rh-PVP were determined. The irradiation wavelength dependence of NADH regeneration was studied. ZnTPPS absorbs photons with a Soret band and Q band, and the quantum efficiencies for NADH regeneration at 420 nm were 0.0012%. The catalytic activity of Rh-PVP was compared with $[Cp^*Rh(bpy)(H_2O)]^{2+}$ for NADH regeneration, and Rh-PVP realized 85% the performance of $[Cp^*Rh(bpy)(H_2O)]^{2+}$ from the initial rate. The photochemical NAD^+ reduction also proceeded in the presence of TiO_2 as a photosensitizer.

The photochemical NADH regeneration system was also applied to enzyme-catalyzed redox reactions. By using the optimized NADH regeneration system, enzymatic reactions with visible-light energy were performed. The enantioselective synthesis of L-lactate with LDH and D-3-hydroxybutyrate with HBDH have been successfully achieved using visible-light energy. Moreover, C–C bond formation from CO_2 to produce L-malate MDH was successfully achieved using visible-light energy.

In addition, in order to improve the catalytic activity of ME in pyruvate carboxylation with CO_2, the effect of metal ions on the ME was studied. Trivalent aluminum and iron ions were found to accelerate the reaction.

4.5 References

1. D. Mandler and I. Willner, "Photochemical fixation of carbon dioxide: enzymic photosynthesis of malic, aspartic, isocitric, and formic acids in artificial media", *J. Chem. Soc., Perkin Trans*. *2*, 1988, 997–1003.
2. T. Itoh, H. Asada, K. Tobioka, Y. Kodera, A. Matsushima, M. Hiroto, H. Nishimura, T. Kamachi, I. Okura and Y. Inada, *Bioconjugate Chem.*, 2000, **11**, 8–13.
3. I. Harary, S. R. Korey and S. Ochoa, "Biosynthesis of dicarboxylic acids by carbon dioxide fixation. VII. Equilibrium of malic enzyme reaction", *J. Biol. Chem.*, 1953, **203**, 595–604.
4. S. Ochoa, A. H. Mehler and A. Kornberg, "Biosynthesis of dicarboxylic acids by carbon dioxide fixation. I. Isolation and properties of an enzyme from pigeon liver catalyzing the reversible oxidative decarboxylation of l-malic acid.", *J. Biol. Chem.*, 1948, **74**, 979–1000.
5. W. J. Rutter and H. A. Lardy, "Purification and properties of pigeon liver malic enzyme", *J. Biol. Chem.*, 1958, **233**, 374 -378.
6. Y. Ohno, T. Nakamori, H. Zheng and S. Suye, "Reverse Reaction of Malic Enzyme for HCO_3^- Fixation into Pyruvic Acid to Synthesize L-Malic Acid with Enzymatic Coenzyme Regeneration", *Biosci., Biotechnol., Biochem.*, 2008, **72**, 1278–1282.
7. H. Zheng, T. Nakamori and S. Suye, "Production of l-malic acid with fixation of HCO_3^- by malic enzyme-catalyzed reaction based on regeneration of coenzyme on electrode modified by layer-by-layer self-assembly method", *J. Biosci. Bioeng.*, 2009, **107**, 16–20.
8. U Kölle, B.-S Kang, P Infelta, P Comte and M Grätzel, "Elektrochemische und pulsradiolytische Reduktion von (Pentamethylcyclopentadienyl)(polypyridyl) rhodium-Komplexen", *Chem. Ber.*, 1989, **122**, 1869–1880.
9. U. Kölle and M. Grätzel, "Organometallic Rhodium(III) Complexes as Catalysts for the Photoreduction of Protons to Hydrogen on Colloidal TiO_2", *Angew. Chem. Int. Edn*, 1987, **26**, 567–570.

10. J. Huang, M. Antonietti and J. Liu, “Bio-inspired carbon nitride mesoporous spheres for artificial photosynthesis: photocatalytic cofactor regeneration for sustainable enzymatic synthesis”, *J. Mater. Chem. A*, 2014, **2**, 7686–7693.
11. R. B. McComb, L. W. Bond, R. W. Burnett, R. C. Keech and G. N. Bowers Jr., “Determination of the molar absorptivity of NADH.”, *Clin. Chem.*, 1976, **22**, 141–150.
12. B. A. Beaupre, M. R. Hoag, J. Roman, F. H. Försterling and G. R. Moran, “Metabolic function for human renalase: oxidation of isomeric forms of β-NAD(P)H that are inhibitory to primary metabolism”, *Biochemistry,* 2015, **54**, 795–806.
13. X. Zhang, L. Song, X. L. Zeng and M.Y. Li, “Effects of electron donors on the TiO_2 photocatalytic reduction of heavy metal ions under visible light”, *Energy Procedia*, 2012, **17. Pt. A**, 422–428.
14. L. Zhiyong, P. Xiangmin and M. Jianxin, “Harm effect distances evaluation of severe accidents for gaseous hydrogen refueling station”, *Int. J. Hydrogen Energy*, 2010, **35**, 1515–1521.
15. S. H. Lee, J. H. Kim and C. B. Park, “Coupling Photocatalysis and Redox Biocatalysis Toward Biocatalyzed Artificial Photosynthesis” *Chem.-A Europ. J.*, 2013, **19**, 4392–4406.
16. H. K. Chenault and G. M. Whitesides, “Regeneration of nicotinamide cofactors for use in organic synthesis” *Appl. Biochem. Biotechnol.*, 1987, **14**, 147–197.
17. Y. Wang, J. Sun, H. Zhang, Z. Zhao and W. Liu “Tetra(4-carboxyphenyl) porphyrin for efficient cofactor regeneration under visible light and its immobilization”, *Catal. Sci. Technol.*, 2018, **8**, 2578–2587.
18. C. B. Grissom and W. W. Cleland, “Isotope effect studies of chicken liver NADP malic enzyme: role of the metal ion and viscosity dependence”, *Biochemistry*, 1988, **27**, 2927–2934.
19. C. C. Kuo, K. Y. Lin, Y. J. Hsu, S.Y. Lin, Y. T. Lin, G. G. Chang and W. Y. Chou, “The roles of Tyr^{91} and Lys^{162} in general acid–base catalysis in the pigeon $NADP^+$-dependent malic enzyme”, *Biochem. J.*, 2008, **411**, 467–473.

Chapter 5

Conclusion

5.1 Summary

The goal of this doctoral work was to establish a CO_2 utilization system that uses visible-light energy and biocatalysts. In this thesis, a novel system that does not incorporate the NAD^+/NADH redox system was proposed. In addition, a novel type of catalyst for NADH regeneration, an Rh colloidal catalyst, was reported.

In Chapter 2, a photoredox system for enzymatic CO_2 fixation using a viologen derivative as a novel, artificial coenzyme for ME was developed. By using this coenzyme, a visible-light-driven C–C bond formation system with ME was developed. In addition, the function of viologen derivatives in the C–C bond formation mechanism was clarified. PV^0 acts as a base and was involved in oxaloacetate production via C–H bond activation and carboxylation of pyruvate by CO_2. In addition, the kinetic parameters of oxaloacetate production based on building a C–C bond of a coupling pyruvate and CO_2 with PCV^0 and ME were determined through the analysis of enzymatic kinetics.

In Chapter 3, the regioselective NAD^+ reduction to enzymatically active NADH using a system comprising a photosensitizer and homogeneously polymer-dispersed metal nanoparticles was carried out. The catalytic activity of homogeneous Rh nanoparticles for NADH regeneration was demonstrated for the first time. The reduction product of NAD^+ was solely 1,4-NADH, which validated the enzymatic assay and HPLC analysis. NADH regeneration mechanisms were also proposed.

By using this system, photochemical conversion using visible light-energy has been successfully achieved, as described in Chapter 4. As models of enantioselective synthesis, LDH-catalyzed pyruvate reduction to L-lactate and HBDH-catalyzed acetoacetate reduction to D-3-hydroxybutyrate were attempted. As a model of C–C bond formation with CO_2 owing to C–H bond activation, MDH catalyzed pyruvate carboxylation with CO_2, and subsequent reduction to L-malate was performed using visible-light energy. This work provides a platform for using Rh nanoparticles as highly efficient homogeneous catalysts for regioselective NADH regeneration, which is central to the design of biological solar-energy conversion and energy storage devices as well as to advance artificial photosynthesis.

5.2 Prospects

In this work, visible-light-driven C–H bond activation and C–C bond formation with CO_2 was developed for the carboxylation of organic molecules using a biocatalyst and photofunctional materials. The systems in this thesis incorporate CO_2 into organic molecules by utilizing the base and reductant produced upon irradiation with visible-light energy. These systems can be expected to lead to new storage methods that fix CO_2 to molecules and contribute to the field of green chemistry. Fig. 5-1 shows the approaches to recycling conversion of CO_2 as an alternative to petrochemical methods.[1]

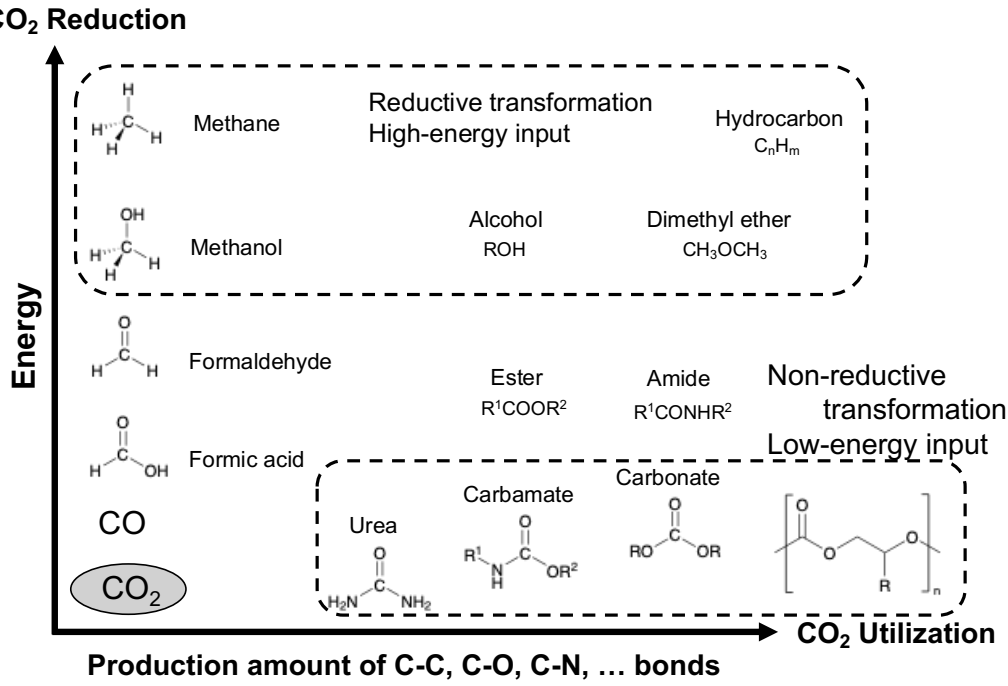

Fig. 5-1. Schematic representation for the approaches to recycling conversions of CO_2 as alternatives to petrochemical methods.

Until now, extensive research efforts have been devoted to CO_2 reduction to CO, formate, formaldehyde, and methanol using electrochemical, photo-electrochemical, and chemical methods including the photoredox systems mentioned in Chapter 1. In contrast, for CO_2 functionalization, new C–C, C–O, and C–N bonds are formed with no formal reduction of the carbon center and thus do not require

significant energy storage. Novel techniques for CO_2 recycling that aim to compete with petrochemistry require new processes that combine both CO_2 reduction and C–C, C–O, and C–N bond formation in order to expand the range of compounds directly available from CO_2.

Enzymes that catalyze CO_2 utilization reactions have the advantage of high reaction-product selectivity. Therefore, in the future, not only will the conversion of CO_2 to C1 fuels such as CO, methanol, and methane be accomplished by using visible-light energy but also chemical product synthesis and innovative CO_2 capture, utilization and storage technology (CCUS).

In addition, most of reported photoredox systems for CO_2 utilization use sacrificial reagents as electron sources. Therefore, there will be a need for photochemical systems that use water as an electron source.

5.3 References

1. C. D. N. Gomes, O. Jacquet, C. Villiers, P. Thuéry, M. Ephritikhine and T. Cantat, "A Diagonal Approach to Chemical Recycling of Carbon Dioxide: Organocatalytic Transformation for the Reductive Functionalization of CO_2", *Angew. Chem., Int. Ed.*, 2012, **51**, 187–190.

Acknowledgements

First, I would like to express my deepest sense of gratitude and appreciation to my principal supervisor Prof. Dr. Yutaka Amao for his kind guidance of my doctoral work. He gave me invaluable suggestions and constant encouragement throughout my doctoral studies. He has taught me a lot, not only about things related to research but also how to set up a life plan, manners, and various other aspects of life. I believe that the six years under his direction will surely lead me to become a full-fledged researcher.

I would like to thank Assoc. Prof. Dr. Masanobu Higashi. He supported me with many scientific suggestions and discussions about this dissertation. I would like to emphasize that they significantly improved the quality of my doctoral work.

I would like to thank Assoc. Prof. Dr. Yasuo Matsubara. He supported me with many scientific suggestions and discussions about this dissertation. He also helped me with the measurements for the HPLC experiments (Capater 3).

I would like to thank Assoc. Prof. Dr. Hiroyuki Takeda, Dr. Hiroyasu Tabe, Dr. Shusaku Ikeyama. They gave me much encouragement during the research and gave me comments that helped me a lot in writing my research paper.

I would like to thank Prof. Dr. Yusuke Yamada at Graduate School of Engineering, Osaka City University. He helped me with the discussion about the enzymatic reactions with an artificial coenzyme. He also helped me with the measurements for the transmission electron microscope experiments (Capater 3).

I would like to thank Prof. Dr. Tomoko Yoshida, Assoc. Prof. Dr. Ritsuko (Mizoguchi) Fujii, Dr. Muneaki Yamamoto, Dr. Masato Akatsuka, Dr. Nami Yamano

at Research Center for Artificial Photosynthesis, Osaka City University, for their helpful supports and kind encouragement.

I would like to thank Mr. Kohei Fujita. He helped me with the experiments in Chapter 2. I would like to thank Mr. Tomoya Ishibashi, Mr. Yusuke Minami, Mr. Ryohei Sato, Mr. Takumi Toyodome, Ms. Yu Kita, and Ms. Mika Takeuchi for their help in my daily life. I would like to thank Ms. Miyuki Fujimura, Ms. Yumiko Muroga, Ms. Manami Ito, Ms. Kaori Murashima, Ms. Mako Kuwata, and Ms. Makiko Miyazaki for their kind encouragement.

I would like to thank Mr. Ryuichi Kano, Mr. Yuma Kato, Ms. Yu (Kudo) Kawaguchi. They encouraged me whenever possible. I appreciate their help and kindness in daily life and support in terms of research.

I would like to thank Mr. Tatsuya Kusumoto, Mr. Hiroki Shinohara, Mr. Hiroki Tabuchi, Ms. Azuki Yasuda, the members of Science Selection Course, Faculty of Science, Osaka City University.

I also thank the members at the Research Center for Artificial Photosynthesis, Osaka City University, and the members of the laboratories where I have been involved in my research.

I would like to thank the teaching staffs including Prof. Dr. Hiroshi Nakajima and Prof. Dr. Toshiyuki Moriuchi, at the Division of Molecular Materials Science, Graduate School of Science, Osaka City University. Prof. Dr. Hiroshi Nakajima and Prof. Dr. Toshiyuki Moriuchi were sub-chief examiners of this dissertation. They told me a precious and impressive story about the mental attitude of a researcher.

Financial support from the JSPS fellowship DC1 is gratefully acknowledged. I would like to thank JSPS for the KAKENHI Grant (Number 19J23723) for a JSPS Research Fellowship.

Finally, I wish to express my gratitude to my parents, Jitsuo, Satomi, my sister Mai, and my brother Teruyuki for their understanding and warm encouragements.

Takayuki Katagiri

Division of Molecular Materials Science
Graduate School of Science, Osaka City University
January 2022

List of the author's works

Publications

Chapter 1

Takayuki Katagiri, Yutaka Amao

"Recent advances in light-driven C–H bond activation and building C–C bonds with CO_2 as a feedstock for carbon capture and utilization technology"

Green Chemistry, 2020, **22** (20), 6682-6713.

Chapter 2

Takayuki Katagiri, Shusaku Ikeyama, Yutaka Amao

"Visible Light-induced Reduction Properties of Diphenylviologen with Water-soluble Porphyrin"

Journal of Photochemistry and Photobiology A: Chemistry, 2018, **358,** 368-373.

Takayuki Katagiri, Kohei Fujita, Shusaku Ikeyama, Yutaka Amao

"Visible light-induced reduction system of diphenylviologen derivative with water-soluble porphyrin for biocatalytic carbon–carbon bond formation from CO_2"

Pure and Applied Chemistry, 2018, **90** (11), 1723-1733.

Takayuki Katagiri, Yutaka Amao

"Double-Electron Reduced Diphenylviologen as a Coenzyme for Biocatalytic Building Carbon–Carbon Bonds from CO_2 as a Carbon Feedstock"

ACS Sustainable Chemistry & Engineering, 2019, **7** (10), 9080-9085.

Chapter3

Takayuki Katagiri, Yutaka Amao

"Visible light driven selective NADH regeneration using a system of water-soluble zinc porphyrin and homogeneously polymer-dispersed rhodium nanoparticles"

New Journal of Chemistry, 2021, **45** (35), 15748-15752.

Chapter 4

Takayuki Katagiri, Yutaka Amao

"Trivalent metal ion promote malic enzyme-catalyzed building carbon-carbon bonds from CO_2 and pyruvate"

New Journal of Chemistry, 2020, **44** (40), 17208-17214.

Selected as Front Cover

Takayuki Katagiri, Yutaka Amao

"Visible light-induced enzymatic reactions using a NADH regeneration system of water-soluble porphyrin and homogeneously rhodium nanoparticles"

Manuscript in preparation.

Other articles

Shusaku Ikeyama, Takayuki Katagiri, Yutaka Amao

"The improvement of formic acid production from CO_2 with visible-light energy and formate dehydrogenase by the function of the viologen derivative with carbamoylmethyl group as an electron carrier"

Journal of Photochemistry and Photobiology A: Chemistry, 2018, **358**, 362-367.

Yutaka Amao, Shusaku Ikeyama, Takayuki Katagiri, Kohei Fujita

"Development of Dye Molecule-biocatalyst Hybrid System with Visible-light Induced Carbon-carbon Bond formation from CO_2 as a Feedstock"

Faraday Discussions, 2017, **198**, 73-81.

Journal of Scientific Society

Takayuki Katagiri, Yutaka Amao

"Photo/biocatalysts hybrid system for C-H bond activation and building C-C bonds from CO_2"

"炭素－水素結合を活性化し二酸化炭素を結合する光触媒・生体触媒複合系"

Photochemistry, **51** (1) 2020, 12-19.

Awards

1. 8th OCARINA International Symposium “POSTER PRIZE”

   (March 2017)

   “Development of a novel electron mediator based on phenylviologen skeleton for enzyme with carbon dioxide fixation”, 8th OCARINA International Symposium,”
2. 第 36 回光がかかわる触媒化学シンポジウム “優秀ポスター賞”

   (June 2017)

   “可視光を用いた二酸化炭素資源化のための色素ーリンゴ酸酵素複合系に関する研究”
3. The 7th IUPAC Conference on Green Chemistry “*Green Chemistry* Poster Prize”

   (October 2017)

   “Visible Light-Induced Reduction Properties of Diphenylviologen with Water-Soluble Zn Porphyrin for Carbon-Carbon Formation from CO_2 with Malic Enzyme”
4. 9th OCARINA International Symposium “POSTER PRIZE”

   (March 2018)

   “Visible light-driven carbon-carbon bond formation from CO_2 as a feedstock with the system containing malic enzyme and dye”
5. The 8th IUPAC Conference on Green Chemistry “Student Scholarship”

   (September 2018)

   “Interaction between diphenylviologen derivative and malic enzyme for carbon-carbon bond formation from CO_2 as a feedstock”
6. Osaka City University distinguished student award (Wakano Award)

   (March 2019)
7. Southeast Asia Catalysis Conference 2019 (SACC2019) “Best Poster Award”

   (May 2019)

   “Biocatalytic carboxylation using CO_2 as the C1 source by malic enzyme and diphenylviologen derivative as an artificial co-enzyme”
8. 第 13 回 GSC Student Travel Grant Award

   (June 2020)

“多電子還元型ジフェニルビオローゲン誘導体とリンゴ酸酵素による二酸化炭素を原料とした有機分子のカルボキシ化に関する研究”

9. 5th EuChemS Conference on Green and Sustainable Chemistry (5th EuGSC) "Best Poster Award"（Royal Society of Chemistry RSC)

(September 2021)

“Regioselective NAD^+ reduction to NADH with dye and homogeneously dispersed rhodium nanoparticles under visible light”

Fund

1. 2019-2022 Mar Grant-in-Aid for JSPS Research Fellow Funding Agency: Japan Society for the Promotion of Science
   JSPS KAKENHI Grant Number: 19J23723
   “機能性電子メディエータによる生体触媒の活性化と二酸化炭素のカルボキシ化”
   Role: PI

Presentation

List of International Conference Talk

【Oral Presentations】

1. Yutaka Amao, Shusaku Ikeyama, Takayuki Katagiri, Kohei Fujita, “Development of Dye Molecule-biocatalyst Hybrid System with Visible-light Induced Carbon-carbon Bond formation from CO_2 as a Feedstock”, Faraday Discussions, Kyoto, Japan, February 2017.
2. Yutaka Amao Shusaku Ikeyama, Takayuki Katagiri, “Porphyrin-biocatalyst Hybrid System with Visible-light Induced Carbon-carbon Bond Formation from CO_2 as a Feedstock”, Light Harvesting Process LHP 2017, Bavaria, Germany, March 2017.
3. Yutaka Amao, Kohei Fujita, Takayuki Katagiri, Shusaku Ikeyama, “Photoredox system with biocatalyst for carbon-carbon bond formation from CO_2 as a feedstock”, 2nd Green and Sustainable Chemistry Conference, Berlin, Germany, May 2017.

4. Takayuki Katagiri, Shusaku Ikeyama, Kohei Fujita, Yutaka Amao, "Development of a novel electron mediator based on phenylviologen for biocatalyst with CO_2 utilization", 16th Korea-Japan Symposium on Catalysis, Sapporo, Japan, May 2017.
5. Yutaka Amao, Kohei Fujita, Takayuki Katagiri, Shusaku Ikeyama, "Visible-light induced carbon-carbon bond formation from CO_2 as a feedstock with the photoredox system consisting of dye and biocatalyst", 21st Annual Green Chemistry & Engineering Conference (GC&E), Reston, U.S.A., June 2017.
6. Yutaka Amao, Takayuki Katagiri, Shusaku Ikeyama, "Photoredox system with dye molecule-biocatalyst for solar to chemicals based on building carbon-carbon bonds from CO_2 as a feedstock", 2nd International Solar Fuel Conference, San Diego, U.S.A., July 2017.
7. Yutaka Amao, Takayuki Katagiri, Shusaku Ikeyama, "Visible-light induced carbon-carbon bond formation from CO_2 as a feedstock with dye molecule-biocatalyst system", 8th International Conference on Green and Sustainable Chemistry Conference (GSC8), Melbourne, Australia, July 2017.
8. Yutaka Amao, Takayuki Katagiri, Shusaku Ikeyama, "Visible Light-induced Carbon-carbon Bond Formation from CO_2 as a Feedstock with Dye Molecule-biocatalyst Hybrid Redox System", 13th European Congress on Catalysis (EUROPACAT 2017), Florence, Italy, August 2017.
9. Yutaka Amao, Takayuki Katagiri, Shusaku Ikeyama, "Visible-light induced building C-C bonds from CO_2 as a feedstock with photosensitizer-biocatalyst system", 7th IUPAC International Conference on Green Chemistry, Moscow, Russia, October 2017.
10. Yutaka Amao, Takayuki Katagiri, Shusaku Ikeyama, "Visible-light driven building C-C bonds from CO_2 as a feedstock with photosensitizer-biocatalyst hybrid system", ECO-BIO 2018, Dublin, Ireland, March 2018.
11. Yutaka Amao, Takayuki Katagiri, Shusaku Ikeyama, "Visible-light driven building C-C bonds from CO_2 with photosensitizer-biocatalyst system", 3rd Green & Sustainable Chemistry Conference, Berlin, Germany, May 2018.
12. Takayuki Ktagiri, Shusaku Ikeyama, Yutaka Amao, "Double-electron reduced

diphenylviologen derivative as a novel co-enzyme for biocatalyst with the function of carbon-carbon bond formation from CO_2", 2018 International Symposium on Advancement and Prospect of Catalysis Science & Technology, Sydney, Australia, July 2018.

13. Yutaka Amao, Takayuki Ktagiri, Shusaku Ikeyama, "Visible light-driven building C-C bonds from CO_2 as a feedstock with photosensitizer-biocatalyst hybrid system", The 8th Tokyo Conference on Advanced Catalytic Science and Technology (TOCAT8), Yokohama, Japan, August 2018.
14. Yutaka Amao, Takayuki Ktagiri, Shusaku Ikeyama, "Visible-Light Driven Carboxylation with CO_2 in the Hybrid System of Biocatalyst and Photocatalytic Dye", 8th IUPAC International Conference on Green Chemistry (ICGC-8), Bangkok, Thailand, September 2018.
15. Takayuki Katagiri, Shusaku Ikeyama, Yutaka Amao, "Visble-Light Driven Carboxylation with CO_2 with The System of Biocatalyst And Photocatalytic Dye", 7th Asia-Oceania Conference on Green and Sustainable Chemistry, Singapore, November 2018.
16. Yutaka Amao, Takayuki Katagiri, "Visible-light driven C-H bond activation and carboxylation of CO_2 with bio-/photocatalytic hybrid system", 4th Green and Sustainable Chemistry Conference 2019, Dresden, Germany, May 2019.
17. Takayuki Katagiri, Shusaku Ikeyama, Yutaka Amao, "Carboxylation of organic molecule by CO_2 with biocatalyst and double-electron reduced diphenylviologen derivative", The 8th Asia-Pacific Congress on Catalysis (APCAT-8), Bangkok, Thailand, August 2019.
18. Takayuki Katagiri, Yutaka Amao, "Biocatalytic carboxylation using CO_2 as the C1 feedstock by malic enzyme and diphenylviologen derivative as an artificial coenzyme with visible light irradiation", The 2021 International Chemical Congress of Pacific Basin Societies (Pacifichem 2021), Online, December 2021.
19. Takayuki Katagiri, Yutaka Amao, "Visible-light-driven regioselective NAD^+ reduction to NADH with the system of water-soluble zinc porphyrin and homogeneously dispersed rhodium nanoparticles", The 2021 International

Chemical Congress of Pacific Basin Societies (Pacifichem 2021), Online, December 2021.

【Poster Presentations】

1. Shusaku Ikeyama, Takayuki Katagiri, Yutaka Amao, "Effect of viologen derivative with carbamoylmetyl group as an electron carrier on the visible light induced formic acid production from CO_2 with zinc porphyrin and formate dehydrogenase", 2017 International Conference on Artificial Photosynthesis, Kyoto, Japan, March 2017.
2. Kohei Fujita, Takayuki Katagiri, Shusaku Ikeyama, Yutaka Amao, "Development of artificial co-enzyme in the visible light-induced malic acid production from CO_2 and pyruvic acid in the presence of malic enzyme", 8th OCARINA International Symposium, Osaka, Japan, March 2017.
3. Takayuki Katagiri, Shusaku Ikeyama, Kohei Fujita, Yutaka Amao, "Development of a novel electron mediator based on phenylviologen skeleton for enzyme with carbon dioxide fixation", 8th OCARINA International Symposium, Osaka, Japan, March 2017.
4. Shusaku Ikeyama, Takayuki Katagiri, Yutaka Amao, "The improvement of formic acid production from CO_2 with the function of visible-light harvesting of water soluble zinc porphyrin and formate dehydrogenase by the effect of the viologen with carbamoylmethyl group as an electron carrier", Light-Harvesting Processes LHP 2017, Bavaria, Germany, March 2017.
5. Takayuki Katagiri, Kohei Fujita, Shusaku Ikeyama, Yutaka Amao, "Development of a novel electron carrier based on phenylviologen for the visible light-induced carbon-carbon bond production from carbon dioxide with malic enzyme", 15th International Conference on Carbon Dioxide Utilization (ICCDU XV), Shanghai, China, July 2017.
6. Takayuki Katagiri, Shusaku Ikeyama, Kohei Fujita, Yutaka Amao, "Visible Light-Induced Reduction Properties of Diphenylviologen with Water-Soluble Zn Porphyrin for Carbon-Carbon Formation from CO_2 with Malic Enzyme", 7th IUPAC International Conference on Green Chemistry, Moscow, Russia, October

2017.

7. Takayuki Katagiri, Shusaku Ikeyama, Yutaka Amao, “Visible light-driven carbon-carbon bond formation from CO_2 as a feedstock with the system containing malic enzyme and dye”, The 9th OCARINA International Symposium Joint mini-symposiums on Structural Biology and Catalysis, Osaka, Japan, March 2018.
8. Takayuki Katagiri, Shusaku Ikeyama, Yutaka Amao, “Studies on the interaction between artificial co-enzyme based on diphenylviologen derivative and malic enzyme for CO_2 utilization”, The 22nd Annual Green Chemistry & Engineering Conference (GC&E), Portland, U.S.A., June 2018.
9. Takayuki Ktagiri, Shusaku Ikeyama, Yutaka Amao, “Kinetic studies of the interaction between malic enzyme and diphenylviologen derivative for CO_2 utilization”, The 18th International Symposium on Relations between Homogeneous and Heterogeneous Catalysis (ISHHC18), Sydney, Australia, July 2018.
10. Takayuki Ktagiri, Shusaku Ikeyama, Yutaka Amao, “Kinetic studies of the interaction between diphenylviologen derivative as a novel co-enzyme and malic enzyme for building carbon-carbon bond from CO_2”, The 8th Tokyo Conference on Advanced Catalytic Science and Technology (TOCAT8), Yokohama, Japan, August 2018.
11. Takayuki Ktagiri, Shusaku Ikeyama, Yutaka Amao, “Interaction between diphenylviologen derivative and malic enzyme for carbon-carbon bond formation from CO_2 as a feedstock”, 8th IUPAC International Conference on Green Chemistry (ICGC-8), Bangkok, Thailand, September 2018.
12. Takayuki Katagiri, Shusaku Ikeyama, Yutaka Amao, “Biocatalytic carboxylation using CO_2 as the C1 source by malic enzyme and diphenylviologen derivative as an artificial co-enzyme”, Southeast Asia Catalysis Conference 2019 (SACC 2019), Singapore, May 2019.
13. Takayuki Katagiri, Shusaku Ikeyama, Yutaka Amao, “ Biocatalytic carboxylation using CO_2 as the C1 source by malic enzyme and diphenylviologen derivative as an artificial co-enzyme”, The 23rd Annual Green Chemistry &

Engineering Conference and 9th International Conference on Green and Sustainable Chemistry, Reston, Virginia, USA., June 2019.

14. Takayuki Katagiri, Shusaku Ikeyama, Yutaka Amao, "Building carbon-carbon bond from CO_2 with malic enzyme and viologen derivative", 4th EuCheMS Conference on Green and Sustainable Chemistry, Tarragona, Spain, September 2019.
15. Takayuki Katagiri, Yutaka Amao, "Promotion of the biocatalytic carboxylation with CO_2 by malic enzyme and viologen derivative in the presence of metal ion", The 24th Annual Green Chemistry & Engineering Conference, Seattle, Virginia, USA., June 2020.
16. Takayuki Katagiri, Yutaka Amao, "Regioselective NAD^+ reduction to NADH with dye and homogeneously dispersed rhodium nanoparticles under visible light", 5th EuChemS Conference on Green and Sustainable Chemistry (5th EuGSC), Online, September 2021.
17. Takayuki Katagiri, Yutaka Amao, "NADH regeneration system with dye and homogeneously dispersed rhodium nanoparticles under visible light", 6th Green & Sustainable Chemistry Conference, Online, November 2021.

List of Domestic Conference Talk

【Oral Presentations】

1. 片桐 毅之, 池山 秀作, 藤田 晃平, 天尾 豊, "脱水素酵素を触媒として用いた可視光駆動型物質変換反応系に有効な新規ビオローゲン電子伝達体の開発", 日本化学会第 97 回春季年会, 神奈川, 2017 年 3 月.
2. 藤田 晃平, 片桐 毅之, 池山 秀作, 天尾 豊, "二酸化炭素固定作用を持つリンゴ酸酵素に働く人工補酵素の開発", 日本化学会第 97 回春季年会, 神奈川, 2017 年 3 月.
3. 池山 秀作, 片桐 毅之, 天尾 豊, "Improvement of the CO_2 reduction to formic acid conversion with formate dehydrogenase via a novel viologen derivative photoreduction", 日本化学会第 97 回春季年会, 神奈川, 2017 年 3 月.
4. 片桐 毅之, 池山 秀作, 藤田 晃平, 天尾 豊, "可視光を利用した二酸化炭

素を原料とする炭素-炭素結合生成を可能とする色素－生体触媒系”, 第 120 回触媒討論会, 愛媛, 2017 年 9 月.

5. 片桐 毅之, 藤田 晃平, 池山 秀作, 天尾 豊, “二酸化炭素資源化のための光増感分子及び生体触媒を用いた可視光駆動型炭素－炭素結合生成系”, 第 47 回石油・石油化学討論会, 鳥取, 2017 年 11 月.
6. 片桐 毅之, 池山 秀作, 天尾 豊, “二酸化炭素資源化機能を持つリンゴ酸酵素と人工補酵素との相互作用に関する研究”, 日本化学会第 98 春季年会, 千葉, 2018 年 3 月.
7. 片桐 毅之, 池山 秀作, 天尾 豊, “二酸化炭素資源化のためのリンゴ酸酵素と新規人工補酵素との相互作用に関する速度論的考察”, 第 122 回触媒討論会, 北海道, 2018 年 9 月.
8. 片桐 毅之, 池山 秀作, 天尾 豊, “二電子還元型ジフェニルビオローゲンを用いたリンゴ酸酵素が触媒する二酸化炭素固定化反応における速度論的解析”, 第 48 回石油・石油化学討論会, 東京, 2018 年 10 月.
9. 片桐 毅之, 池山 秀作, 天尾 豊, “人工補酵素ジフェニルビオローゲン誘導体とリンゴ酸酵素による二酸化炭素を原料とした有機分子のカルボキシ化”, 日本化学会第 99 春季年会, 兵庫, 2019 年 3 月.
10. 片桐 毅之, 池山 秀作, 天尾 豊, "生体触媒と人工補酵素ジフェニルビオローゲン誘導体を用いた二酸化炭素の固定化", 第 124 回触媒討論会, 長崎, 2019 年 9 月.
11. 片桐 毅之, 池山 秀作, 天尾 豊, “リンゴ酸酵素が触媒する二酸化炭素固定反応における多電子蓄積ジフェニルビオローゲン誘導体の機能に関する研究”, 第 49 回石油・石油化学討論会, 山形, 2019 年 10 月.
12. 片桐 毅之, 池山 秀作, 天尾 豊, “Effect of metal ion on the CO_2 addition by malic enzyme with viologen derivative”, 日本化学会第 100 春季年会, 千葉, 2020 年 3 月.
13. 片桐 毅之、天尾 豊, “リンゴ酸酵素が触媒する二酸化炭素のカルボキシ化に対する補因子の影響”, 第 128 回触媒討論会, オンライン開催, 2020 年 9 月.
14. 片桐 毅之、天尾 豊, “リンゴ酸酵素が触媒する二酸化炭素固定反応に対する補因子の効果”, 第 50 回石油・石油化学討論会, 熊本, 2020 年 11 月.

15. 片桐 毅之, 天尾 豊, “リンゴ酸酵素が触媒する二酸化炭素付加反応における金属補因子効果”, 日本化学会第 101 春季年会, オンライン開催, 2021 年 3 月.
16. 片桐 毅之, 天尾 豊, “水溶性亜鉛ポルフィリンおよびロジウム微粒子による可視光駆動型 NADH 再生系” 第 128 回触媒討論会, オンライン開催, 2021 年 9 月.
17. 片桐 毅之, 東 正信, 天尾 豊, “ロジウム微粒子および水溶性亜鉛ポルフィリンを用いた NADH 再生のための光酸化還元系”, 第 51 回石油・石油化学討論会, 北海道, 2021 年 11 月.
18. 片桐 毅之, 東 正信, 天尾 豊, 日本化学会第 102 春季年会, 兵庫, 2022 年 3 月.

【Poster Presentations】

1. 片桐 毅之, 池山 秀作, 藤田 晃平, 天尾 豊, “Dye/malic enzyme composite system for visible-light induced malic acid production from CO_2 and pyruvic acid” 触媒学会西日本支部第 8 回触媒科学研究発表会, 大阪, 2017 年 6 月.
2. 片桐 毅之, 池山 秀作, 藤田 晃平, 天尾 豊, “可視光を用いた二酸化炭素資源化のための色素ーリンゴ酸酵素複合系に関する研究”, 第 36 回光がかかわる触媒化学シンポジウム, 大阪, 2017 年 6 月.
3. 池山 秀作, 片桐 毅之, 天尾 豊, “新規電子伝達体の開発による可視光を駆動力として用いた生体触媒の CO_2 還元触媒活性利用技術の向上”, 第 36 回光がかかわる触媒化学シンポジウム, 大阪, 2017 年 6 月.
4. 片桐 毅之, 池山 秀作, 天尾 豊, “Evaluation of catalytic activity of malic enzyme for CO_2 fixation by two-electron reduced form of diphenylviologen”, 触媒学会西日本支部第 9 回触媒科学研究発表会, 愛知, 2018 年 6 月.
5. 片桐 毅之, 池山 秀作, 天尾 豊, "CO_2 fixation with malic enzyme and diphenylviologen derivative as a co-enzyme", 第 10 回触媒科学研究発表会, 鳥取, 2019 年 6 月.
6. 片桐 毅之, 池山 秀作, 天尾 豊, "生体触媒と二電子還元型ジフェニルビオローゲン誘導体を用いた二酸化炭素の有機分子への固定化", 第 8 回 JACI/GSC シンポジウム, 東京, 2019 年 6 月.

7. 片桐 毅之, 天尾 豊, “リンゴ酸酵素を触媒として用いた可視光をエネルギー源とする二酸化炭素資源化”, 第 9 回 JACI/GSC シンポジウム, オンライン開催, 2020 年 6 月.
8. 片桐 毅之, 天尾 豊, “ロジウムナノ微粒子を触媒として用いた NAD^+光還元反応”, 第 12 回触媒科学研究発表会, オンライン開催, 2021 年 6 月.

【Other Presentation】

1. 片桐 毅之, “可視光を用いた二酸化炭素の資源化のための新規ビオローゲン電子伝達体の分子設計・合成及びその特性についての研究”, 2016 年度「サマーチャレンジ在り方検討会」及び「合同研究発表会」, 茨城, 2017 年 3 月.
2. 片桐 毅之, “可視光を用いた二酸化炭素資源化のための色素ー生体触媒系”, 第 38 回触媒学会若手会「夏の研修会」, 滋賀, 2017 年 8 月.
3. 片桐 毅之, “可視光による二酸化炭素資源化を目指して～光増感分子ーリンゴ酸酵素光レドックス系～”, 2017 年度「サマーチャレンジ在り方検討会」及び「合同研究発表会」, 茨城, 2018 年 2 月.
4. 片桐 毅之, “二電子還元型ジフェニルビオローゲン誘導体とリンゴ酸酵素による二酸化炭素を原料とした有機分子のカルボキシ化に関する研究”, 2018 年度「サマーチャレンジ世代間交流会」, 茨城, 2019 年 2 月.